UNIVERSIDADE FEDERAL DO RIO GRANDE DO SUL
INSTITUTO DE QUÍMICA
PROGRAMA DE PÓS-GRADUAÇÃO EM QUÍMICA

Sandra Valeria Mendes de Moraes

SÍNTESE E CARACTERIZAÇÃO DE HÍBRIDOS A BASE DE SÍLICA CONTENDO AMINAS ALIFÁTICAS E AROMÁTICAS

Tese apresentada como requisito parcial para
a obtenção do grau de Doutor em Química

Prof. Dr. Edílson Valmir Benvenutti
Orientador
Prof. Dr[a] Márcia Russman Gallas
Co-orientadora

UNIVERSIDADE FEDERAL DO RIO GRANDE DO SUL
INSTITUTO DE QUÍMICA
PROGRAMA DE PÓS-GRADUAÇÃO EM QUÍMICA

SÍNTESE E CARACTERIZAÇÃO DE HÍBRIDOS A BASE DE SÍLICA CONTENDO AMINAS ALIFÁTICAS E AROMÁTICAS

Sandra Valeria Mendes de Moraes

DEDICATÓRIA

Dedico este trabalho ao meu pai que sempre lutou para que seus filhos tivessem a melhor educação que a força do seu trabalho pudesse oferecer. Ele certamente estaria orgulhoso deste momento.

AGRADECIMENTOS

Ao professor Dr. Edílson V. Benenutti por acredtitar que é possível orientar alunos que trabalham em outras instituições públicas ou privadas e fazê-lo com dedicação, eficiência e empenho. Agradeço ainda por ter se tornado um amigo para a vida inteira.

À professora Dr[a] Márcia R. Gallas, co-orientadora, pela amizade, pela orientação técnica e prática na utilização de altas pressões e pelas inúmeras discussões que foram fundamentais no desenvolvimento desse trabalho.

Aos membros da banca professor Dr. Yoshitaka Gushinkem, professor Dr. Éder Lima, professor Dr. João Henrique Z. dos Santos e professor Dr. Cláudio Perotonni.

Aos professores doutores celso C. Moro e Tânia M. H. Costa pelas inúmeras discussões.

Às amigas Joana B. Passos e Marina T. Laranjo pela amizade e valorosa contribuição durante o período em que foram alunas de iniciação científica.

Aos amigos Flávio A. Pavan e daniel R. Azolin pela amizade e auxílio.

Às amigas Débora S. F. Gay, leliz T. Arenas e Andréa Marins de Oliveira, pelo incentivo, carinho e amizade que sempre demonstraram por mim.

Ao Exército Brasileiro e em especial aos comandantes do Colégio Militar de Porto Alegre por apoiarem seus subordinados a fazer pós-graduação.

A minha mãe e irmãos por serem especiais.

Ao meu amado Giuliano brasil Graciolli por me compreender e me fazer feliz.

SUMÁRIO

RESUMO

Nesse trabalho foram sintetizados híbridos organo-inorgânicos à base de sílica contendo aminas aromáticas e alifáticas, usando-se os métodos sol-gel e enxerto nas sínteses. Os híbridos obtidos foram caracterizados usando-se isotermas de adsorção e dessorção de nitrogênio, microscopia eletrônica de varredura e termoanálise no infravermelho. Alguns dos híbridos sintetizados mostraram potencialidade na adsorção de espécies químicas de interesse ambiental. Os híbridos sintetizados foram, difenilaminapropil sílica, *p*-anisidinapropil sílica, *p*-fenilenodiaminapropil sílica e o 7-amino-4-azaheptil sílica.

A influência da presença de titânia na matriz inorgânica foi investigada para o híbrido difenilaminapropil sílica. Observou-se que a adição de titânia, embora reduza a porosidade do híbrido, melhora as propriedades de adsorção de compostos aromáticos nitrogenados.

O híbrido 7-amino-4-azaheptil sílica apresentou características promissoras para a utilização como material adsorvente, tendo mostrado potencialidade para o uso na pré-concentração de íons Fe (III) e Cu (II).

Os materiais híbridos: difenilaminapropil sílica, *p*-anisidinapropil sílica, *p*-fenilenodiaminapropil sílica, obtidos a partir do método sol-gel de síntese, foram também processados em altas pressões. A morfologia dos xerogéis híbridos foi estudada antes e após esse processamento, tendo sido possível avaliar os efeitos produzidos pela presença de orgânicos nas matrizes sólidas. O processamento em altas pressões mostrou-se adequado para densificação de materiais híbridos, evitando-se assim o uso de tratamento térmico que poderia levar a decomposição de orgânicos. Entretanto, foi observado que a presença dos grupos orgânicos nos poros inibe parcialmente a densificação, sendo que um mecanismo de inibição foi proposto. A densificação dos xerogéis híbridos depende não apenas da pressão aplicada, mas também da natureza do grupo orgânico presente nos poros.

ABSTRACT

In this work it was synthesized sílica based organo-inorganic hybrids containing aliphatic and aromatic amines, using the sol-gel and grafting methods. The obtained hybrids were characterized using nitrogen adsorption-desorption isotherms, scanning electron microscopy and infrared thermal analysis. Some hybrids presented potentiality to adsorb chemical species of environmental interest. The synthesized hybrids were biphenylaminepropyl silica, *p*-anisidinepropyl silica, *p-phenylene*diaminepropyl silica and 7-amine-4-azaheptyl silica.

The influence of the presence of titania in the inorganic matrix was investigated for the biphenylaminepropyl silica hybrid. It was observed that the titania addition results in a porosity decreasing and in an improvement of adsorption properties for N-containing aromatic compounds.

The 7-amine-4-azaheptyl silica hybrid presented promising characteristics as sorbent material, with potentiality to be used for Fe(III) and Cu(II) pre-concentration.

The hybrid materials: biphenylaminepropyl silica, *p*-anisidinepropyl silica, *p-phenylene*diaminepropyl silica obtained by the sol-gel synthesis method were also processed using high pressure. The hybrid xerogels morphology was studied before and after the high pressure processing, being possible to evaluate the effects of the organics in the solid matrix.

The high pressure processing was satisfactory to compact hybrid materials, avoiding the thermal treatment which could result in organic decomposition. However, it was observed that the organic presence in the pores partially inhibits the compaction, and an inhibition mechanism was proposed. The hybrid xerogels compaction depends on the applied pressure and also on the organic group presented in the pores.

LISTA DE ARTIGOS PUBLICADOS E TRABALHOS APRESENTADOS EM CONGRESSO

Artigos

1- Moraes, S. V. M; Moro, C. C.; Costa, T. M. H.; Gallas, M. R.; Benvenutti, E. V.; *High Pres. Res.* **2006**, 26, 1.

2- Moraes, S. V. M.; Laranjo, M. T.; Zat, M.; Costa, T. M. H.; Gallas, M. R.; Benvenutti, E. V.; *Apll. Phys. A*, **2005**, 81, 1053.

3- Moraes, S. V. M.; Brasil, J. L.; Milcharek, C. D., Martins, L. C.; Laranjo, M. T. H.; Gallas, M. R.; Benvenutti, E. V.; Lima, E. C.; *Spectochem. Acta, Part A*, **2005**, 62, 398.

4- Moraes, S. V. M.; Tisott, M. M.; Millcharek, C. D.; Brasil, J. L.; Costa, T. M. H., Gallas, M. R.;Benvenutti, E. V.; Lima E. C.; *Anal. Sci*. **2005**, 21, 273.

5- Moraes, S.V.M.; Passos, J. B.; Schossler, P.; Camarão, E. B;.Moro, C. C.; Costa, T. M H.; Benvenutti, E. V.; *Talanta*, **2003**, 59, 1039.

Trabalhos

1- Moraes, S. V. M., Laranjo, M. T., Brasil, J. L., Costa, T. M. H., Lima, E. C., Tissot, M. M., Gallas, M. R., Benvenutti, E. V. Uso do híbrido diaminopropanopropril/sílica em sistemas de pré-concentração em fluxo para a determinação de Fe (III) em amostars de águas naturais. In: Congresso Latino Americano de Química, 2004, Salvador, V. QA p28.

2- Moraes, S. V. M., Laranjo, M. T., Moro C. C., Stefani, V., Costa, T. M. H., Gallas, M. R., Benvenutti, E. V. Estudo da influência das altas pressões nas propriedades ópticas dos xerogéis híbridos anilina/sílica e p-anisidina. In: XXVI Congresso Latino Americano de Química, 27ª Reunião Anual da SBQ, 2004, Salvador, v. QM p.233.

3- Moraes, S. V. M., Laranjo, M. T, Stefani, V., Costa, T. M. H., Gallas, M. R., Benvenutti, E. V. Estudo das propriedades ópticas de gel de sílica modificado com rodamina 6G. In: XII Encontro de Química da Região Sul, 2004, Garapuava, v. QI, 025.

4- Moraes, S. V. M., Laranjo, M. T, Moro, C. C., Gallas, M. R., Costa, T. M., Benvenutti, E. V. Morphological changes produced by high-pressure processing in p-anisidine/silica hybrid xerogel. In: 2ª Reunião da Rede de Nanobiotecnologia, 2003, Campinas.

5- Moraes, S. V. M., Vinade, M. T. , Moro, C. C., Costa, T. M. H., Gallas, M. R.. Efeito das altas pressões na morfologia de xerogéis híbridos: bifenilaminapropilsilica e bifenilaminaproprilsilicatitânia,In:, 26ª Reunião Anual da Sociedade Brasileira de Química, Poços de Calda, 2003, v. QM p.111

6- Moraes, S. V. M., Zat, M., laranjo, M. T., Costa, T. M. H., Gallas, M. R., Benvenutti, E. V., High-pressure effects on p-phenylediamine/sílica and p-anisidine/sílica hybrid xerogels. In: II Encontro de SBPMAT, Rio de Janeiro, 2003, p.18.

7- Moraes, S. V. M., Passos, J. B., Moro, C. C., Costa, T. M. H., Benvenutti, E. V. propriedades dos xerogéis bifenilproprilsílica e bifenilproprilsilica titânia. In: 25ª reunião Anual da SBQ, Poços de Caldas, 2002, p. QM108.

1. INTRODUÇÃO

Nos últimos 20 anos a comunidade científica tem concentrado esforços para o desenvolvimento de novos materiais e para o aperfeiçoamento de materiais já existentes face a necessidade crescente de desenvolvimento tecnológico que atenda aos anseios da sociedade moderna [1-9]. Alguns exemplos de materiais desenvolvidos podem ser citados, como o desenvolvimento dos biomateriais para a substituição de ossos, dentes e até órgãos [9-12], de materiais para a indústria farmacêutica [13], de sensores utilizados no controle de poluição [4, 14], de materiais para as indústrias de aviação e de navegação [5], entre tantos outros. Uma classe muito importante desses materiais é a dos híbridos, que associam, numa mesma matriz, componente orgânico e inorgânico. Como resultado da soma das contribuições individuais de cada componente, propriedades como resistência mecânica [15-18], porosidade [19] e capacidade de adsorção de substâncias químicas são muitas vezes superiores às propriedades dos componentes individuais [20-22].

A sílica gel é o suporte inorgânico mais utilizado na obtenção de materiais híbridos organo-inorgânicos. Sua superfície rica em grupos silanóis (Si-OH) permite a adsorção física de diversos compostos e possibilita ainda reações químicas com diferentes grupos orgânicos [19, 21, 22]. Os dois procedimentos mais importantes de obtenção de híbridos a base de sílica são o método enxerto e o método sol-gel. No primeiro utiliza-se uma sílica com características predefinidas e, a partir de reações químicas, adicionam-se grupos orgânicos à sua superfície [23, 24]. Já no método sol-gel, a formação da sílica ocorre simultaneamente à adição dos grupos orgânicos e conseqüentemente esses grupos ficam dispersos em toda estrutura do material, em nível molecular [25]. No Instituto de Química da UFRGS, especificamente pelo grupo de Química do Estado Sólido e Superfícies, no Laboratório de Sólidos e Superfícies (LSS), estão sendo desenvolvidos novos materiais híbridos organo-inorgânico a base de sílica e de aminas, contendo grupos orgânicos aromáticos e alifáticos [26-31]. Esses híbridos, também chamados de sílica organofuncionalizadas, têm apresentado diversas aplicações na adsorção de substâncias químicas, na construção de sensores eletroquímicos, de dispositivos ópticos e ainda são utilizados como carreadores de fármacos.

Neste trabalho o híbrido difenilaminapropril sílica foi sintetizado pela primeira vez. Suas características e propriedades foram investigadas, bem como a influência da adição de titânia à sua estrutura. A potencialidade de uso desse novo híbrido como fase

estacionária na adsorção de compostos aromáticos nitrogenados, de interesse ambiental, foi investigada através do método de extração em fase sólida. A utilização de sílicas organofuncionalizadas como fases estacionárias em técnicas de extração em fase sólida e técnicas cromatográficas tem sido amplamente estudada. A vantagem é que além de apresentarem boa estabilidade térmica, esses materiais possuem propriedades mecânicas e microestruturais do suporte inorgânico, e o comportamento químico do componente orgânico presente pode variar conforme o grupo orgânico utilizado [15-18, 22, 25]. É importante destacar que as propriedades adsorventes dessas sílicas são, em geral, determinadas pela associação das propriedades dos componentes orgânicos e inorgânicos [20, 21, 26].

Outra etapa do trabalho foi estudar o efeito do processamento em altas pressões na estrutura de híbridos obtidos pelo método sol-gel. A compactação em condições tão extremas pode ser uma alternativa para o controle das propriedades desses materiais, já que o método sol-gel, apesar de bastante eficaz, é muito sensível. Qualquer modificação nos parâmetros de síntese, como por exemplo, temperatura de gelificação, quantidade de água e pH do meio, pode levar à formação de híbridos com propriedades diferentes, tornando difícil a reprodução exata dos materiais [19, 21, 32- 36]. Estudar procedimentos que possam controlar ou modificar algumas dessas propriedades, como por exemplo, a porosidade, é uma alternativa bastante interessante.

A compactação em altas pressões de materiais híbridos organo-inorgânicos pode ser também uma opção à tradicional etapa de sinterização térmica, utilizada na densificação dos materiais, já que a fase orgânica presente nesses híbridos não é estável em temperatura elevada [29, 37, 38]. A densificação dos materiais em altas pressões, sem aquecimento, ocorre por meio de um processo chamado sinterização a frio, que será discutido neste trabalho.

Os materiais estudados foram compactados em pressões que variam entre 3,5 e 7,7 GPa, no Laboratório de Altas Pressões e Materiais Avançados (LAPMA), do Instituto de Física da UFRGS. Inicialmente foi compactado o híbrido inédito, difenilaminapropril sílica, a fim de investigar as alterações na microestrutura desse material, causadas por esse processamento. A compactação desse híbrido após adição de titânia também foi estudada. Numa etapa posterior os híbridos *p*-fenilenodiaminapropril sílica e *p*-anisidinapropril sílica, obtidos *via* método sol-gel, também foram processados em altas pressões, com a finalidade de aprofundar este estudo, e assim verificar o

comportamento de outros híbridos a base de sílica e de aminas aromáticas quando submetidos a condições tão extremas de pressão. Deve-se destacar que a compactação em altas pressões desse tipo de híbrido é um estudo inédito.

Ainda como parte desse trabalho, o híbrido 7-amino-4-azaheptil sílica foi sintetizado pelo método enxerto com o objetivo de avaliar sua utilização na adsorção e pré-concentração de íons metálicos, especificamente íons de cobre e ferro, e ainda estudar o método utilizado industrialmente para a produção de materiais híbridos. A utilização de sílica organofuncionalizada como adsorvente químico tem sido bastante estudada [20, 39-41] e a presença de grupos quelantes na superfície da sílica, como no caso do híbrido estudado, permite vários ciclos de pré-concentração, num processo de retenção e dessorção. A pré-concentração de íons metálicos é uma alternativa para aumentar o poder de detecção de técnicas analíticas menos sensíveis e mais acessíveis do ponto de vista econômico, como a espectrofotometria no UV e visível e a espectrometria de absorção atômica de chama.

Este trabalho, então, teve como objetivos: Relacionar as características microestruturais dos materiais híbridos síntetisados pelo método sol-gel com as condições experimentais de síntese; estudar potenciais aplicações para os materiais híbridos preparados, a partir das características obtidas; estudar o mecanismo de compactação em altas pressões dos xerogeis híbridos. Para alcançar tais objetivos foi sintetizado o híbrido difenilaminapropril sílica pelo método sol-gel estudando-se o efeito da presença da titânia na microestrutura desse material.Investigou-se o efeito da compactação em altas pressões na microestrutura desse material antes e depois da adição de titânia. Foi investigado ainda o efeito da compactação em altas pressões utilizando dois outros híbridos obtidos pelo método sol-gel: o *p*-anisidinapropril sílica e o *p*-fenilenodiaminapropril sílica. Esse processamento pode ser uma alternativa aos métodos tradicionais de sinterização, ou ainda, uma forma de controlar e/ou modificar as características microestruturais dos materiais híbridos, obtidos pelo método sol-gel. Nesse trabalho também foi sintetizado o híbrido 7-amino-4-azaheptil sílica pelo método enxerto com o objetivo de avaliar a potencialidade desse material na adsorção de íons metálicos.

Na caracterização dos diversos materiais obtidos determinou-se a área superficial e a distribuição de poros pelos métodos BET [42] e BJH [43], respectivamente. A microestrutura dos híbridos foi avaliada também por microscopia eletrônica de

varredura. Já a estabilidade desses materiais foi determinada por termoanálise no infravermelho [37, 44].

2. MATERIAIS HÍBRIDOS

Atualmente a síntese de materiais híbridos organo-inorgânicos tem despertado grande interesse nos pesquisadores em função da versatilidade no que diz respeito às suas propriedades. A mistura de dois componentes distintos dá origem a um novo material, cujas características são resultantes da soma das contribuições individuais de cada componente [22, 45, 46]. Essa combinação possibilita o aperfeiçoamento dos materiais já existentes e a produção de novos materiais com potencialidade em diversas aplicações tecnológicas, tais como: sensores eletroquímicos [25, 47-49], adsorventes químicos [39, 40], fase estacionária para cromatografia [21, 41, 50, 51], suporte de catalisadores [52], revestimento [53, 54], dispositivos ópticos [1, 55, 56], etc.

Existem duas classes principais de materiais híbridos que são as Classes I e II, as mesmas estão relacionadas à natureza química da interface organo-inorgânica. Nos híbridos de Classe I, os componentes estão ligados entre si por interações do tipo van der Waals, interações eletrostáticas ou ligações de hidrogênio. [41, 47, 57] Esses híbridos podem ser obtidos pela mistura homogênea de um componente orgânico com precursores inorgânicos em um solvente único. Durante a formação da matriz inorgânica, a partir das reações de hidrólise e condensação, os grupos orgânicos são aprisionados na matriz à medida que a rede está sendo formada [47].

Os híbridos de Classe II são aqueles em que a natureza química da interface é predominantemente covalente. Tais materiais podem ser preparados pela reação entre um precursor inorgânico, do tipo $Si(OR)_4$, e um precursor orgânico, hidrolisável, do tipo R'-$Si(OR)_3$, ou ainda, pela reação da superfície da sílica gel com silanos bifuncionais: Y_3Si-R [47, 57]. Os híbridos sintetizados e estudados no presente trabalho são de Classe II, nos quais os componentes orgânico e inorgânico estão fortemente ligados e foram sintetizados pelos métodos enxerto e sol-gel. Nesses híbridos o componente orgânico mostra-se mais resistente à lixiviação por solventes além de ser termicamente mais estável que nos híbridos de Classe I.

2.1 Método enxerto

Os grupos silanóis, presentes na superfície de géis de sílica, tornam essa matriz propícia para a imobilização de diferentes substâncias [23, 52]. Como já foi dito anteriormente, a modificação de superfícies como a sílica tem como objetivo principal associar, na mesma matriz, características físicas e químicas de diferentes materiais. O método enxerto é o método mais tradicionalmente utilizado para a obtenção de materiais híbridos. Esse método é utilizado industrialmente e consiste na reação dos grupos silanóis da superfície da sílica com os grupos a serem ancorados [23, 24, 52, 58].

A obtenção de materiais híbridos pelo método enxerto requer a ativação dos grupos silanóis, por meio da eliminação da água residual, o que pode ser alcançado com o aquecimento da sílica sob vácuo [52]. Após a ativação dos grupos silanóis, a imobilização de grupos funcionais pode ser realizada por meio de reações da matriz de sílica ativada com silanos bifuncionais: $Y_3Si\text{-}R$ [23, 52]. A aplicabilidade desses grupos silanos está relacionada às características do grupo R, onde Y pode ser um haleto, um grupo amina, porém, é mais comum encontrá-lo como grupo alcóxido, que reage facilmente com substratos hidroxilados, liberando álcool para o meio reacional [23]. Entretanto, mesmo após a organofuncionalização, diversos grupos silanóis permanecem inalterados na superfície do material e podem ser desativados, se necessário, reagindo esses silanóis com pequenos grupos, como por exemplo, o $Cl\text{-}Si(CH_3)_3$.

É importante destacar que, no método enxerto, a incorporação dos grupos orgânicos ocorre apenas na superfície, assim, todas as propriedades físicas da matriz são mantidas no material híbrido [59]. Já as propriedades químicas do material passam a ser definidas pelos grupos imobilizados na superfície. Os grupos imobilizados ligam-se fortemente à superfície da matriz ficando dispersos de forma homogênea nessa superfície, o que se explica pela formação de uma monocamada [34, 60]. Neste trabalho, foi utilizada uma sílica gel comercial da marca Merck, de granulometria 0,2-0,5 mm, diâmetro médio de poro de 10 nm e área superficial de aproximadamente 250 m^2g^{-1}.

2.2 Método sol-gel

O processo sol-gel é uma rota atrativa na preparação de materiais híbridos, quando comparado ao tradicional método enxerto, já que propriedades como volume e distribuição de poros, tamanho e forma de partículas, quantidade de matéria orgânica e área superficial podem ser modificadas através da manipulação dos parâmetros de síntese [19, 34, 61, 62].

O método sol-gel também permite a obtenção de materiais com alto grau de pureza e, como a síntese é realizada à temperatura ambiente, é possível incorporar biomoléculas à rede inorgânica sem degradá-las, como por exemplo, a incorporação de enzimas em matrizes inorgânicas para a construção de biossensores [25, 57, 63]. Os materiais sintetizados por essa *via* podem ter diferentes configurações como monolitos, fibras, corpos cerâmicos, filmes, membranas e pós, configurações que dependem dos parâmetros utilizados durante a síntese [34]. Essa versatilidade do método sol-gel é muito importante para a área de ciências de materiais, já que, de forma simples, são sintetizados materiais com diferentes texturas, estruturas, configurações, composições, características químicas e, conseqüentemente, podem ser sintetizados materiais para diversas aplicações. Entretanto, deve-se destacar que a reprodução desses materiais depende de um controle rígido nos parâmetros de síntese [36, 64- 67].

O processo sol-gel consiste em uma transição de sistema sol para um sistema gel, em que sol é o termo utilizado para definir uma dispersão de partículas coloidais entre 1 a 100 nm, estáveis em um fluido e o termo gel define o sistema formado por uma estrutura rígida tridimensional de partículas coloidais (gel coloidal) ou de cadeia polimérica (gel polimérico). No gel coloidal ocorre agregação de partículas primárias, já nos géis poliméricos a agregação ocorre pela interação de longas cadeias poliméricas [25].

A síntese de sílica pelo método sol-gel consiste basicamente na hidrólise (reação 1) e policondensação de alcoxisilanos (reações 2a e 2b), em geral tetraetilortosilicato (TEOS) ou tetrametilortosilicato (TMOS), em meio alcoólico, resultando numa rede interligada de sílica [68]. Na etapa de hidrólise grupos alcóxidos são substituídos por hidroxilas com a eliminação de álcool. Nas etapas seguintes (policondensação) ocorrem as condensações aquosas e alcóolica [69]. As reações, mostradas a seguir, são realizadas em meio alcoólico, já que os alcoxisilanos e a água não são miscíveis. A hidrólise de

alcoxisilanos ocorre por mecanismo SN_2 e nessa etapa são formados os grupos silanóis (SI-OH) enquanto que na condensação são formados os grupos silanos (Si-O-Si).

$$Si(OR)_4 + H_2O \rightarrow (RO)_3Si\text{-}OH + ROH \quad (1) \quad \text{hidrólise}$$

$$\equiv SiOH + OH\text{-}Si \equiv \rightarrow \equiv Si\text{-}O\text{-}Si \equiv + H_2O \quad (2a) \quad \text{condensação}$$

$$\equiv Si\text{-}OH + RO\text{-}Si \equiv \rightarrow \equiv Si\text{-}O\text{-}Si \equiv + ROH \quad (2b) \quad \text{condensação}$$

Os mecanismos envolvidos durante a transição sol-gel são bastante complexos, pois muitas das reações de condensação ocorrem simultaneamente às reações de hidrólise [25]. Em função da baixa reatividade dos alcóxidos são utilizados catalisadores para acelerar a reação, que podem ser ácidos, básicos ou nucleofílicos [69].

2.2.1 Hidrólise catalisada por ácido

Sob condições ácidas, ocorre a protonação do grupo alcóxido seguido do ataque nucleofílico da água. Na Figura 1 é mostrado um esquema desse mecanismo, no qual há formação de um intermediário pentacoordenado, com inversão do tetraedro de silício. A diminuição do impedimento estérico em torno do átomo de silício e a presença de substituintes doadores de elétrons, que estabilizam a carga positiva do estado de transição, são fatores que favorecem a hidrólise [68].

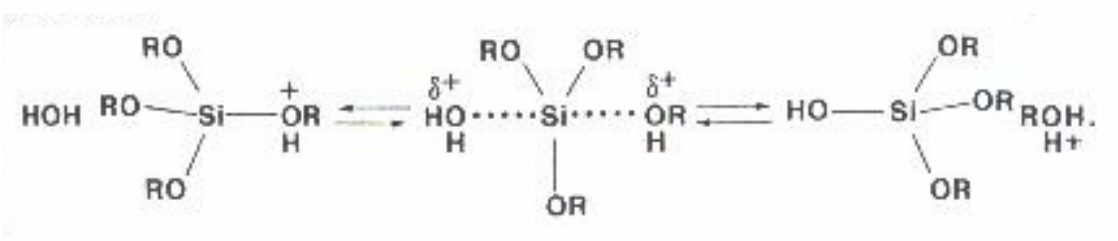

Figura 1. Mecanismo da hidrólise catalisada por ácido.

2.2.2 Hidrólise catalisada por base

O mecanismo da hidrólise catalisada por base consiste no ataque nucleofílico ao átomo de silício pela hidroxila. Iller [69] e Keef [70] propuseram que íons hidroxilas substituam grupos alcóxidos com inversão do tetraedro. Esse mecanismo depende mais

dos fatores estéricos que dos indutivos, já que nesse mecanismo o estado de transição tem pouca carga. Na Figura 2, abaixo, é mostrado um esquema desse mecanismo.

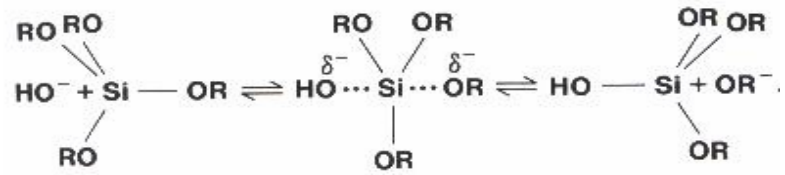

Figura 2. Mecanismo da hidrólise catalisada por base.

Pohl e Osterholtz [71] propuseram um mecanismo que envolve dois estados de transição: no primeiro, um intermediário pentacoordenado se forma. Este por sua vez, forma um segundo estado de transição em que um dos ligantes adquire carga e que se completa com a saída do grupo alcóxido.

2.2.3 Hidrólise catalisada por agente nucleofílico

O mecanismo envolvido nessa hidrólise é muito semelhante ao da catálise básica. Segundo Brinker e Scherer [72], numa primeira etapa rápida e reversível, há formação de um intermediário pentacoordenado; já numa segunda etapa, lenta, o intermediário sofre ataque nucleofílico da água levando à formação de um sistema hexacoordenado com posterior transferência de próton e eliminação de um grupo ROH [72, 73, 74]. Nas Figuras 3 e 4 são mostradas respectivamente, a etapa rápida e a etapa lenta desse mecanismo. Na síntese dos materiais estudados neste trabalho, utilizou-se F^- como agente nucleofílico.

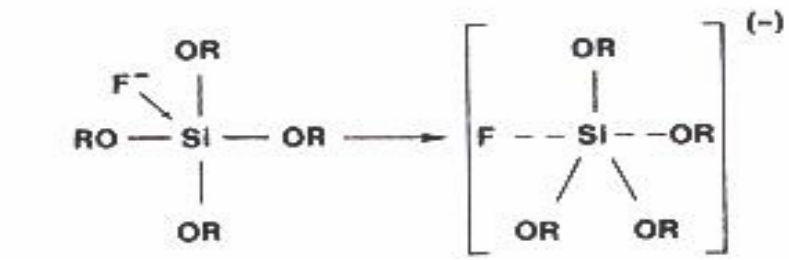

Figura 3. Etapa rápida da síntese catalisada por F^-

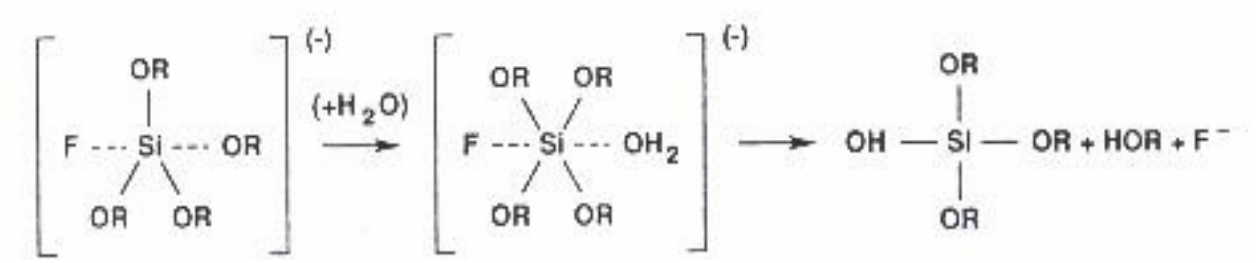

Figura 4. Etapa lenta da hidrólise catalisada por F^-

2.2.4 Transição sol-gel

No estágio inicial da polimerização, os grupos silanóis estão parcialmente desprotonados promovendo uma barreira de repulsão que estabiliza o sol. A evaporação do solvente e o consumo de água pela hidrólise dos alcóxidos promovem a concentração do meio e a desestabilização da suspensão. O ponto de gel ocorre quando pode ser observado um rápido aumento na viscosidade do sol. Nesse ponto a massa sólida torna-se interconectada, contudo, mensurá-lo é extremamente difícil [73].

Durante o último estágio da gelificação, a água e o solvente orgânico evaporam dos poros e ocorre um encolhimento do monolito, em alguns casos o volume final do xerogel é menor que 10% do volume inicial do gel [34, 36, 51]. É nessa etapa também que ocorre o aparecimento de trincas no material. Na etapa seguinte há o envelhecimento do gel com evaporação do solvente [34, 51].

A velocidade de hidrólise e condensação depende de vários parâmetros, dentre eles, a natureza e a concentração do catalisador utilizado, a razão molar H_2O/Si, o tipo de precursor alcóxido e o pH do meio reacional. Conseqüentemente a microestrutura do gel obtido será também afetada pelas condições de síntese [25, 32, 36]. Sabe-se que, em pH elevado, a condensação ocorre preferencialmente entre oligômeros ramificados levando à formação de géis particulados que se tornam, após a secagem, materiais mesoporosos [25, 73, 74]. Um material microporoso e mais denso pode ser sintetizado em meio ácido. Nessas condições, a condensação ocorre preferencialmente entre os grupos silanóis presentes em monômeros ou no final de cadeia polimérica, formando géis de cadeias poliméricas entrelaçadas que, após a secagem, formam uma matriz microporosa [72].

Estudos já demonstraram também que a adição de grande quantidade de água acelera a velocidade de hidrólise e diminui a velocidade de agregação, levando à formação de microporos que resultarão em géis com maior área superficial [25, 32, 75].

Quando a razão molar H_2O/Si é baixa há formação de uma cadeia polimérica com excesso de orgânicos residuais, devido à presença de alcóxidos não hidrolisados. Razão molar H_2O/Si pequena e pH do meio reacional baixo são condições ideais para obtenção de material na forma de fibras, por exemplo [34].

É importante ressaltar ainda que outros parâmetros de síntese podem ser utilizados para controlar as características finais do gel. Estudos mostram que a microestrutura do xerogel está diretamente relacionada à quantidade e ao tipo de matéria orgânica incorporada, ao tipo de solvente utilizado, ao tipo e à quantidade de catalisador, ao pH do meio, à temperatura de gelificação e à secagem do gel [32- 34, 36]. Por exemplo, o excesso de solvente diminui a tendência de agregação aumentando a porosidade do produto final, já a adição de surfactantes é utilizada para reduzir a tensão superficial, estabilizando pequenas partículas e, conseqüentemente, aumentar a área superficial [34].

Modificações nos parâmetros de secagem do gel, como os de temperatura e tempo de envelhecimento, também são realizadas para alterar as características finais desses géis [30, 33, 36]. Define-se como tempo de envelhecimento o tempo estabelecido entre o ponto de gelificação e a secagem do gel. Essa etapa permite uma série de mudanças no produto final, o que pode ser realizado a partir do controle do tempo de envelhecimento e da temperatura [76, 77]. A secagem pode ocorrer em temperatura e pressão ambientes ou em condições supercríticas, que podem ser alcançadas com autoclave em presença de CO_2, N_2O, EtOH, etc [34]. A secagem em condições supercríticas evita o aparecimento de trincas no monolito, melhorando as propriedades mecânicas do material sintetizado [34]. Quando a secagem ocorre em condições ambientes o produto final é denominado xerogel e em condições supercríticas, é chamado de aerogel [72].

As propriedades de híbridos obtidos *via* sol-gel são distintas e muitas vezes superiores às propriedades originais dos componentes individuais, sendo uma alternativa para a produção de novos materiais que supram as limitações de materiais ditos convencionais, ou seja, materiais orgânico e inorgânico na sua forma pura [25]. Os grupos orgânicos podem ser adicionados à estrutura da sílica (matriz inorgânica) a partir da escolha de organosilanos apropriados ($R\text{-}Si(OR)_3$) que sofrerão hidrólise e policondensação simultaneamente com TEOS ou TMOS, formando ligações covalentes entre a sílica e o organosilano [30]. Assim, os grupos serão inseridos em toda a estrutura e

não apenas na superfície. Quando a dispersão ocorre em nível molecular esses materiais são também chamados nanocompósitos, em que um dos componentes do híbrido serve de matriz na qual o segundo componente está disperso [57].

A síntese de nanocompósitos permite a obtenção de materiais com propriedades físicas, químicas e mecânicas de alta qualidade [57, 78, 79]. Além da versatilidade, a possibilidade de obtenção de namomateriais faz do método sol-gel uma rota sintética bastante interessante. Entretanto, ainda há vários fatores a serem estudados pelos pesquisadores, já que os mecanismos de síntese ainda não foram totalmente compreendidos, pois inúmeras são as variáveis que afetam essa rota sintética e nesse caso, em que o sol-gel é de híbridos, o número de variáveis aumenta se comparado a géis de sílica pura.

3. MÉTODO DE PROCESSAMENTO-TÉCNICA DE ALTA PRESSÃO

Algumas aplicações tecnológicas exigem que o material tenha uma forma geométrica específica e com elevada resistência mecânica. Isso é geralmente alcançado com a compactação do pó e posterior densificação desse material, por meio de tratamento térmico em temperatura elevada, chamado de sinterização [2, 80]. Esse processo convencional de densificação de materiais não é viável para híbridos contendo grupos orgânicos, pois em temperaturas elevadas, a matéria orgânica sofre decomposição [37]. Uma alternativa viável para compactação e densificação desses pós em temperatura ambiente é a utilização da técnica de alta pressão, disponível no Laboratório de Altas Pressões e Materiais Avançados, do Instituto de Física da UFRGS e já utilizada em trabalhos anteriores [81-86], em diversas colaborações com o LSS.

A importância da pressão como variável experimental no estado sólido, surge do fato de ser o único modo de se variar o parâmetro de rede de um modo eficaz e controlado. Pode-se causar uma variação de até 10 % na distância interatômica, causando efeito drástico em propriedades físicas dos materiais. Uma boa revisão dessa técnica pode ser encontrada em Sherman e Sttudtmuller [87]. O termo alta pressão usualmente define pressões acima de 1,0 GPa. Nesse trabalho utilizamos pressões entre 3,5 e 7,7 GPa.

A técnica de altas pressões foi utilizada em trabalhos anteriores [81, 84] no estudo da compactação de sílica produzida pelo método sol-gel. Nestes trabalhos foi sugerido um mecanismo de sinterização a frio que explica o processo de compactação da sílica em alta pressão e em temperatura ambiente. No mecanismo proposto, a alta pressão produz uma aproximação entre os grupos silanóis com conseqüente desidroxilação formando uma rede de siloxanos, em que a sílica pura sofre uma redução de cerca de 99% de sua área superficial, em função do fechamento de poros. Na Figura 5 é mostrado o mecanismo sugerido para esse processo.

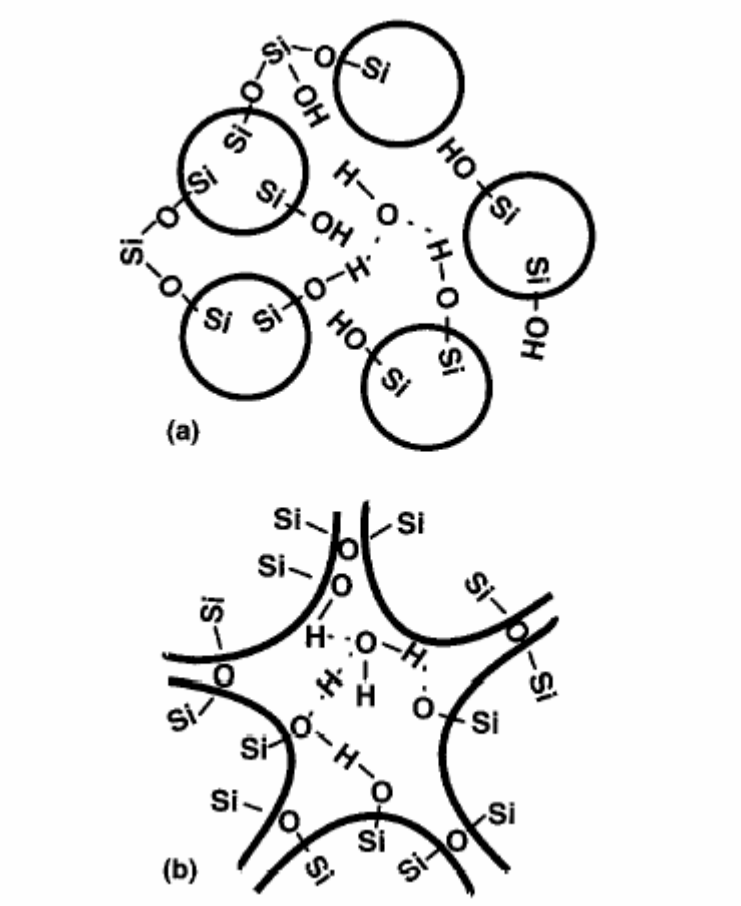

Figura 5. Mecanismo de sinterização a frio da sílica pura. (a) aproximação dos grupos silanóis da sílica; (b) formação dos grupos siloxanos.

Em trabalhos recentes [82, 89], realizados pelo grupo de Estado Sólido e Superfícies e pelo Grupo de Física de Altas Pressões e Materiais Avançados foi visto que a sinterização a frio pode ser utilizado com sucesso no processamento de materiais híbridos, contendo corantes orgânicos dispersos em sílica obtida pelo método sol gel, com o objetivo de produzir materiais com propriedades ópticas. É importante destacar que dispersões em nível molecular foram alcançadas nesses trabalhos, entretanto, apenas para baixas concentrações de grupos orgânicos (10^{2-} a 10^{-3} mmol org/mmol TEOS). A compactação em altas pressões de híbridos sintetizados pelo método sol-gel com concentração de orgânico elevada, como a realizada neste trabalho, é um estudo inédito. As características microestruturais dos híbridos antes e depois da compactação foram avaliadas a fim de se verificar as modificações provocadas por esse processamento.

Os mecanismos de sinterização a frio dependem da adesão, da deformação plástica e da geração de pulsos aleatórios de temperatura, que ocorrem durante a compactação em pressões tão elevadas. É importante destacar que em sistemas sólidos a interação em nível molecular torna-se difícil porque o contato entre as superfícies não é suficiente, a aplicação de pressão aumenta esse contato, possibilitando que forças de interação secundárias como de Van der Waals e ligações de hidrogênio possam atuar ou até mesmo as forças de natureza química. [81, 84].

No processo de sinterização a frio, a deformação plástica é considerada um mecanismo importante e ocorrerá se a tensão de cisalhamento causada pela pressão for maior que a tensão de escoamento entre as partículas. Essa deformação será responsável pelo fechamento dos poros [88].

Neste trabalho utilizamos uma câmara do tipo toroidal para o processamento em alta pressão [90]. Essas câmaras são uma evolução de um aparelho chamado bigorna de Bridgman, em que cones truncados de metal duro são suportados por vários anéis de aço montados com interferência e utilizam o efeito chamado "suporte maciço". O cintamento desses núcleos permite que o mesmo opere num regime de compressão ou com pequenos esforços de tração, viabilizando sua utilização [87]. Na Figura 6 apresentamos um esquema do sistema utilizado.

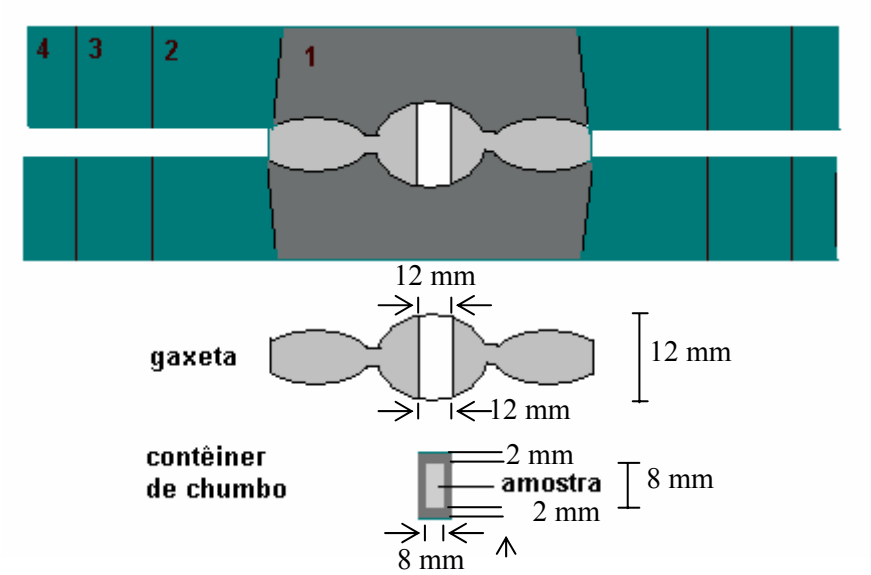

Figura 6. Esquema de um sistema tipo toroidal com a representação da gaxeta, do contêiner de chumbo e da amostra.

Essas câmaras são constituídas por duas metades simétricas que apresentam cavidades esféricas centrais que aumentam o volume útil. Entre as câmaras é utilizado um disco deformável, de material compressível (cerâmico) e com alto coeficiente interno, que mantém a amostra no centro dos pistões. O disco, denominado gaxeta, mostrada na Figura 6, evita o contato direto entre as câmaras, aumenta o atrito e não permite a extrusão da amostra. A gaxeta possui perfil semelhante ao da câmara correspondente e propicia uma distribuição gradual da pressão sobre os pistões, sendo máxima no centro, junto à amostra, e mínima nas extremidades. A força de compressão aplicada sobre a câmara deforma a gaxeta, levando ao escoamento de material e ao desenvolvimento de uma intensa força de atrito dentro da mesma e nas superfícies de contato com a matriz. As propriedades do material e a forma geométrica da gaxeta são fatores importantes para a manutenção de um estado o mais isostático possível [85, 87, 90].

A geração de alta pressão está limitada à resistência dos materiais disponíveis e associada à geometria do sistema. Esta é normalmente realizada pela aplicação de uma força uniaxial a um meio transmissor de pressão, no qual a amostra encontra-se confinada. Neste trabalho, as amostras foram colocadas em contêiner de chumbo com volume interno de aproximadamente 0,35 cm^3 que, na seqüência, foi encaixado na gaxeta. Na Figura 7 é mostrada uma foto do conjunto.

Figura 7. Fotografia da gaxeta e do contêiner de chumbo.

O contêiner de chumbo age como meio transmissor de pressão quasi-hidrostático e esse meio transforma a força uniaxial aplicada em uma pressão uniforme sobre toda a amostra ou seja, o mais hidrostática possível. O chumbo, por possuir uma baixa tensão de cisalhamento, mostrou-se o meio sólido ideal, além de ser estável sob pressão e de fácil manuseio. A hidrostaticidade do meio transmissor de pressão é fundamental para a compactação dos pós, pois evita o surgimento de tensões de cisalhamento.

Para gerar alta pressão nas câmaras toroidais é necessária a aplicação de uma força, que é obtida através de prensas hidráulicas de grande porte. Nesse trabalho foi utilizada uma prensa de 1000 tonf, cuja fotografia é apresentada na Figura 8. Na Figura 9, pode-se observar uma fotografia das câmaras toroidais e do sistema gaxeta-amostra após a compactação. A pressão sobre a amostra é gerada pela compressão da gaxeta entre os pistões através da força aplicada pela prensa. A determinação da pressão efetiva sobre a amostra é fundamental, entretanto, não pode ser calculada diretamente utilizando apenas a razão entre a força aplicada e a área efetiva, pois essas câmaras toroidais apresentam um perfil complexo, além disso, há que se levar em consideração a gaxeta que é deformada no processo.

Figura 8. Fotografia da prensa de 1000 tonf do LAPMA IF/UFRGS.

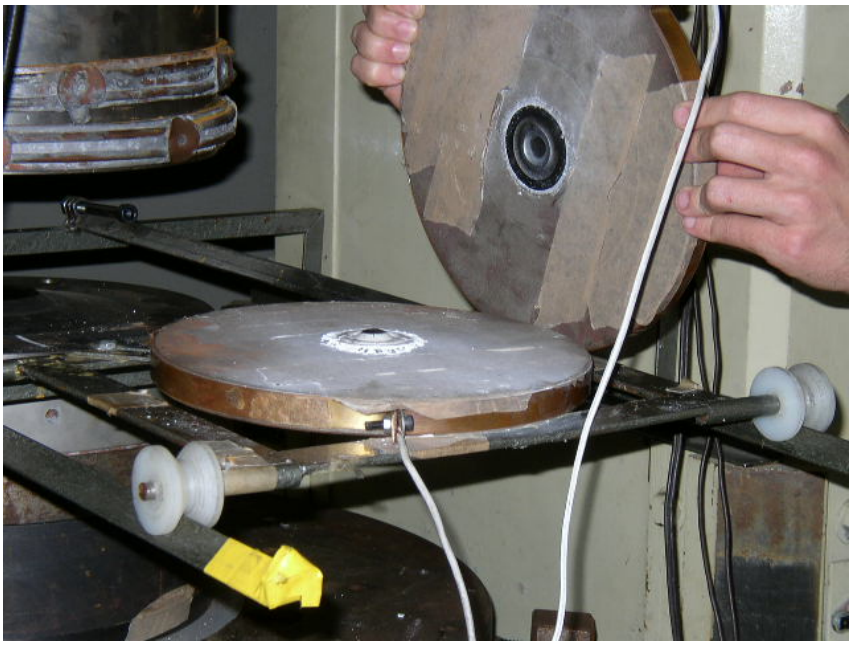

Figura 9- Fotografia das câmaras toroidais e do sistema gaxeta-amostra após a compactação.

A calibração da pressão do sistema é imprescindível e, para isso, são usadas técnicas de calibração que se baseiam no fato de alguns materiais variarem a sua resistividade ao sofrerem transições de fase, causadas pelo aumento da pressão. Essa calibração pode ser feita utilizando-se metais que apresentam transições de fase bem definidas em determinadas pressões, como o itérbio e o bismuto. Esses metais podem ser chamados de sensores de pressão e são colocados numa montagem especial, junto ao contêiner de chumbo. Ao passar uma corrente constante por esses calibrantes mede-se a tensão, que varia proporcionalmente à resistência do sistema. A determinação de alguns pontos torna possível traçar uma curva de calibração que relaciona a força aplicada pela prensa com a pressão na amostra (em GPa), determinada pela transição de fase no calibrante [87]. É importante ressaltar que a curva de calibração é extremamente dependente da configuração utilizada no experimento, porém, totalmente reprodutível se as condições forem mantidas. Para cada lote de gaxetas confeccionadas é feita uma calibração. Na Figura 10, apresentamos curvas típicas de um procedimento de calibração de pressão feitas no presente trabalho. Na Figura 10 a, pode-se observar as transições de fase (quedas bruscas de tensão) para o Bi e o Yb, que ocorrem em pressões bem definidas e para uma determinada força aplicada. Na Figura 10 b temos a

curva de calibração propriamente dita, que relaciona a força aplicada com a pressão efetiva na amostra. Esta é a curva utilizada para os processamentos. Neste trabalho aplicamos pressões entre 3,5 e 7,7 GPa.

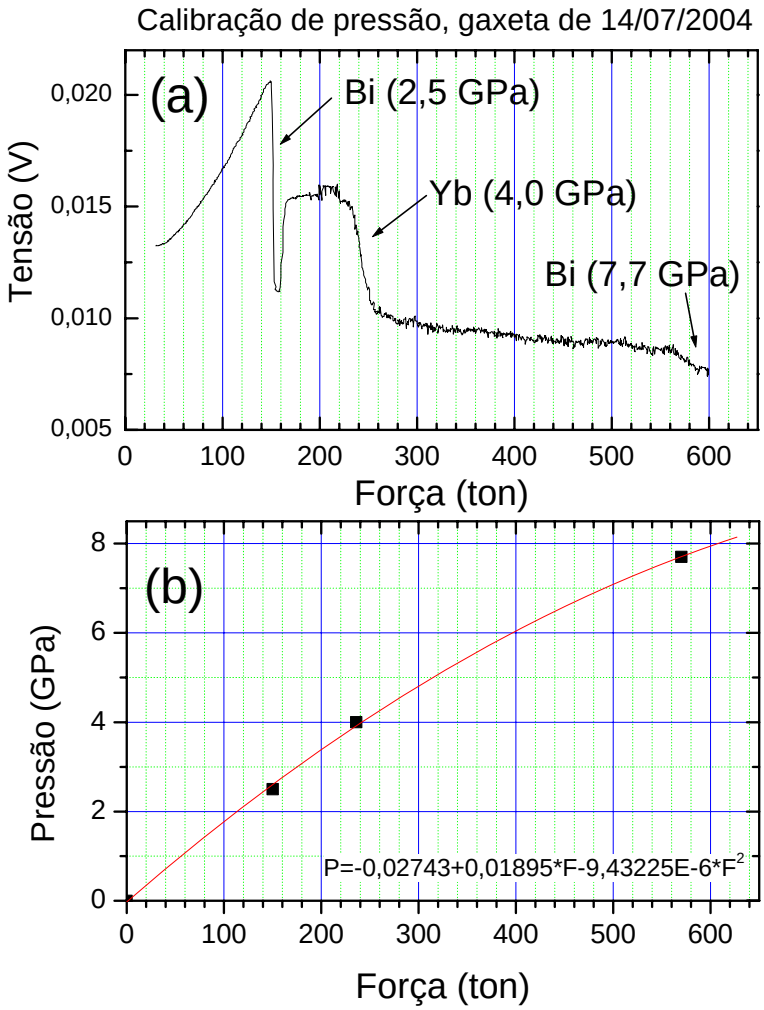

Figura 10. Curva de calibração de pressão com itérbio e bismuto com calibrantes. (a) transição de fase do itérbio e do bismuto; (b) curva de calibração.

4. TÉCNICAS DE CARACTERIZAÇÃO

Neste trabalho foram utilizadas, para a caracterização microestrutura das amostras, isotermas de adsorção e dessorção de N_2 e a análise por microscopia eletrônica de varredura. Já a estabilidade térmica foi determinada por termoanálise no infravermelho. Essas técnicas serão descritas resumidamente nessa seção.

4.1- Isotermas de adsorção e dessorção de N_2

A área superficial total de um sólido por unidade de massa pode ser obtida pelo método BET, que recebeu esse nome em homenagem aos cientistas Brunauer, Emmett e Teller [42]. Esse método consiste na determinação do volume de gás adsorvido em uma monocamada, a partir da sua isoterma de adsorção física. Tal isoterma é obtida à temperatura de ebulição do gás. Essa isoterma relaciona a quantidade do gás adsorvido em equilíbrio com sua pressão de vapor ou concentração na fase gasosa.

Pode-se explicar o método BET através da teoria das multicamadas, em que o equilíbrio que se estabelece entre a fase gasosa e a fase adsorvida conduz a uma distribuição de porções da superfície cobertas por um número de moléculas que pode variar de zero a infinito, sendo essa distribuição uma função da pressão de equilíbrio. Considera-se que a formação das multicamadas é equivalente à condensação de adsorvato líquido sobre a superfície. O gás mais utilizado para essa determinação é o N_2, entretanto, Ar e He também são usados. Para que a equação BET possa ser deduzida é necessário fazer as seguintes considerações:

a) em cada camada, a velocidade de adsorção é igual a velocidade de dessorção;
b) o calor de adsorção a partir da segunda camada é constante e igual ao calor de condensação;
c) quando $P= P_0$ o vapor condensa como um líquido ordinário e o número de camadas é infinito.

A partir dessas premissas chega-se então a equação BET:

$$P/ n^a (P_0 - P) = 1/ n^a{}_m C + (C-1/n^a C) (P/P_0)$$

Onde:

P = pressão de equilíbrio

P_0 = pressão de saturação

n^a = n° de mol do gás adsorvido

n^a_m = n° de mol do gás adsorvido numa monocamada

$C = \exp [(E_L - E_1)/RT]$

E_L= energia de adsorção a partir da 2^a camada

E_1= energia de adsorção da 1^a camada

R= constante dos gases

T= temperatura absoluta

O gráfico de $P/ n^a_m (P_0 - P)$ em função de P/P_0 resulta em uma reta. A partir dos valores dos coeficientes linear e angular da reta, a e b, respectivamente, a área superficial pode ser obtida segundo a equação abaixo:

$$S_{BET} = [1/(a+b)] Na_m$$

Em que $\mathbf{S_{BET}}$ é a área superficial; **N,** o número de Avogadro; e **a,** a área da molécula.

A adsorção de nitrogênio (N_2), é indicada também para a determinação da distribuição de tamanho e de volume de poros em materiais mesoporosos e os dados são obtidos também a partir de isotermas de adsorção-desorção do gás. Considerando que os poros são capilares, esses dados são tratados pelo método BJH [43], segundo a equação de Kelvin:

$$\text{Ln}\,(P/Po) = -(2\gamma M_v \cos\theta / RTr_m)$$

Onde:

P = pressão crítica de condensação

γ = tensão superficial do líquido;

M_v = volume molar do adsorvato;

R = constante universal dos gases;

T = temperatura absoluta;

θ = ângulo de contato entre o sólido e a fase condensada;
r_m = raio de curvatura médio do menisco do líquido.

É importante ressaltar que as medidas são feitas nas curvas descendentes (dessorção) por que a evaporação ocorre a uma pressão mais baixa que a condensação. O valor mínimo de diâmetro de poro em que se pode considerar condensação capilar pelo equilíbrio $N_{2\ líq}$ / $N_{2\ gás}$ é de cerca de 10 Å e o limite máximo de aplicação da equação de Kelvin é em torno de 250 Å.

Neste trabalho, aproximadamente 200 mg de cada híbrido foram desgaseificados numa linha de vácuo a 150°C. As isotermas de adsorção-dessorção de nitrogênio foram determinadas utilizando uma aparelhagem construída no LSS com um sistema de vácuo que emprega uma bomba turbo molecular e as medidas de pressão são realizadas utilizando um barômetro capilar de Hg.

4.2 Espectroscopia no infravermelho

A espectroscopia no infravermelho é uma técnica muito importante de identificação molecular. Essa técnica se baseia na propriedade que determinadas moléculas têm de absorver radiações eletromagnéticas na região do infravermelho, que compreende as radiações com comprimento de onda na faixa de 0,78 a 2,5 μm. A radiação infravermelha, quando absorvida pela amostra, converte-se em energia de vibração e energia de rotação molecular, dando origem a um espectro de vibração-rotação, que costuma aparecer como uma série de bandas [91]. As posições das bandas no espectro de infravermelho são apresentadas em número de onda ($1/\lambda$) e a intensidade das bandas é expressa em transmitância (T) ou absorbância (A). Onde $A = \log_{10} 1/T$

As vibrações moleculares podem ocorrer por deformações axiais e deformações angulares, onde a vibração de deformação axial corresponde ao movimento ao longo do eixo da ligação e a deformação angular a variações de ângulos das ligações. O espectro vibracional molecular poderá ser observado no infravermelho sempre que as vibrações resultarem em variação no momento dipolar da molécula. Apenas nessas condições o campo elétrico alternado da radiação pode interagir com a molécula e causar variações na amplitude de um de seus movimentos [91].

4.2.1 Análise térmica no infravermelho

A estabilidade térmica dos materiais híbridos foi estudada neste trabalho a partir da análise térmica no infravermelho. Para esse estudo utiliza-se uma aparelhagem construída no LSS que permite o aquecimento da amostra sob vácuo, chamada de cela de infravermelho (IV). Cerca de 100 mg de cada amostra são compactados na forma de pastilha a aproximadamente 55 MPa. As pastilhas são aquecidas, na cela de IV, numa taxa de 3°C/ min sob vácuo (10^{-2} Torr), por uma hora, em cada temperatura do tratamento térmico. Após cada aquecimento a cela é retirada da linha de vácuo e é deslocada até o equipamento Shimadzu, modelo 8300. Os espectros foram obtidos com resolução de 4 cm^{-1} de resolução e 100 varreduras. Essa análise é realizada à temperatura ambiente. Na Figura 11 é apresentada uma representação esquemática da cela de IV.

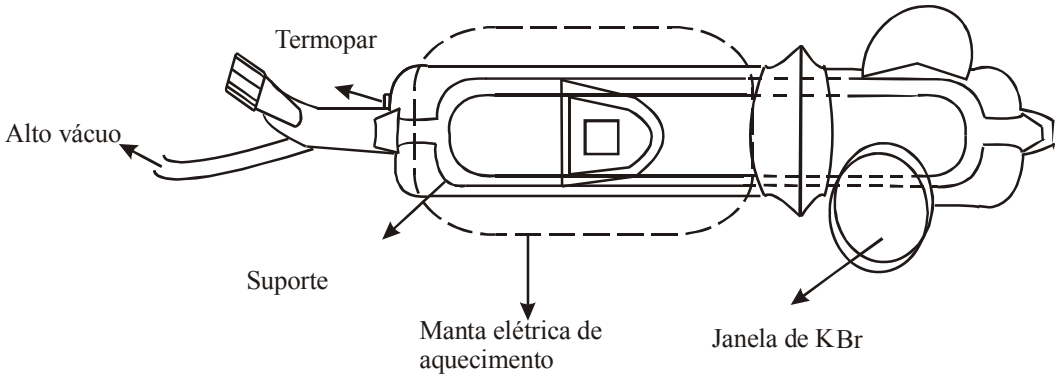

Figura 11- Representação esquemática da cela de IV, utilizada no tratamento térmico da amostra.

A cela, que é feita de quartzo, é constituída de duas partes. Em uma, há um forno elétrico envolvendo a parede externa, possibilitando que a amostra seja aquecida, sem que haja exposição à atmosfera externa. Na segunda parte, existem duas janelas externas de KBr que permitem que a amostra seja submetida ao feixe de infravermelho. As duas partes são interligadas por um trilho, no qual está encaixado um suporte móvel onde a amostra, na forma de pastilha, é fixada. Esse trilho permite que a amostra, após o aquecimento, seja exposta ao feixe de infravermelho através das janelas

de KBr, que estão na outra extremidade da cela, sem a necessidade de abri-la. As amostras estudadas nesse trabalho foram tratadas termicamente em temperaturas que variaram de 100 a 450°C, sob vácuo. Esse tratamento térmico tem demonstrado ser um método eficaz para estudar a estabilidade térmica dos híbridos organo-inorgânico [37, 44], a partir do monitoramento da variação de intensidade das bandas que aparecem no espectro desses materiais, após cada aquecimento. Na Figura 12, é possível verificar uma fotografia da cela acoplada à linha de vácuo utilizada nesse trabalho.

Figura 12- Fotografia da linha de vácuo e da cela utilizada no tratamento térmico das amostras.

4.3 Microscopia eletrônica de varredura (MEV)

A análise por microscopia eletrônica de varredura (MEV) é um método muito utilizado na caracterização microestrutural de materiais sólidos. Esse método consiste na varredura de pontos da amostra por um fino feixe de elétrons altamente energético. Da interação entre esse feixe de elétrons e a superfície da amostra são emitidas radiações como elétrons secundários, elétrons retroespalhados, raios X, fóton, etc. Essas radiações emitidas podem gerar informações sobre a amostra tais como: microestrutura, topografia e mapeamento de elementos químicos.[91] O equipamento utilizado para esse tipo de análise é o microscópio eletrônico de varredura, capaz de produzir imagens de alta

ampliação (até 300.000 x) e resolução . Neste trabalho, utilizou-se o aparelho Joel modelo ISM, com 20 kV e aumento máximo de 30000 vezes. Já a análise elementar foi realizada utilizando um detector Noran acoplado a esse mesmo microscópio. Inicialmente cada amostra analisada por MEV, nesse trabalho, foi dispersa num suporte de alumínio sobre uma fita condutora de dupla face e coberta com um filme de ouro com o auxilio de um metalizador Baltec SCD 050.

Na realização da análise por microscopia eletrônica de varredura, o feixe de elétrons que incidirá sobre a amostra é produzido a partir do aquecimento de um filamento de tungstênio, sob uma diferença de potencial. Esse aquecimento permite que os elétrons ultrapassem a barreira de energia necessária para escapar do material. É utilizado um filamento de tungstênio (eletrodo negativo) pois esse metal possibilita a obtenção de um feixe de elétrons com alta densidade, bem abaixo da sua temperatura de fusão, que é de 3410 °C.

A diferença de potencial a que está submetido o filamento atrai fortemente os elétrons gerados, resultando numa aceleração em direção ao eletrodo positivo. Entretanto, é preciso corrigir o percurso do feixe, o que é realizado através de lentes denominadas condensadoras. Essas lentes têm a função de colimar o feixe de elétrons o máximo possível e alinhá-lo até a lente denominada objetiva, que irá ajustar o foco antes que o feixe incida sobre a amostra.

Quando esse feixe de elétrons incide sobre a amostra ele pode interagir tanto com o núcleo quanto com a nuvem eletrônica dos átomos que constituem a amostra. No caso da interação do feixe com o núcleo, os elétrons são retroespalhados pela ação das forças coulombianas e perdem pouca energia, podendo então alcançar regiões mais profundas da amostra, porém com perda de resolução. Essa interação permite efetuar a análise elementar da amostra, já que o espalhamento depende do número atômico. Já os elétrons de menor energia, presentes nas camadas mais externas dos átomos, podem ser arrancados tanto pela interação com o feixe de elétrons incidente, quando estes estão penetrando na amostra, quanto pela interação com os elétrons retroespalhados, quando esses elétrons estão deixando a amostra. Esses elétrons arrancados do material são chamados de elétrons secundários, e possuem energia menor que 50 eV. É importante destacar que de todos os sinais que podem ser utilizados para análise das amostras por MEV, esse é o mais utilizado. Em função da baixa energia desses elétrons, a profundidade máxima da análise é de 50 nm. Esses elétrons mais externos são

arrancados em todos as direções, como consequência de choques inelásticos, permitindo dessa forma avaliar a microestrutura da amostra estudada. Ainda como consequência da interação do feixe de elétrons com a amostra emissões de raios X são geradas. A interação desse feixe com elétrons de níveis mais internos, provoca a emissão de raios X característicos da amostra. Isso ocorre porque os elétrons internos, ao serem emitidos, permitem que elétrons de níveis de energia superiores sofram transição e ocupem os níveis vazios, emitindo a diferença de energia na forma de raios X, característico do elemento químico. Esse fato permite a análise elementar da amostra.

5. REFERÊNCIAS BIBLIOGRÁFICAS

1- Lyubarskii, S. V.; Lyubarskii, N. K.; *J. Opt. Technol.* **2005**, 10, 792.

2- Callister, W.D. J.; *Mater. Science and Engeneering and Introduction,* John Wiley & Sons. Inc., New York, **1996.**

3- Kazmerski, L. L.; *J. Electron. Spetrosc. Relat. Phenom*. **2006**, 150, 105.

4- Balshaw, M. D., Philbert, M.; Suk, A. W.; *Toxicol. Sci.* **2005**, 88, 298.

5-Miracle, D. B.; *Composites Sci. Thecnol*. **2005**, 65, 2526.

6- Morales, A. J.; Aranda, P.; Gálvan, J. C.; *J. Mater. Proces. Tecnol.* **2003**, 143, 5.

7- Oshi, T.; *J. Non-Cryst. Solids,* **2003**, 332, 80.

8- Wang, E.; Chow, F. K.; Kwan, V.; Chin, T.; Wong, C.; Bocarsly, A.; *Anal. Chim. Acta,* **2001**, 495, 45.

9- Kino, R.; Ikoma, T.; Monkawa, A.; Yunoki, S.; Munekata, M.; Tanaka, J.; Asakuta, T.; *J. Appl. Polym. Sci.* **2006**, 99, 2822.

10- Staige, M. P.; Pietak, A. M.; Huandmai, J; Dias, G.; *Biomaterials*; **2006**, 27, 1728.

11- Correlo, V. M.; Boesal, L. F.; Bhattacharrya, M.; *Macromol. Mater. Eng*. **2005**, 290, 1157.

12- Wu, C. T.; Chang, J.; Ni, S. Y.; Wang, J. Y.; *J. Biomed. Mater. Res., Part A*, **2006**, 76, 73.

13- Perioli, L.; Ambrogi, V.; Bertini, B.; Ricci, M.; Nocchetti, M.; Latterini, L.; Rossi, C.; *Eur. J. Pharmaceutics Biopharmaceutics*, **2006**, 62, 185.

14- Riu, J.; Maroto, A.; Rius, F. X.; *Talanta*, **2006**, 69, 288.

15- Kattti, A.; Shimpi, N.; Roy, S.; Lu, H. B.; Fabrizio, E. F.; Dass, A.; Capadona, L. A.; Leventis, N.; *Chem. Mater*. **2006**, 18, 285.

16- Patwardhan, S. V.; Tari, V. P.; Hassan, M.; Agashe, N. R.; *Eur. Polym. J*. **2006**, 42, 167.

17- Hussain, H.; Rehman, H. U.; Ahmad, Z.; *J. Sol-Gel Sci. Technol.* **2005**, 36, 239.

18- Chevalier, Y.; Grillet, A. C.; Rahmi, M. I.; Liére, C.; *Mater. Sci. Eng. C*, **2002**, 21, 143.

19- Boury, B.; Corriu, R. J. P.; *Adv. Mater*. **2000**, 12, 989.

20- Arakari, L. N. H.; Augusto, V. L. S. F.; Aguiar, F. P.; Fonseca, M. G. da; Espínola, J. G. P.; *Thermochim. Acta*, **2006**, 440, 176.

21- Vansant, E. F.; Van der Voot, P.; Vrancken, K. C.; *Studies in Surface Science and Catalysis Characterization and Chemical Modification of the Silica Surface*, Elsevier, Amsterdam, **1995.**

22- Pesek, J. I.; Leigh, I. E.; Leigh I. E.; *Chemical Modified Surfaces*, Royal Society of Chemistry, London, **1994**.

23- Deshler, U.; Kleinnschmit; Panster, P.; *Agew. Chem. Int.* **1986**, 25, 236.

24- Etienne, M.; Walcarius, A.; *Talanta*, **2003**, 59, 1173.

25- Alfaya, A. A. S.; Kubota, L. T.; *Quim. Nova*, **2002**, 25, 835.

26- Pavan, F. A; Costa, T. M. H.; Benvenutti, E. V.; *Colloids Surf. A*, **2003**, 226, 95.

27- Pavan, F. A; Magalhães, W. F.; Luca, M. A. de; Moro, C. C.; Costa, T. M. H.; Benvenutti, E. V.; *J. Non-Cryst. Solids,* **2002**, 311,54.

28- Pavan,. F. A .; Leal, S.; Costa, T. M. H.; Benvenutti, E. V.; *J. Sol-Gel Sci. Technol*. **2002**, 23,129.

29- Pavan, F. A.; Gobbi, S. A.; Moro, C. C.; Costa, T. M. H.; *J. Sol–Gel Sci. Technol*. **2002**, 23, 219.

30- Pavan, F. A.; Hoffmann, H. S.; Gushikem, Y.; Costa, T. M H.; Benvenutti, E. V.; *Mater. Lett.* **2002**, 55, 378.

31- Pavan, F. A; Lucho, M. S. A.; Gonçalves; S.; Costa, T.M. H.; Benvenutti, E.V.; *J. Colloid Interface Sci.* **2003**, 263, 688.

32- Azolin, D. R.; Moro, C. C; Costa, T. M. H; Benvenutti, E.; *J. Non-Crystal. Solids,* **2004,** 337, 201.

33- Gay, D.; Gushikem, C. C.; Costa, T. M. H.; Benvenutti, E. V.; *J. Sol-Gel Sci. Technol*. **2005**, 34, 189.

34- Lev, O.; Tsionsky, M.; Rabnovich; L.; Glezer, V.; Sampath, S.; Pankratov, I.; *J. Anal. Chem.* **1995**, 67, 23A.

35- Lindberg, R.; Sjorblom, J.; Sundholm, G.; *Colloids Surf. A,* **1995**, 99, 79.

36- Husing, N.; Schubert, U.; *Angew. Chemi. Int. Ed.*.**1998**, 37, 22.

37- Foschiera, J. L.; Pizzaloto, T. M.; Benvenutti, E. V.; *J Braz. Chem. Soc.* **2001**, 2, 159.

38- Pavan, A. F.; Franken, L.; Moreira, A. C.; Costa, T. M. H.; Benvenutti, E. V.; Gushinken, Y.; *J. Colloid Interface Sci.* **2001**, 241, 413.

39- Quintanilla, D. P.; Hierro, I. del; Hermosilla, F. C.; Farjado, M.; Sierra, I.; *Anal. Bional. Chem*. **2006**, 384, 827.

40- Hassanien, M.; Sherbini, A. S. K.; *Talanta*, **2006**, 68, 1550.

41- He, L.; Toh, C. S.; *Anal. Chim*. **2006**, 1, 556.

42- Brunauer, P. H.; Emmett, E. T.; *J. Am. Chem. Soc*.**1938**, 60, 309.

43- Barret, E. P; Joyner, L. G.; Halenda, P. P.; *J. Am. Chem. Soc*.**1951**, 73, 373.

44- Pavan, F. A; Gobbi, S. A; Costa, T. M. H.; Benvenutti, E. V.; *J. Therm. Anal. Colorim*. **2002**, 68, 199.

45- Kickelbick, G. B. F.; Boury, B.; Corriu, R. J. P.; Le Strat, V.; *Chem. Mater*. **2000**, 12, 3249.

46- Novak, B. M.; *Adv. Mater*. **1993**, 6, 422.

47- Sanchez, C.; Soler-Illia; G. J. A. A.; Ribot, F.; Grosso, D.; *C. R. Chimie 6,* **2003**; 1131.

48- Lee, C. W.; Parka, H. S.; Kima, J. G.; Choilb, B. K.; Jooc, S. W.; Gonga, M. S.; *Sens. Actuators B*, **2005**, 109, 315.

49- Gushikem, Y.; Franco, D. W.; *Polyhedron*, **2000**, 19, 2277.

50- Kaszynska, M. S.; Jaszczot, K.; Koodziejczy, A.; *Talanta*, **2006**, 68, 1560.

51- Silva, C. R.; Jardim, I. C. S.; Collins, C. H.; Airold, C.; *Quim. Nova*, **2004**, 27, 270.

52- Arakari, N. H. L.; Airold, C; *Quim. Nova,* **1999**, 22, 246.

53- Khramov, A. N.; Balbyshev, V. N.; Voevodin, N. N; Donley, M. S.; *Prog. Org. Coat*. **2003**, 47, 207.

54- Hofacker, S.; Mechtel, M.; Mager, M.; Kraus, *Prog. Org. Coat*., **2002**, 159.

55- Bentivegna, F.; Canva, M.; *J. Sol-Gel Sci. Technol*. **1997**, 9, 33.

56- Costa ,T. M. H.; Stefani, V.; Balzaretti, N; Francisco, L. T. S. T; Gallas, M. R.; Jornada, J. A. H.; *J. Non-Cryst. Solids*, **1997**, 221, 157.

57- Esteves, A. C. C.; Timmons, A. B.; Trindade, T.; *Quim. Nova*; **2004**, 5, 798.

58- Gambaro, A.; Kutoba, L. T.; Gushikem, Y.; Airold, C.; Granjeiro, J. M.; Taga, E. M.; Alcantara, E. F. C.; *J. Colloid Interf. Sci*. **1997**, 185, 313.

59- Chevalier, Y.; Grillet, A. C.; Rahmi, M. I.; Lière, C.; Masure, M.; Hérmery, P.; Babenneau, F.; *Mat. Sci. Eng*. C. **2002**, 21, 143.

60- Cónsul, J. M. D.; Baibich, I. M.; Benvenutti, E. V.; T.; *Quim. Nova*; 2005, 28, 393.

61- Novak, B. M.; *Adv. Mater*. **1993**, 6, 422.

62- Airold, C; Farias R. F. De, *Quim. Nova,* **2004**, 27, 84.

63- Jerzy, Z.; *J. Sol-Gel Sci. Technol.* **1997**, 8, 17.

64- Shea, K. J.; Loy, D. A.; *Chem. Mater*. **2001**, 13, 3306.

65- Kickelbick, G. B. F.; Boury, B.; Corriu, R. J. P.; Le Strat, V.; *Chem. Mater***. 2000**, 12, 3249.

66- Peets, M. P. J.; t. N. M.; Van Bommel, M. J.; *J. Sol-Gel Sci Tecnol.* **1998**, 13, 71

67- Uhlmann, D. R.; *J. Sol-Gel Technol.* **1998**, 13, 153.

68- Brinker, C. J.;. Scherer, G. W.*; Sol–Gel Science*, Academic Press, San Diego, **1990**.

69- Iler, R.K.; *The Chemistry of Silica*, Wiley, New York, **1979**.

70- Keefer, K.D.; Brinker, C.J.; Clark, D.E.; Ulrich, D.R.; *Better Ceramics Through Chemistry*, North-Holland, New York, 1**984**.

71- Pohl, E.R.; Osterholts, F.D.; Ishida, H.; G. Kumar; *Molecular Characterization of composite Interface*, Plenium, New York, **1985**.

72- Brinker, C. J.; Scherer, G. W.; J. *Non-Cryst. Solids,* **1998**, 100, 31.

73- Corriu, R.J.P.; Leclercq, D.; Vioux, A; Pauthe, M.; and *J. Phalippou in Ultrastructura Processing of Advanced Ceramics*. **1988**, 113.

74- Corriu, R.J.P.; Leclercq, D.; Angew.*Chem. Int Engl.* **1996**, 35, 1420.

75- Sakka, S.; Kozuka, H.; *J. Non-Cryst. Solids*, **1988**, 100, 142

76- Scherer, G. W.; Haereid, S.; Nielsen, E.; Einarsrud, M.; *J. Non-Cryst. Solids,* **1996**, 202, 42.

77- Takahashi, R.; Nakanishi, K.; Soga, N.; *J. Non-Cryst. Solids,* **1995**, 189,66.

78- Scottner, G.; *Chem. Mater. Sci*. **2001**, 13, 3422.

79- Cerveau, G.; Corriu, R. J.; Framely, E.; *Chem. Mater*. **2001**, 13, 3373.

80- German, R. M.; *Fundamentals of Sintering*, ASM International, **1991.**.

81- Costa, T. M. H; Compactação em altas pressões de pós nanométricos de gel de sílica e alumina γ, tese de doutorado, IF, UFRGS, 1997

82- Costa, T. M. H.; Hoffmann; H. S.; Benvenutti, E. V.; Stefani, V.; Gallas, M. R.; *Optical Mater*. **2005**, 27, 43.

83- Costa, T. M. H.; Gallas, M. R; Benvenutti, E. V.; Jornada, J. A. H.; *J. Phys. Chem. B,* **1999,** 103, 4278.

84- Costa, T. M. H.; Gallas, M. R.; Benvenutti, E. V.; Jornada, J. A. H.; *J. Non-Cryst. Solids*, **1997**, 220, 195.

85- Rosa, A. R., Efeito das altas pressõesna compactação de pós nanométricos de alumina, Dissertação de Mestrado, UFRGS-PPGEMM, **1995**.

86- Gallas, M. R., Rosa, A. R., Costa, T. M. H., Jornada, J. A. H.; *J. Mater. Res*. **1997**, 12, 764.

87- Sherman, W. F; Stadmuller, A. A.; *Experimental Techniques and High-pressure Research,* John Wiley & Sons Ltd., New York, **1987**.

88- Gutmanas, E. Y.; Rabinkin, A.; Roittberg, M.; *on Cold Sintering Under High Pressure*, Pergamon Press, **1980**.

89- Costa, T. M. H.; Stefani, V.; Gallas, M. R; Balzaretti, N. M.; *J. Non-Cryst. Solids*, **2004**, v. 333, 221.

90- Khvostantsev, L. G.; *High Temp-High Press*, **1984**, 16, 165.

91- Stuart, B.; George, B.; Mlcntyre, *Modern Infrared Spectroscopy*, John Willey&Sons, Ltda, New York, **1998**.

92- Goldstein, J. I.; Newbury, D. E.; Echilin, P.; Joy, D. C.; Romig, A. D.; Lyman, C. E.; Fiori, C; Lifshin, E.; *Scanning Electron Microscopy and X-Ray Microanalysis; Plenum Press*, New York, 1994.

Available online at www.sciencedirect.com
SCIENCE DIRECT®
Talanta 59 (2003) 1039–1044
Talanta
www.elsevier.com/locate/talanta

Silica–titania sol–gel hybrid materials: synthesis, characterization and potential application in solid phase extraction

Sandra V.M. de Moraes [a], Joana B. Passos [a], Patricia Schossler [b], Elina B. Caramão [b], Celso C. Moro [a], Tania M.H. Costa [a], Edilson V. Benvenutti [a,*]

[a] *Laboratório de Sólidos e Superfícies, Instituto de Química, UFRGS, CP 15003, 91501-970 Porto Alegre, RS, Brazil*
[b] *Laboratório de Química Ambiental, Instituto de Química, UFRGS, CP 15003, 91501-970 Porto Alegre, RS, Brazil*

Received 16 July 2002; received in revised form 11 December 2002; accepted 16 December 2002

Abstract

The biphenilaminepropylsilica and biphenilaminepropylsilicatitania were synthesized by sol–gel method, in two steps: (a) biphenylamine reacts with chloropropyltrimethoxysilane and (b) the product of reaction was polycondensed with tetraethylorthosilicate (TEOS) or TEOS and titanium isopropoxide. The sol–gel materials were characterized using infrared spectroscopy and N_2 adsorption–desorption isotherms and they were employed as sorbents for carcinogenic N-containing compound retention, in aqueous solution, using the SPE technique. The N-containing compounds adsorption was influenced by the titania presence and the sorption process seems to happen in the pores with higher organic density.

Keywords: Xerogel; Hybrid materials; Nanometric pores; Solid phase extraction; Quinolines

1. Introduction

Over the decade, organofunctionalized silicas have been very used as sorbent materials for solid phase extraction (SPE) and also for chromatographic techniques [1–6]. Organofunctionalized silica particles present mechanical and morphological properties of the inorganic support and their chemical behavior, in general, are related to the organic groups immobilized on the surface. Therefore, the sorption properties of these materials are determined by the association of the inorganic and organic phases properties. Grafting method has been very used as a synthesis method to obtain organofunctionalized silicas. This method involves the immobilization of an organic functional group, frequently using an organosilane as an intermediate reagent [7–9].

Another possibility to obtain organofunctionalized silicas is the sol–gel method, using alkoxysilanes $R–Si(OR)_3$ and tetraethylorthosilicate

* Corresponding author. Tel.: +55-51-3316-7209; fax: +55-51-3316-7304.
E-mail address: edilson@iq.ufrgs.br (E.V. Benvenutti).

0039-9140/03/$ - see front matter © 2003 Elsevier Science B.V. All rights reserved.
doi:10.1016/S0039-9140(03)00005-5

(TEOS) or tetramethylorthosilicate (TMOS) as precursor [10–13]. The polycondensation of alkoxysilanes is performed at room temperature and it can be described in three reactions: (i) hydrolysis; (ii) silanol condensation and; (iii) silanol–alcohol condensation [10–13]. The sol–gel synthesis presents some advantages if compared with the grafting method, it allows to obtain different physicochemical characteristics on the resulting materials like surface area, particle shape and size, porosity and organic functionalization grade [14–16], associated to the possibility to obtain binary oxides as inorganic phases. It was reported that other inorganic matrices, like titania, can present different selectivity for a large variety of sorbates, when compared with silica matrix [17], therefore, the use of binary oxides systems instead of pure silica, as inorganic phase, could serve to improve the surface selectivity in the adsorption process. Besides a small molar percentage of titania can be used to reduces the thermal expansion coefficient of silica [18], that could improve their stationary phase properties. Nevertheless to our knowledge, hybrid materials systems, obtained by sol–gel method, were very little used as sorbent in SPE process. There are some reports for metal extraction [19], solid phase microextraction [20], or immunoaffinity columns [21].

In recent papers it was presented a easy procedure to obtain appropriated organic alkoxides as sol–gel precursor reagent to obtain the hybrid silica based materials anilinepropylsilica and *p*-anisidinepropylsilica. The resulting nanometric powders were thermally very stable [12,22], and their organic phases presented a good resistance to leaching by solvents [23]. In the present paper, a new organic precursor was synthesized, $(C_6H_5)_2N(CH_2)_3Si(OCH_3)_3$, and the hybrid material was obtained with two inorganic components, silica and titania:silica (1:9). The insertion of titania in the inorganic phase was made using titanium isopropoxide that is a very common precursor reagent for titania synthesis in binary oxide systems [24,25]. The influence of titanium oxide on the silica matrix porosity and on the adsorption properties were studied. The retention ability of the hybrid material for some carcinogenic N-containing compounds, from aqueous samples, was investigated using SPE and GC/MSD analysis.

2. Experimental

2.1. Reagents and solvents used

All reagents and solvents were analytical grade purchased from Merck. The extractor solvents, hexane and isopropylamine, were twice distilled before use. A standard solution of isoquinoline, quinoline, fluorene (IS), phenanthridine, acridine and 7,8-benzoquinoline at 100 mg l^{-1} in acetone pesticide residue grade was obtained from individual stock solutions, also in acetone pesticide residue grade, at 1000 mg l^{-1}. A spike solution, containing 1 mg l^{-1} of each compound, was prepared, from the standard solution, using twice distilled water as solvent. Fluorene was used as internal standard reference (IS). The N-containing compounds and the IS were purchased from Sigma-Aldrich.

2.2. Syntheses of hybrid materials

Biphenylamine $(C_6H_5)_2NH$ was firstly activated using sodium hydride in 10 ml of a mixture of aprotic solvent (toluene:thf) (1:1) for 30 min, and the $(CH_3O)_3Si(CH_2)_3Cl$ (CPTMS) was added. The quantity used was stoichiometric for biphenylamine, CPTMS, and NaH, the value was 8.0 mmol. The mixture was stirred under argon at solvent-reflux temperature for a period of 10 h. The solution was than centrifuged, to eliminate the byproduct sodium chloride. The product of reaction, biphenylaminepropyltrimethoxysilane (bPAPS) was then used as organic sol–gel precursor reagent. The bPAPS was added to the inorganic precursor solution mixture, containing 5 ml of TEOS and 0.75 ml of titanium isopropoxide, 5 ml of ethyl alcohol, 1.6 ml of water and 0.1 ml of HF (40%), stirred for 20 min and stored for a week, just covered without sealing, for gelation. The resulting materials were designated as bPhe/SiO_2 and bPhe/SiO_2/TiO_2 for the samples titania free and containing 10% of titania, respectively. The materials were then comminuted and

washed extensively with various solvents and finally dried for 1 h, in an oven, at 100 °C.

2.3. Elemental analysis

The organic phase content were analyzed using a CHN Perkin–Elmer M CHNS/O Analyzer, model 2400. The analysis was performed in triplicate, after heating materials at 100 °C, under vacuum, for 1 h.

2.4. Infrared measurements

Self-supporting disks of the materials, with an area of 5 cm^2, weighing approximately 100 mg, were prepared. The disks were heated for 1 h at 200 °C, under vacuum (10^{-2} Torr), using an IR cell [9]. The self-supporting disks were analyzed in the infrared region using a Shimadzu FTIR, model 8300. The spectra were obtained with a resolution of 4 cm^{-1}, with 100 scans.

2.5. N_2-isotherms

The nitrogen adsorption–desorption isotherms of previous degassed solids, at 150 °C, were determined at liquid nitrogen boiling point in a homemade volumetric apparatus, with a vacuum line system employing a turbo molecular Edward vacuum pump. The pressure measurements are made using capillary Hg barometer and also an active Pirani gauge. The specific surface areas of hybrid materials were determined from the Brunauer, Emmett and Teller (BET) [26] multipoint method and the pore size distribution was obtained using Barret, Joyner, and Halenda (BJH) method [27].

2.6. Pre-concentration

The hybrid materials were employed as sorbent using the SPE method. The sorbent (500 mg) was packed in a glass column (15 × 1 cm) and was firstly treated by washing with 5 ml of hexane, 5 ml of dichloromethane, 5 ml of methanol and 20 ml of twice distilled water. The spike solution (100 ml at 1 mg l^{-1}) was passed through the adsorption bed at a rate of 5 ml min^{-1}. The N-containing compounds adsorbed in the solid phase surface were released using three aliquots (10 ml each) of hexane:isopropylamine mixture (1:10). The IS substance reference was than added in the same concentration (1 mg l^{-1}). Before the GC/MSD analysis the solution volume was reduced to 1 ml using nitrogen stream (200 ml min^{-1}) at room temperature.

2.7. GC/MSD data acquisition

The GC/MSD data analysis was performed in a Shimadzu equipment model QP5050A using a HP-5 capillary column—60 m × 0.25 mm × 0.25 μm. The operation conditions were: column temperature 100 °C, hold 5 min, heat to 190 °C at 4 °C min^{-1}, hold 1 min, heat to 210 °C at 1 °C min^{-1} and hold 5 min; injector temperature 280 °C, column flow 1 ml min^{-1}; interface temperature 280 °C. The MS analysis was made in the SIM mode using electron impact ionization with electron energy of 70 eV. The monitored ions, that correspond to the N-containing compounds in the standard mixture, were 129 for isoquinoline and quinoline; 166 for fluorene (IS); and 179 for phenanthridine, acridine and 7,8-benzoquinoline. The volume injected in the split mode (1:20) was 1 μl.

3. Results and discussion

In the first synthesis step, the reaction between the biphenylamine and CPTMS was made in aprotic solvent mixture toluene–thf, using NaH as base activator, as illustrated in Eqs. (1) and (2).

$$NH\text{–}(C_6H_5)_2 + NaH \rightarrow N\text{–}(C_6H_5)_2Na^+ + H_2 \quad (1)$$

$$(CH_3O)_3Si(CH_2)_3Cl + N\text{–}(C_6H_5)_2Na^+ \rightarrow (CH_3O)_3Si(CH_2)_3N\text{–}(C_6H_5)_2 + NaCl \quad (2)$$

The reaction product (Eq. (2)) was then used as organic precursor. The gelation was carried out by the addition of TEOS or TEOS and titanium isopropoxide in the Ti/Si molar ratio of 0.11, and the resulting hybrid materials were assigned as bPhe/SiO_2 and bPhe/SiO_2/TiO_2, respectively.

Table 1
Elemental CHN analysis and morphological properties

Sol–gel material	Organic content (mmol g^{-1})[a]	Surface area (m^2 g^{-1})	Pore volume (cm^3)	Pore diameter predominant (nm)
bPhe/SiO_2	1.42±0.05	112±10	0.26±0.02	Smaller than 8 and ca. 37 nm
bPhe/SiO_2/TiO_2	1.46±0.05	38±4	0.04±0.01	Smaller than 7

[a] mmol of biphenyl groups per gram of material.

The use of sodium hydride as base activator results in drastic reduction in the reaction time [28]. Additionally, the insoluble byproduct NaCl can be easily separated from the organic medium by centrifugation. In the absence of NaH there is a formation of HCl, that reacts with the biphenylamine, resulting in the organic salt, which is more difficult to separate from the organic medium [9].

The organic phase content, obtained by CHN analysis, for bPhe/SiO_2 and bPhe/SiO_2/TiO_2, are presented in the Table 1. The achieved values for organic loading were very extensive if compared with that obtained by the grafting process, for other aromatic amines, where the maximum quantity grafted was 0.42 mmol g^{-1} [9]. The organic incorporation can be also observed from the infrared analysis presented in the Fig. 1. It can be observed in the spectra, two very strong bands at 1591 and 1495 cm^{-1} corresponding to the aromatic ring stretching modes of biphenyl groups. The presence of these infrared bands after heating up to 200 °C, under vacuum, is an evidence that the organic phase are strongly bonded to the surface, in the covalent form. The typical silica overton bands, with a maximum in 1865 cm^{-1} [29], corresponding to the inorganic phase, can be also observed in the spectra. In the Fig. 1, the spectrum B of the sample that contain 10% of titania, shows a broadening in the aromatic ring infrared absorption if compared with the spectrum A, obtained for titania free sample. This broadening could be interpreted considering the proximity of biphenyl groups, since the surface area of the bPhe/SiO_2/TiO_2 is approximately three times lower than bPhe/SiO_2 (see Table 1), while the organic content is the same for both samples (Table 1). Therefore, the organic surface density, in the bPhe/SiO_2/TiO_2 sample, should be higher, resulting in a great interaction between the biphenyl groups. This organic surface density can be estimated assuming that the organic groups uniformly cover the surface. Thus the surface density of the biphenyl groups, d (groups nm^2), is defined as [12]:

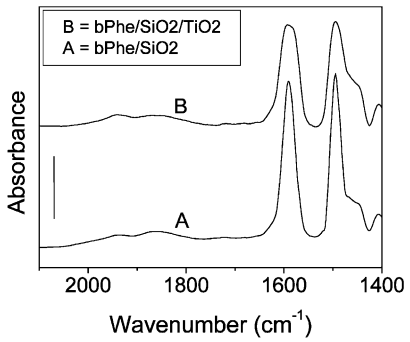

Fig. 1. Absorbance infrared spectra of materials, obtained at room temperature, after been heated up to 200 °C for 1 h, in vacuum. The bar value is 1.

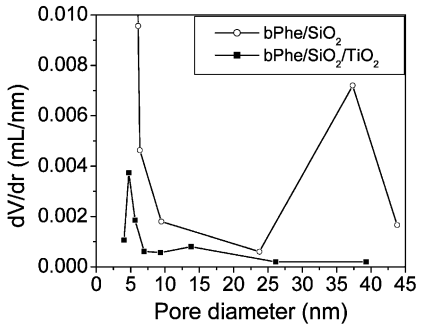

Fig. 2. BJH mesopore size distribution for sol–gel hybrid materials.

Table 2
SPE results

Analyte	Standard	bPhe/SiO_2 ($n=5$)[a]		bPhe/SiO_2/TiO_2 ($n=5$)[a]	
	RR[b]	RR[b]	Rec. %[c]	RR[b]	Rec. %[c]
Isoquinoline	1.50	0.89	59.2±5.9	0.89	59.6±5.9
Quinoline	1.33	0.74	56.0±5.6	0.50	37.3±3.7
Fluorene (IS)	1.00	1.00	100.0	1.00	100.0
Phenanthridine	1.38	1.00	63.1±6.3	0.87	72.7±7.3
Acridine	1.07	0.77	68.4±6.8	0.73	72.2±7.2
7,8-benzoquinoline	0.82	0.41	50.5±5.1	0.60	73.5±7.4

[a] The overall methodology shows a medium error of 10% for five replicates.
[b] RR, relative response factor.
[c] Rec.%, recovery percentual.

$$d = (\mathrm{Nf}.N)/S_{\mathrm{BET}}$$

where Nf is the organic coverage (mol g^{-1}), N is the Avogadro number (groups mol^{-1}) and S_{BET} is the surface area (nm^2 g^{-1}). The organic densities achieved were 7.6 and 23.1 biphenyl groups nm^{-2} of the surface, for bPhe/SiO_2 and bPhe/SiO_2/TiO_2 samples, respectively.

From the N_2 adsorption–desorption isotherms it was obtained the pore size distribution using the BJH method [27]. This method allows to determine the mesopores distribution (diameter between 2 and 50 nm). The results are presented in the Fig. 2. For bPhe/SiO_2 material, two distinct pore diameter regions appears (i) small pores with diameter lower than 8 nm and (ii) another region with larger pores with a maximum diameter in approximately 37 nm, while for bPhe/SiO_2/TiO_2, there is, predominantly, pores with diameter lower than 7 nm. Additionally the pore volume were also higher for bPhe/SiO_2 than bPhe/SiO_2/TiO_2 (see Table 1) indicating a higher porosity for bPhe/SiO_2 than bPhe/SiO_2/TiO_2. These results can explain the lower BET surface area observed for bPhe/SiO_2/TiO_2 in relation to bPhe/SiO_2 (Table 1). Therefore, the insertion of titania in the inorganic phase produced marked morphological changes.

In the pre-concentration study, the hybrid material was employed as sorbent using SPE technique. It was used aqueous solution of some N-containing compounds that, in recent years, are been considered a new group of potential mutagen and carcinogenic compounds, which can be formed in proteinaceous foods prepared at high temperature [30–33]. The technique was firstly developed according the description in the Section 2, using three aliquots. However, considering that no peaks were obtained in the chromatographic analysis of the third aliquot, only two aliquots of 10 ml of hexane:isopropylamine mixture (1:10) were enough to extract the analytes. Both aliquots were merged and the total volume (20 ml) was reduced to 1 ml and analyzed according the Section 2. The results obtained are presented in the Table 2. Except for quinoline that shows better results for bPhe/SiO_2, the N-containing compounds recovering percents were equal or more elevated for bPhe/SiO_2/TiO_2 than for bPhe/SiO_2 material (Table 2). Considering that both materials present a same organic content, this difference could be interpreted taking into account two components: (i) the adsorption is influenced by the inorganic phase differences or (ii) the adsorption process is influenced by the organic groups density in the pore surface. In the first case the bPhe/SiO_2/TiO_2 material, that contain 10% of titania, presents higher N-containing compounds recovering due to the higher dipole moment of TiO–H groups related to the SiO–H groups in the surface [17], since the N-containing compounds present appreciable polarity. In the second case the adsorption occurs preferentially in pores with

higher organic density that are present in the bPhe/SiO_2/TiO_2 material.

4. Conclusions

Biphenylamine propylsilica and biphenylamine propylsilicatitania were obtained by a satisfactory way. The organic phase was incorporated and it was thermally stable at least 200 °C, in vacuum. The titania presence in the inorganic phase produces a reduction in the surface area, in the pore volume and also differences in the pore size distribution. The hybrid sol–gel materials when used in SPE process, as sorbent for N-containing compounds, in a general way, present higher recovering percents for the material containing titania. The sorption process is influenced by the titania presence and should occur preferentially in pores with higher organic density.

Acknowledgements

J.B.P. is indebted to Fapergs for her grant. The authors also thank FINEP/CTPETRO for financial support.

References

[1] Y. Yamini, M. Chaloosi, H. Ebrahimzadeh, Talanta 56 (2002) 797.
[2] Y. Bereznitski, M. Jaroniec, J. Chromatogr. A 828 (1998) 51.
[3] M. Shamsipur, A. Avanes, M.K. Rofouei, H. Sharghi, G. Aghapour, Talanta 54 (2001) 863.
[4] D. Barceló, M.F. Alpendurada, Chromatographia 42 (1996) 704.
[5] B. Varga, G. Kiss, I. Ganszky, A. Gelencser, Z. Krivacsy, Talanta 55 (2001) 561.
[6] U. Deschler, P. Kleinschmit, P. Panster, Angew. Chem. Int. Ed. Engl. 25 (1986) 236.
[7] C.H. Lochmüller, A.S. Colborn, M.L. Hunnicutt, J.M. Harris, Anal. Chem. 55 (1983) 1344.
[8] N.H. Arakaki, C. Airoldi, Quim. Nova 22 (1999) 246.
[9] J.L. Foschiera, T.M. Pizzolato, E.V. Benvenutti, J. Braz, Chem. Soc. 12 (2001) 159.
[10] C.J. Brinker, G.W. Scherer, Sol–Gel Science, Academic Press, London, 1990.
[11] L.L. Hench, J.K. West, Chem. Rev. 90 (1990) 33.
[12] F.A. Pavan, L. Franken, C.A. Moreira, T.M.H. Costa, E.V. Benvenutti, Y. Gushikem, J. Colloid Interf. Sci. 241 (2001) 413.
[13] O. Lev, M. Tsionsky, L. Rabinovich, V. Glazer, S. Sampath, I. Pankratov, J. Gun, Anal. Chem. 67 (1995) 22A.
[14] M.M. Collinson, Crit. Rev. Anal. Chem. 29 (1999) 289.
[15] F.A. Pavan, H.S. Hoffmann, Y. Gushikem, T.M.H. Costa, E.V. Benvenutti, Mater. Lett. 55 (2002) 378.
[16] F.A. Pavan, W.F. de Magalhães, M.A. de Luca, C.C. Moro, T.M.H. Costa, E.V. Benvenutti, J. Non-Cryst. Solids 311 (2002) 54.
[17] J. Winkler, S. Marmé, J. Chromatogr. A 888 (2000) 51.
[18] D. Gerlich, M. Wolf, I. Yaacov, B. Nissenson, J. Non-Cryst. Solids 21 (1976) 243.
[19] J. Seneviratne, J.A. Cox, Talanta 52 (2000) 801.
[20] S.L. Chong, D. Wang, J.D. Hayes, B.W. Wilhite, A. Malik, Anal. Chem. 69 (1997) 3889.
[21] M. Cichna, P. Markl, D. Knopp, R. Niessner, Chem. Mater. 9 (1997) 2640.
[22] F.A. Pavan, S.A. Gobbi, T.M.H. Costa, E.V. Benvenutti, J. Therm. Anal. Calorim. 68 (2002) 199.
[23] L. Franken, L.S. dos Santos, E.B. Caramão, T.M.H. Costa, E.V. Benvenutti, Quim. Nova 25 (2002) 563.
[24] I.M.M. Salvato, F.M.A. Margaça, J. Teixeira, J. Non-Cryst. Solids 163 (1993) 115.
[25] H.S. Hoffamnn, P.B. Staudt, T.M.H. Costa, C.C. Moro, E.V. Benvenutti, Surf. Interf. Anal. 33 (2002) 631.
[26] S. Brunauer, P.H. Emmett, E. Teller, J. Am. Chem. Soc. 60 (1938) 309.
[27] E.P. Barret, L.G. Joyner, P.P. Halenda, J. Am. Chem. Soc. 73 (1951) 373.
[28] F.A. Pavan, S. Leal, T.M.H. Costa, E.V. Benvenutti, Y. Gushikem, J. Sol–Gel Sci. Technol. 23 (2002) 129.
[29] T.M.H. Costa, M.R. Gallas, E.V. Benvenutti, J.A.H. da Jornada, J. Non-Cryst. Solids 220 (1997) 195.
[30] J.J. Sauvain, T.V. Due, C.K. Huynh, Fresenius J. Anal. Chem. 371 (2001) 966.
[31] F.M. Lanças, M.A. Barbirato, Fuel Sci. Technol. Int. 12 (1994) 507.
[32] B. Janoszka, U. Blaszczyk, L. Warzecha, M. Strózyk, A.D. Bodzek, D. Bodzek, J. Chromatogr. A 938 (2001) 155.
[33] R.D. Klassen, D. Lewis, B.P.Y. Lau, N.P. Sen, Food Res. Int. 35 (2002) 837.

High Pressure Research
Vol. 26, No. 1, March 2006, 11–21

Taylor & Francis
Taylor & Francis Group

Effects of the high pressure on the morphology of silica-based hybrid xerogels

SANDRA V. M. DE MORAES†, CELSO C. MORO†, TANIA M. H. COSTA†, MARCIA R. GALLAS‡ and EDILSON V. BENVENUTTI*†

†LSS, Instituto de Química, UFRGS, CP 15003, 91501-970 Porto Alegre, RS, Brazil
‡LAPMA, Instituto de Física, UFRGS, CP 15051, 91501-970 Porto Alegre, RS, Brazil

(Received 4 November 2005; revised 18 November 2005; in final form 18 November 2005)

The hybrid biphenylamine propylsilica (bPhe/SiO_2) and biphenylamine propylsilicatitania xerogels were obtained by the sol-gel synthesis. The bPhe/SiO_2 material showed higher porosity and higher thermal stability of the organic component. These materials were submitted to high-pressure processing (3.5 and 6.0 GPa) and the changes in their morphological properties were investigated by using scanning electron microscopy, N_2 adsorption–desorption isotherms and infrared spectroscopy. The high-pressure processing produces changes in the morphological structure of hybrid materials caused by the compaction of the aggregated particles and the blocking of the pores with the entrapment of organics through the cold sintering process. However, when the organics are covalently bonded to the surface, this mechanism can be partially inhibited.

Keywords: Amorphous materials; Sol-gel chemistry; Microstructure

1. Introduction

The sol-gel method is an attractive route to prepare several hybrid materials with interesting properties, which allows their potential application as sorbents, sensors, catalysts, optical and electrochemical devices [1–5]. This method presents many advantages when compared with the classical procedure, as grafting reactions over inorganic powders, because the materials properties such as porosity, organic content and surface area can be controlled starting from the choice of the experimental conditions [6–9]. Furthermore, the synthesis can be performed at room temperature. Glasses of different oxides, binary and ternary systems, have also been obtained by the sol-gel method [10–12].

In previous papers, an efficient procedure was presented to obtain appropriate organic alkoxides as precursor reagent for the sol-gel synthesis of hybrid anilinepropylsilica and *p*-anisidinepropylsilica [8, 13]. The resulting nanometric powders were thermally stable up to 300 °C. The study of the synthesis of hybrid materials, similar to that cited above and

*Corresponding author. Tel.: +55 51 3316 7209; Fax: +55 51 3316 7304; Email: benvenutti@iq.ufrgs.br

High Pressure Research
ISSN 0895-7959 print/ISSN 1477-2299 online © 2006 Taylor & Francis
http://www.tandf.co.uk/journals
DOI: 10.1080/08957950500508421

containing binary Si/Ti oxide phases, can bring about materials with interesting properties. It was reported that the use of the binary oxides systems silica/titania, instead of pure silica, could serve to increase the surface selectivity in the adsorption process [14] and can be used to reduce the thermal expansion coefficient of silica [15].

The high-pressure technique at near 5.0 GPa (49,000 a.t.m.) has been used to compact nanometric inorganic powders to improve mechanical and optical properties of processed materials [16, 17]. A cold sintering mechanism was proposed for this compaction, at high pressure and room temperature. In this process, a reduction occurs in the surface area because of the formation of a microstructure with closed pores [17]. Afterwards, our group has proposed to apply this model on encapsulation of organic species in inorganic matrices, obtaining a new process to produce doped compact starting from hybrid sol-gel materials [18, 19]. This procedure is performed at room temperature without damage to the chemical and physical properties of organic species; however, high organic concentration can partially hinder the cold sintering process [19].

Aiming to explore the preparation of new hybrid materials and to make further investigation on mechanism of cold sintering for hybrid systems, in the present work, we have used the sol-gel method and the high-pressure technique, up to 6.0 GPa (59,200 a.t.m.), in the preparation and processing of new hybrid xerogels. The hybrids were obtained by using biphenylamine as organic precursor and two inorganic components, silica and titania:silica (1:9). The effect of high pressure in the morphology of the xerogels, mainly in their porosity, was investigated. The hybrid materials, before and after the high-pressure process, were characterized by using infrared spectroscopy, elemental analysis, scanning electron microscopy (SEM) and nitrogen adsorption–desorption isotherms.

2. Experimental

2.1 *Syntheses of the hybrid materials*

Biphenylamine $(C_6H_5)_2NH$ was first activated using sodium hydride in 10 ml of a mixture of aprotic solvent (toluene:thf) (1:1) for 30 min and then 3-chloropropyltrimethoxisilane (CPTMS) was added. The quantities used were stoichiometric (8 mmol) for biphenylamine, CPTMS and NaH, according to equations (1) and (2). The mixture was stirred under argon at solvent-reflux temperature for a period of 10 h. The resulting solution was centrifuged to eliminate the byproduct sodium chloride. The product of reaction, biphenylaminepropyl-trimethoxysilane (bPAPS), was then used as organic sol-gel precursor reagent. The bPAPS was added to the inorganic precursor solution mixture, containing 5 ml of tetraethylorthosilicate (TEOS), 5 ml of ethanol, 1.6 ml of water and 0.1 ml of HF (40%), stirred for 20 min and stored for 1 week, just covered without sealing, for gelation. The resulting material was designated as bPhe/SiO_2. For the hybrid containing 10% of titania, it was made by a previous hydrolysis of the TEOS for 20 min and after a titanium isopropoxide (TIPOT) solution (0.55 ml) was added. The mixture was stirred for 20 min and the obtained xerogel material was designated as biphenylamine propylsilica (bPhe/SiO_2/TiO_2). The hybrid materials were then comminuted (lower than 250 mesh), washed extensively with various solvents and finally dried for 1 h, in an oven, at 100 °C.

2.2 *Elemental analysis*

The organic phase content was analysed using a CHN Perkin Elmer M CHNS/O Analyzer, model 2400. The analysis was performed in triplicate, after heating the materials at 100 °C, under vacuum, for 1 h.

2.3 *Infrared measurements*

Self-supporting discs, prepared by the compaction of pure powdered samples at near 55 MPa, with an area of 5 cm^2, weighing ~100 mg, were prepared. The disc thickness should be sufficiently small to allow the use of the transmission technique. The discs were heated with a heat rate of 3 °C min^{-1}, at 100, 200, 300, 400 and 450 °C, under vacuum (1 Pa), remaining 1 h in each temperature, using an IR cell [20]. The self-supporting discs were analysed at room temperature in the infrared region using a Shimadzu FTIR, model 8300. The spectra were obtained with a resolution of 4 cm^{-1}, with a minimum of 100 scans.

2.4 *Scanning electron microscopy*

The materials were analysed by SEM in a Jeol equipment, model JSM 5800, with 20 kV and a maximum magnification of 30,000×.

2.5 *EDS elemental analysis*

The EDS analysis was made using a Noran detector in a Jeol equipment, model JSM 5800, with 20 kV, with an acquisition time of 100 s and magnification of 100×.

2.6 *X-ray diffraction*

The xerogel samples were submitted to XRD analysis using Cu Kα radiation as source. The equipment was a Siemens Diffractometer D500.

2.7 *N_2-isotherms*

The nitrogen adsorption–desorption isotherms of previous degassed solids, at 150 °C, were determined at liquid nitrogen boiling point in a homemade volumetric apparatus, with a vacuum line system employing a turbo molecular Edward vacuum pump. The pressure measurements were made using capillary Hg barometer and an active Pirani gauge. The apparatus was frequently checked with an alumina Aldrich standard reference (150 mesh, 5.8 nm and 155 m^2 g^{-1}). The specific surface areas of the hybrid materials were determined from the BET (Brunauer, Emmett and Teller) [21] multipoint method and the pore size distribution curves were obtained using BJH (Barret, Joyner and Halenda) method [22].

2.8 *High-pressure experiments*

For the high-pressure experiments, the xerogel powders were initially precompacted in a piston–cylinder type die to ~0.1 GPa. The volume of precompacted samples was ~0.35 cm^3 (diameter of 8 mm and height of 7 mm). The samples were then placed in a Pb container which acted as a pressure transmitting medium. The high-pressure processing was accomplished in a toroidal-type chamber at 3.5 GPa (34,500 a.t.m.) and 6.0 GPa (59,200 a.t.m.), at room temperature [23].

3. Results and discussion

3.1 *Synthesis of hybrid materials*

The synthesis procedure of the organic precursor (bPAPS), used in this work, was recently described for similar systems [14]. In the reaction of biphenylamine with CPTMS, first the biphenylamine was activated with sodium hydride in aprotic solvent mixture, as illustrated in equations (1) and (2). The use of NaH as base activator results in reduction in the reaction time [24]. Furthermore, the insoluble byproduct NaCl can be easily separated from the organic medium by centrifugation. In the absence of NaH, there is a formation of HCl, which reacts with the biphenylamine, resulting in the organic salt, which is more difficult to separate from the organic medium [20].

$$NH{-}(C_6H_5)_2 + NaH \longrightarrow {}^{-}N{-}(C_6H_5)_2Na^{+} + H_2 \quad (1)$$

$$(CH_3O)_3Si(CH_2)_3Cl + {}^{-}N{-}(C_6H_5)_2Na^{+} \longrightarrow (CH_3O)_3Si(CH_2)_3N{-}(C_6H_5)_2 + NaCl \quad (2)$$

The organic precursor obtained in equation (2) (bPAPS) was then added to the inorganic precursor solution containing TEOS or TEOS and TIPOT, to gelation. The resulting hybrid materials were assigned as bPhe/SiO_2 and bPhe/SiO_2/TiO_2, respectively. In the bPhe/SiO_2/TiO_2 case, the Ti/Si atomic ratio, determined by using EDS analysis, was 0.11 (table 1). This relation ensures an amorphous material with the titanium dispersed atomically in the tetrahedral silica structure, substituting the Si sites [25, 26], and considering that X-ray diffraction analysis did not show any titania or silica crystalline phase.

The idealized gelation step for bPhe/SiO_2 material is illustrated by equation (3).

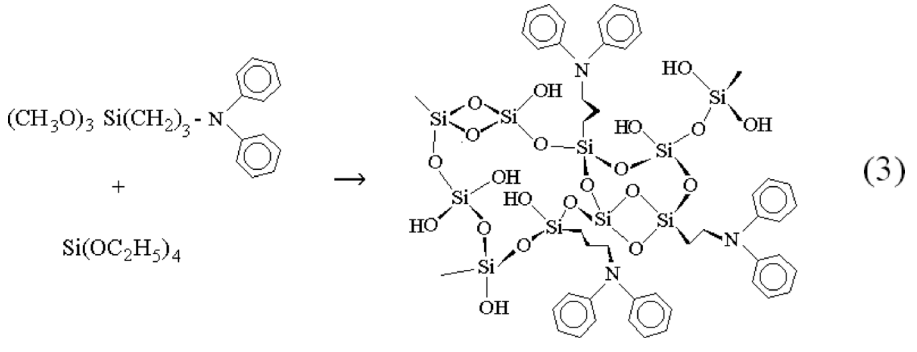

(3)

Table 1. Elemental composition and morphological data.

Material	Sample (GPa)	Organic content (mmol g^{-1})†	Atomic ratio Ti/Si‡	Surface area (m^2 g^{-1})	Pore volume (ml g^{-1})
bPhe/SiO_2	Powdered	1.42 ± 0.05		112 ± 7	0.26 ± 0.02
	Pressed 3.5			46 ± 5	0.05 ± 0.02
	Pressed 6.0			40 ± 5	0.04 ± 0.02
bPhe/SiO_2/TiO_2	Powdered	1.46 ± 0.05	0.11 ± 0.02	38 ± 5	0.04 ± 0.02
	Pressed 3.5			<3	<0.01
	Pressed 6.0			<3	<0.01

†mmol of organic groups per gram of xerogel.
‡obtained from the EDS analysis.

The organic incorporation values obtained by using the CHN elemental analysis were 1.42 and 1.46 ± 0.05 mmol of organic groups per gram of xerogel, for bPhe/SiO_2 and bPhe/SiO_2/TiO_2, respectively (table 1).

3.2 *SEM analysis*

The SEM analyses show different images for the bPhe/SiO_2 and bPhe/SiO_2/TiO_2 materials, as can be seen in figures 1 and 2, respectively. The bPhe/SiO_2 powdered sample has a mesoporous structure (figure 1a and b), whereas, in the powdered bPhe/SiO_2/TiO_2 sample, the nanoparticles are very close in the agglomerates, and thus it was observed only macropores (figures 2a and b). From figures 1c and 2c, it is evident that the pressed samples at 3.5 GPa are more compact and their pore structures are not visible in this scale. The application of higher pressure (6 GPa) causes no significant changes in the bPhe/SiO_2 (figure 1d); however, in the bPhe/SiO_2/TiO_2 case, it results in a fractured microstructure (figure 2d).

3.3 *Infrared analysis*

Figures 3 and 4 show the infrared spectra of the powdered and pressed samples of the hybrid materials, bPhe/SiO_2 and bPhe/SiO_2/TiO_2, respectively, obtained at room temperature, in

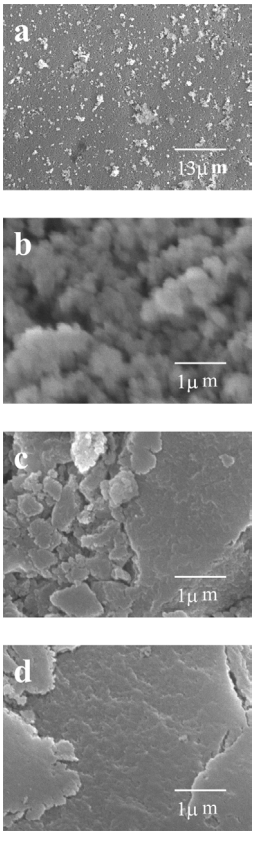

Figure 1. SEM images of bPhe/SiO_2 hybrid xerogel. (a and b) Powdered sample; (c) pressed at 3.5 GPa; (d) pressed at 6.0 GPa. The magnification was 2000× for image (a) and 30,000× for images (b, c and d).

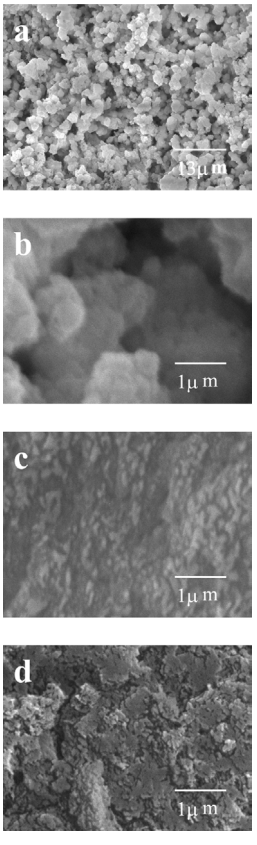

Figure 2. SEM images of bPhe/SiO_2/TiO_2 hybrid xerogel. (a and b) Powdered sample; (c) pressed at 3.5 GPa; (d) pressed at 6.0 GPa. The magnification was 2000× for image (a) and 30,000× for images (b, c and d).

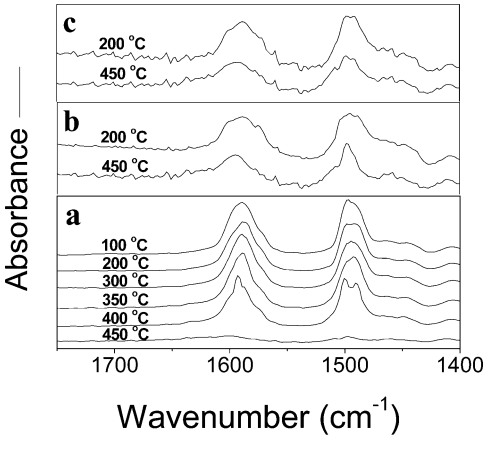

Figure 3. FTIR absorbance spectra of the bPhe/SiO_2 xerogel, obtained at room temperature, after heating in vacuum to temperatures ranging from 100 to 450 °C. (a) Powdered sample; (b) pressed at 3.5 GPa; (c) pressed at 6.0 GPa. The bar value is 2 for (a) and 0.6 for (b and c).

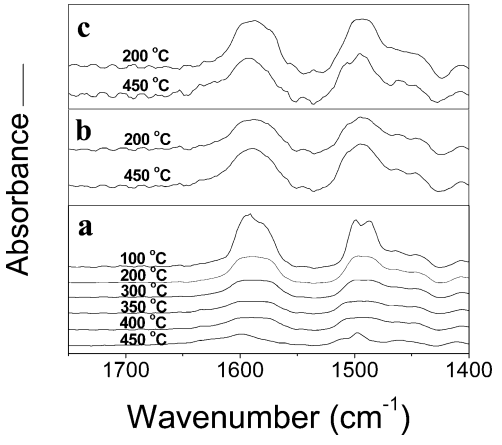

Figure 4. FTIR absorbance spectra of the xerogel bPhe/SiO_2/TiO_2, obtained at room temperature, after heating in vacuum to temperatures ranging from 100 to 450 °C. (a) Powdered sample; (b) pressed at 3.5 GPa; (c) pressed at 6.0 GPa. The bar value is 2 for (a) and 0.5 for (b and c).

vacuum. The aromatic ring modes at ∼1590 and 1495 cm^{-1} are very strong in the spectra; therefore, the band area of these absorption modes can be used to estimate the thermal stability of the organics [27]. The infrared band areas of the organics, obtained for the samples heat treated from 100 to 450 °C, are presented in the table 2. The overtone band of silica at ∼1870 cm^{-1} was used as a reference band. This normalization was necessary, considering the heterogeneity in disc thickness and for taking into account the position changes of the infrared beam.

It was observed in figure 3a that the organic phase of the powdered bPhe/SiO_2 sample is thermally stable because the infrared band areas of the organics are almost constant up to 400 °C (table 2). This high thermal stability is an indication that the organic groups are strongly

Table 2. Infrared band areas of aromatic phenyl group, obtained from the spectra of materials heated under vacuum.

Material	Sample (GPa)	Thermal treatment (°C)	IR band area (cm^{-1} abs)†
bPhe/SiO2	Powdered	100	3.1
		200	3.4
		300	3.1
		350	3.0
		400	2.7
		450	0.56
	Pressed at 3.5	200	3.0
		450	1.1
	Pressed at 6.0	200	3.3
		450	1.6
bPhe/SiO2/TiO2	Powdered	100	3.5
		200	2.4
		300	1.9
		350	1.6
		400	1.4
		450	1.1
	Pressed at 3.5	200	2.6
		450	2.7
		200	2.6
	Pressed at 6.0	450	2.0

†band area of phenyl ring at 1590 cm^{-1}/silica overtone band area at 1870 cm^{-1}.

bonded to the surface of the hybrid bPhe/SiO_2 material. Further thermal treatment (450 °C) results in a decrease in the band area, indicating that at this temperature the chemical bond was disrupted and the organic groups were desorbed from the surface [27]. However, for the powdered bPhe/SiO_2/TiO_2 sample, the increase in the temperature produces a progressive decrease in the infrared band area (figure 4a and table 2), indicating a lower thermal stability than that observed for the bPhe/SiO_2 material. Therefore, for the bPhe/SiO_2/TiO_2 sample, we propose that a fraction of the organic groups is not directly bonded to the surface of the silica/titania matrix, but some of the organosilane precursors are linked to each other forming oligomeric species which were gradually desorbed with the increasing temperature up to 200 °C. Nevertheless, a considerable organic band is present in the spectrum of the powdered bPhe/SiO_2/TiO_2 sample, even after heating up to 300 °C (table 2), and this band is related to organics chemically bonded to the silica/titania matrix. In addition, we can consider that the remained band after heating up to 450 °C can be explained by the retention of the organics in closed pores formed during the polycondensation and drying process [27, 28].

Considering now the spectra of the pressed samples, for the bPhe/SiO_2 material, in the spectra obtained after thermal treatment from 200 to 450 °C, a decrease in the organic band area was observed (table 2), indicating a considerable amount of open pores, even after applying 6 GPa of pressure (figure 3c). However, it is worth to observe a remaining band area (of 1.1 at 3.5 GPa and 1.6 at 6.0 GPa), higher than the powdered samples (0.56), heated at the same temperature. Considering the previous discussion, the high-pressure processing produced the partial closing of the pores and consequently the entrapment of the organics. For the bPhe/SiO_2/TiO_2, the infrared band area of the organics remains constant for samples pressed at 3.5 GPa, after thermal treatment up to 450 °C (figure 4b and table 2). On the other hand, when the bPhe/SiO_2/TiO_2 material was pressed at 6 GPa, the infrared spectrum of the sample heat treated up to 450 °C showed a slight band area reduction. This could be explained by the formation of cracks during the high-pressure compaction as evidenced by SEM image shown in figure 2d. These cracks allow the liberation of organics, which as shown in table 2 are not so strongly bonded when compared with the bPhe/SiO_2 material.

3.4 *N_2 isotherms*

The N_2 adsorption–desorption results are shown in table 1. The bPhe/SiO_2 sample has a BET surface area nearly three times larger than that obtained for the powdered bPhe/SiO_2/TiO_2 sample, according to the previous results reported for similar systems containing titania crystalline phase and silica [29]. However, in the present work, the lower porosity of the bPhe/SiO_2/TiO_2 when compared with the bPhe/SiO_2 material could not be explained by this same way because the samples did not show titania or silica crystalline phases. In both samples, the high-pressure processing produces a decrease in the BET surface area as well as in the pore volume.

The mesopore size distribution curves of the bPhe/SiO_2 and bPhe/SiO_2/TiO_2 materials, obtained by using the BJH method [22], are shown in figures 5 and 6, respectively. It was possible to observe that the porosity is higher for powdered samples than in the pressed ones. In the bPhe/SiO_2 case, the powdered sample presents two distinct mesopore diameter regions: (1) small pores with diameter <8 nm and (2) larger pores with average diameter of $\sim$37 nm (figure 5). The powdered bPhe/SiO_2/TiO_2 sample has mainly mesopores with 5 nm diameter, however, with a lower amount of small pores in relation to bPhe/SiO_2 powdered sample (see the scales of figures 5 and 6). After applying pressure, the pores of the bPhe/SiO_2/TiO_2 material were not detected by the used technique (figure 6).

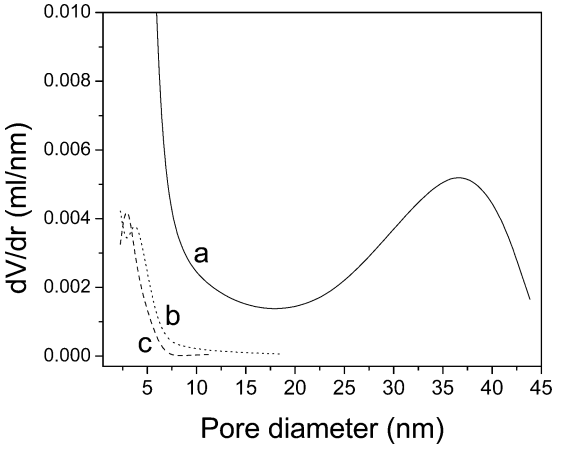

Figure 5. Pore size distribution of the bPhe/SiO_2 xerogel, obtained by the BJH method. (a) Powdered sample; (b) pressed at 3.5 GPa; (c) pressed at 6.0 GPa.

3.5 *Further discussion*

It was recently reported that high-pressure processing (up to 0.52 GPa) produces some decrease in the silica surface area, which was accompanied by a decrease in the pore volume [30]. These effects were attributed mainly to the decrease in the external surface area owing to the aggregation of particles, as the diameter of the main pores remains almost constant. In the present work, the pressure applied was nearly 10 times higher and the effects were more impressive, including closing of the pores containing organics. However, in the sample bPhe/SiO_2, surprisingly, a considerable amount of small open pores with diameter <5 nm is still observed, even after applying pressures of 6 GPa (figure 5 and table 1). This fact can also be confirmed by the reduction in the infrared band area of organics in the pressed sample, after the thermal treatment up to 450 °C (table 2), which means an organic desorption. These results can be interpreted by taking into account the presence of the surface pendant organic groups that prevent the complete reaction between silanol groups hindering the cold sintering process [17, 19].

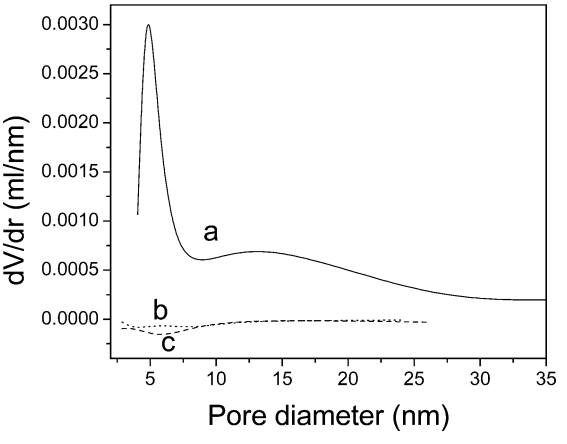

Figure 6. Pore size distribution of the bPhe/SiO_2/TiO_2 xerogel, obtained by the BJH method. (a) Powdered sample; (b) pressed at 3.5 GPa; (c) pressed at 6.0 GPa.

For the pressed bPhe/SiO_2/TiO_2 sample at 3.5 GPa, no opened pores were observed. This compaction was evident from the pore size distribution curves of figure 6, from the porosity data of the table 1 and also from the band area data showed in the table 2, where all organics remained trapped in the matrix. In this case, we proposed that there is no inhibition of cold sintering because the organics, in the oligomeric form, have higher mobility to accommodate during the compaction. However, after applying 6.0 GPa, the bPhe/SiO_2/TiO_2 sample shows a slight infrared band area reduction after thermal treatment. This could be caused by liberation of organics through the cracks formed in the microstructure during the compaction as observed in the SEM images (figure 2d and discussed earlier). These cracks were caused by the energy dissipation during the high-pressure compaction that was already observed in materials with low porosity [19].

4. Conclusions

In this work, the combination of the sol-gel method and a high-pressure technique was successful in the preparation and processing of new hybrid xerogels. The organic phase of the powdered bPhe/SiO_2 sample was thermally stable up to 400 °C, indicating that the organics are covalently bonded to the surface. For the bPhe/SiO_2/TiO_2 material, the thermal treatment produces a progressive desorption of the organics, because in this sample, the organics are in oligomeric form. From the SEM and N_2-isotherms, we conclude that the powdered bPhe/SiO_2 sample has a higher porosity than the powdered bPhe/SiO_2/TiO_2. The high-pressure processing produces a remarkable reduction in the surface area and pore volume. These effects are due to the compaction of the aggregated particles and also to the blocking of the pores. The closing of the pores results in organics entrapment, and this was more evident in the bPhe/SiO_2/TiO_2 material. In the bPhe/SiO_2 material, the cold sintering was partially hindered, possibly by the presence of organics bonded on the silica surface. This study helped us to improve our understanding about the mechanisms of compaction of hybrid materials at high pressure. The high pressure processing can be used as a complementary tool to promote the encapsulation of organic species in inorganic solid media, enabling the preparation of a lot of new hybrid sol-gel-based materials.

Acknowledgements

We thank FAPERGS, CNPq for financial support and grants. We also thank to CME – UFRGS for the use of the SEM.

References

[1] C. Sanchez, B. Lebeau, F. Chaput *et al.*, Adv. Mater. **15** 1969 (2003).
[2] A. Walcarius, Chem. Mater. **3** 3351 (1997).
[3] N.M. Jose and L.A.S.D. Prado, Quim. Nova **28** 281 (2005).
[4] A.M. Lazarin, Y. Gushikem and J. Braz, Chem. Soc. **13** 88 (2002).
[5] W. Li, D.P. Fries and A. Malik, J. Chromatogr. A **1044** 23 (2004).
[6] V. Rao and M.M. Kulkarni, Mater. Res. Bull. **37** 1667 (2002).
[7] U. Schubert, N. Hüsing and A. Lorenz, Chem. Mater. **7** 2010 (1995).
[8] D.S.F. Gay, Y. Gushikem, C.C. Moro *et al.*, J. Sol Gel Sci. Technol. **34** 189 (2005).
[9] G. Wu, J. Wang, J. Shen *et al.*, Mater. Res. Bull. **36** 2127 (2001).
[10] P. Innocenzi, A. Sassi, G. Brusatin *et al.*, Chem. Mater. **13** 3635 (2001).
[11] A. Pirson, A. Mohsine, P. Marchot *et al.*, J. Sol Gel Sci. Technol. **4** 179 (1995).
[12] I. Kimura, T. Kase, Y. Taguchi *et al.*, Mater. Res. Bull. **38** 585 (2003).
[13] L. Franken, L.S. Santos, E.B. Caramão *et al.*, Quim. Nova **25** 563 (2002).
[14] S.V.M. de Moraes, J.B. Passos, P. Schossler *et al.*, Talanta **59** 1039 (2003).

[15] J. Winkler and S. Marmé, J. Chromatog. A **888** 51 (2000).
[16] T.M.H. Costa, M.R. Gallas, E.V. Benvenutti *et al.*, J. Phys. Chem. B **103** 4278 (1999).
[17] T.M.H. Costa, M.R. Gallas, E.V. Benvenutti *et al.*, J. Non Cryst. Solids **220** 195 (1997).
[18] T.M.H. Costa, H.S. Hoffmann, E.V. Benvenutti *et al.*, Opt. Mater. **27** 1819 (2005).
[19] S.V.M. de Moraes, M.T. Laranjo, M. Zat *et al.*, Appl. Phys. A **81** 1053 (2005).
[20] J.L. Foschiera, T.M. Pizzolato and E.V. Benvenutti, J. Braz. Chem. Soc. **12** 159 (2001).
[21] S. Brunauer, P.H. Emmett and E. Teller, J. Am. Chem. Soc. **60** 309 (1938).
[22] E.P. Barret, L.G. Joyner and P.P. Halenda, J. Am. Chem. Soc. **73** 373 (1951).
[23] M.R. Gallas, A.R. Rosa, T.M.H. Costa *et al.*, J. Mater. Res. **12** 764 (1997).
[24] F.A. Pavan, S. Leal, T.M.H. Costa *et al.*, J. Sol Gel Sci. Technol. **23** 129 (2002).
[25] G.W. Wallidge, R. Anderson, G. Mountjoy *et al.*, J. Mater. Sci. **39** 6743 (2004).
[26] R. Anderson, G. Mountjoy, M.E. Smith *et al.*, J. Non Cryst. Solids **232–234** 72 (1998).
[27] F.A. Pavan, S.A. Gobbi, T.M.H. Costa *et al.*, J. Therm. Anal. Calorim. **68** 199 (2002).
[28] B. Boury, R.J.P. Corriu and V.L. Strat, Chem. Mater. **11** 2796 (1999).
[29] J.Y. Zheng, J.B. Pang, K.Y. Qiu *et al.*, Micropor. Mesopor. Mater. **49** 189 (2001).
[30] M.A. Springuel-Huet, J.L. Bonardet, A. Gédéon *et al.*, Micropor. Mesopor. Mater. **44**/**45** 775 (2001).

Appl. Phys. A (2004)
DOI: 10.1007/s00339-004-2945-y

Applied Physics A
Materials Science & Processing

S.V.M. DE MORAES[1]
M.T. LARANJO[1]
M. ZAT[1]
T.M.H. COSTA[1]
M.R. GALLAS[2]
E.V. BENVENUTTI[1,✉]

High-pressure effects on nanometric hybrid xerogels, *p*-phenylenediamine/silica and *p*-anisidine/silica

[1] LSS, Instituto de Química, UFRGS, CP 15 003, 91 501-970, Porto Alegre, RS, Brazil
[2] LAPMA, Instituto de Física, UFRGS, CP 15 051, 91 501-970, Porto Alegre, RS, Brazil

Received: 16 March 2004/Accepted: 31 May 2004
Published online: 29 July 2004 •

ABSTRACT The hybrid xerogels *p*-phenylenediamine/silica and *p*-anisidine/silica were prepared with different surface areas and porosities and they were processed at high pressure (7.7 GPa or ∼ 76 000 atm) in a quasi-hydrostatic medium at room temperature. The morphologies of the materials were studied before and after the high-pressure treatment by using N_2 adsorption–desorption isotherms, scanning electron microscopy and infrared thermal analysis. The porous hybrid *p*-phenylenediamine/silica presented after the high-pressure treatment a surface-area reduction and an entrapment of organics in closed pores. However, the less porous hybrid *p*-anisidine/silica showed a surprising behavior, a pressure-induced increase in surface area with opening of pores. We propose a mechanism based on the inhibition of the cold sintering process by the organics to explain these results.

PACS 81.20.-n; 81.40.Vw; 81.05.-t

1 Introduction

The sol–gel method is an attractive route to prepare several silica-based materials, with promising properties that allow their potential application as sorbents, sensors, catalysts and optical and electrochemical devices [1–8]. The sol–gel method to prepare silica consists basically in the hydrolysis (Scheme 1) and polycondensation of alkoxysilanes in tetraethylorthosilicate (TEOS) or tetramethylorthosilicate (TMOS) (Schemes 2a and 2b) that result in a cross-linked silica network [9].

$$\mathrm{Si(OR)_4 + H_2O \rightarrow (RO)_3Si{-}OH + ROH} \quad (1)$$

$$\equiv \mathrm{SiOH + OH{-}Si} \equiv \rightarrow \equiv \mathrm{Si{-}O{-}Si} \equiv + \mathrm{H_2O} \quad (2a)$$

$$\equiv \mathrm{Si{-}OH + RO{-}Si} \equiv \rightarrow \equiv \mathrm{Si{-}O{-}Si} \equiv + \mathrm{ROH} \quad (2b)$$

Thus, it is possible to insert several organic groups in the silica structure by choosing an appropriate organosilane ($\mathrm{R{-}Si(OR)_3}$) to be hydrolyzed and polycondensed simultaneously with the TEOS or TMOS. The resulting hybrid materials present a very stable organic phase [10, 11].

The high-pressure technique is an effective tool to be used for compaction of silica-based powder materials, improving mechanical, optical and morphological properties [12–16]. Costa et al. [17] proposed a cold sintering mechanism to explain the compaction of a pure silica system at room temperature. The high-pressure compaction produces an approach of silanol groups that react to form bridged siloxanes, resulting in a more cross-linked and compacted silica network. In this process the pure silica undergoes a drastic reduction in the surface area, near 100 times, due to the formation of a microstructure with closed pores.

In the present work, the high-pressure technique was used to compact, at room temperature, the hybrid-based silica, *p*-phenylenediamine/silica (*p*-PhAS/silica) and *p*-anisidine/silica (*p*-ANS/silica). The high-pressure effects on silica-containing organics were investigated by using infrared spectroscopy, N_2 adsorption–desorption isotherms and scanning electron microscopy.

2 Experimental

2.1 *Synthesis*

For the synthesis of the sol–gel organic precursors the *p*-phenylenediamine and *p*-anisidine were activated with sodium hydride in 10 ml of aprotic solvents mixture (toluene:thf) (Merck) (1:1) for 30 min, and 3-chloropropyltrimethoxysilane (CPTMS, Merck) was added. The quantities used were stoichiometric (5 mmol) for *p*-phenylenediamine (Merck), *p*-anisidine, CPTMS and NaH (Acros). The mixtures were stirred under argon at solvent-reflux temperature for a period of 5 h. The solutions were then centrifuged, and the supernatants that contain the *p*-phenylenediaminepropyltrimethoxysilane (*p*-PhAS) or *p*-anisidinepropyltrimethoxysilane (*p*-ANS) were used as sol–gel organic precursors in the two gelation processes. Afterwards, tetraethylorthosilicate (TEOS, Acros) (5 ml), ethyl alcohol (Merck) (5 ml), HF (0.1 ml, Synth) and water in stoichiometric ratio with Si $r = 4/1$ (1.6 ml) were added to the precursor solutions, under stirring. The gelations occur by a fluoride nucleophilic catalytic process, at pH ∼ 10. The mixtures were stored for a week, just covered without sealing, for gelation and solvent evaporation. The resulting xerogels were then extensively washed using the following solvents: toluene, thf, ethyl alcohol, distilled water and ethyl ether. The xerogels were finally dried for 30 min in an oven at 100 °C. The resulting xerogel powders were designated *p*-PhAS/silica and *p*-ANS/silica.

✉ Fax: +55-51/3316-7304, E-mail: edilson@iq.ufrgs.br

2.2 *High-pressure technique*

For the high-pressure technique, the xerogel powders were initially pre-compacted in a piston–cylinder-type die to approximately 0.1 GPa. The volume of pre-compacted samples was about 0.35 cm^3 (diameter of 8 mm and height of 7 mm). The samples were then placed in a Pb container which acted as a quasi-hydrostatic pressure-transmitting medium. The high-pressure processing was accomplished in a toroidal-type chamber at 7.7 ± 0.5 GPa ($\sim$ 76 000 atm) at room temperature [18]. The pressure calibration was accomplished by the fixed-points method [19].

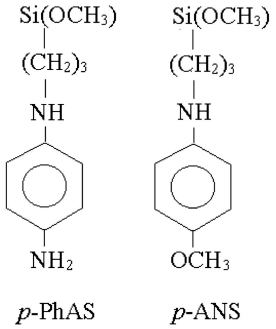

FIGURE 1 Sol–gel organic precursors used

2.3 *Infrared analysis*

Self-supporting disks of the materials were prepared, with an area of 5 cm^2, weighing $\sim$ 100 mg. The disks were heated in a temperature range from 100 to 450 °C under vacuum (10^{-2} Torr, 1 Torr = 133.3 Pa), for 1 h. The infrared cell used in this work was described elsewhere [20]. The equipment used was a Shimadzu Fourier-transform infrared (FTIR) spectrometer, model 8300. The spectra were obtained with a resolution of 4 cm^{-1}, with 100 scans.

2.4 N_2 *isotherms*

The nitrogen adsorption–desorption isotherms of previously degassed solids, at 150 °C, were determined at liquid-nitrogen boiling point in a home-made volumetric apparatus, with a vacuum-line system employing a turbomolecular Edwards vacuum pump. The pressure measurements were made using a capillary Hg barometer. The specific surface areas of the hybrid materials were determined using the BET (Brunauer, Emmett and Teller) [21] multipoint method and the pore-size distribution was obtained using the BJH (Barret, Joyner and Halenda) method [22].

2.5 *Scanning electron microscopy*

The hybrid xerogel materials were analyzed with a Jeol model JSM 5800 scanning electron microscope (SEM), with 20 kV and 60 000 times magnification.

3 Results and discussion

The synthesis of the sol–gel organic precursors employing a SN_2 reaction between 3-chloropropyltrimethoxysilane (CPTMS) and aromatic amines has been described by using sodium hydride as a base activator [23]. The organic precursors *p*-PhAS and *p*-ANS, synthesized in this work, are illustrated in Fig. 1.

In the presence of tetraethylorthosilicate (TEOS), water and HF catalyst, the organic precursors undergo hydrolysis and polycondensation. The resulting hybrid xerogel materials present a covalent organic–inorganic interface, and the organics can be dispersed in open pores or trapped in closed pores [11].

Infrared thermal analysis is a very effective tool to investigate the presence and the distribution of the organic phase in hybrid xerogel materials with a covalent organic–inorganic interface. The analysis is based on the evolution of the infrared band areas of the organics in relation to the thermal treatment [11]. The band area of the organics dispersed in open pores, when covalently bonded, is almost constant up to 300 °C. However, these organics are completely desorbed when heat treated up to 450 °C, in vacuum. The remaining organic bands that do not vanish are attributed to trapped organics in closed pores [11]. Thus, it is possible to calculate the relative organic coverage, i.e. organic groups that are really on the surface, in open pores. This is obtained by subtracting the band areas corresponding to the organic trapped groups from the band areas of the organic total content. The organic band-area values are obtained by using the overtone silica band at $\sim$ 1870 cm^{-1} as a reference band. This normalization was necessary, considering the heterogeneity in the disk's thickness, so as to take into account the position changes of the infrared beam.

The infrared spectra of the *p*-PhAS/silica and *p*-ANS/silica materials are presented in Figs. 2 and 3, respectively. The great organic thermal stability observed for the powdered samples heat treated up to 400 °C, in the vacuum cell, is evidence that these groups are strongly bonded to the surface in the covalent form. It is possible to observe that the fraction of organics that remained in the powdered

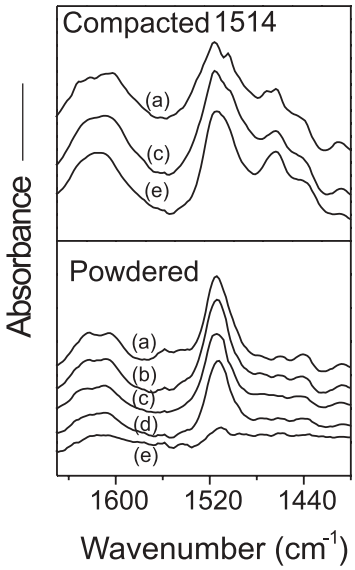

FIGURE 2 Infrared spectra of powdered and compacted (7.7 GPa) *p*-PhAS/silica samples, obtained after heat treatment in vacuum for 1 h up to: (a) 100; (b) 200; (c) 300; (d) 400 and (e) 450 °C. The bar value is 0.5 for both powdered and compacted samples

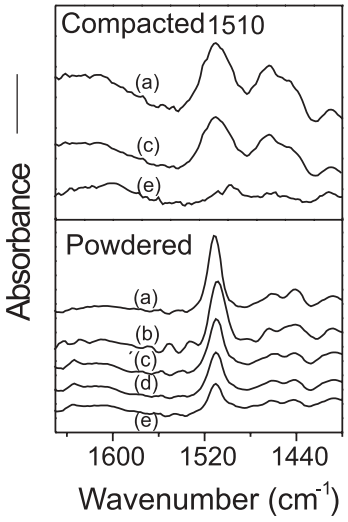

FIGURE 3 Infrared spectra of powdered and compacted (7.7 GPa) *p*-ANS/silica samples, obtained after heat treatment in vacuum for 1 h up to: (a) 100; (b) 200; (c) 300; (d) 400 and (e) 450 °C. The bar value is 0.5 and 0.2 for powdered and compacted samples, respectively

p-ANS/silica material, even after heat treatment up to 450 °C, is 57% (Table 1), higher than the fraction observed for the *p*-PhAS/silica material, which is only 10%. The relative remaining organic grade indicates the presence of organics in closed pores [11]. Therefore, the powdered *p*-ANS/silica material presents a larger fraction of organic groups trapped in closed pores than the powdered *p*-PhAS/silica material. These results are in agreement with the surface-area and pore-volume measurements presented in Table 1. The surface-area and pore-volume values of the powdered *p*-ANS/silica material are lower (near 40%) than the values for the powdered *p*-PhAS/silica material.

The infrared spectra of the *p*-PhAS/silica and *p*-ANS/silica compacted samples at 7.7 GPa are also shown in Figs. 2 and 3, respectively. It is possible to observe that the high-pressure processing closed some existing pores for *p*-PhAS/silica material, since the relative remaining organic grade, estimated from the spectra of the samples heat treated up to 450 °C, increased from 10 to 77% after applying the high pressure (Table 1). Confirming these results, the surface area and pore volume of the compacted *p*-PhAS/silica sample also decreased from 175 to 65 $m^2\ g^{-1}$ and from 0.30 to 0.07 $cm^3\ g^{-1}$, respectively (Table 1). For the compacted *p*-ANS/silica sample, the relative remaining organic grade of 25% was lower than that obtained for the powdered sample, which was 57% (Table 1), indicating that, for this sample, the high-pressure processing, surprisingly, promoted the opening of pores and this fact made possible the organics liberation during the thermal treatment, in the vacuum cell. These results are also confirmed by surface-area data that show a higher value for this sample after the high-pressure processing. The *p*-ANS/silica results are unexpected if compared with that obtained for pure silica gel [17] and even for a *p*-PhAS/silica sample.

The pore size distribution curves, obtained from the N_2 desorption isotherms, are presented in Fig. 4. It is possible to observe that the *p*-PhAS/silica material presents a higher porosity than the powdered *p*-ANS/silica material. The high-pressure processing produces a closing of the pores for *p*-PhAS/silica material; on the other hand, no measurable effect can be detected for the *p*-ANS/silica material.

Costa et al. [17] reported that when pure silica gel is submitted to similar high-pressure values, the surface area undergoes a drastic reduction, decreasing from 300 to 3 $m^2\ g^{-1}$. This effect was interpreted as a consequence of the surface dehydroxylation, i.e. conversion of silanol to siloxane groups, induced by the higher silanol proximity in the compacted samples [17]. In the present work, for the porous *p*-PhAS/silica that is a hybrid material, the closing of the pores was not too impressive, since after the high-pressure processing, the surface area and pore volume decrease by about 50% (Table 1), but even so a fraction of open pores remained. In this case, the surface pendant organic groups prevented the complete reaction between the silanol groups, hindering the cold sintering process, as represented in Fig. 5.

On the other hand, for the *p*-ANS/silica hybrid material, which presents a very low porosity even in the powdered form, the changes were totally unexpected. The high-pressure pro-

Sample	Thermal treatment/ °C	IR band area/ Abs.cm^{-1} (Relative remaining organic grade/%)	Surface area/$m^2\ g^{-1}$	Pore volume/ $cm^3\ g^{-1}$
Powdered p-PhAS/ silica	100	2.1 (100)	175	0.30
	200	2.1 (100)		
	300	2.1 (100)		
	400	2.0 (95)		
	450	0.2 (10)		
Compacted p-PhAS/ silica	150	2.2 (100)	65	0.07
	300	2.2 (100)		
	450	1.7 (77)		
Powdered p-ANS/ silica	100	2.1 (100)	65	0.13
	200	2.1 (100)		
	300	1.7 (81)		
	350	1.6 (76)		
	450	1.2 (57)		
Compacted p-ANS/ silica	150	1.6 (100)	90	0.08
	300	1.2 (75)		
	450	0.4 (25)		

TABLE 1 Infrared band areas of aromatic ring stretching and porosity data of hybrid materials

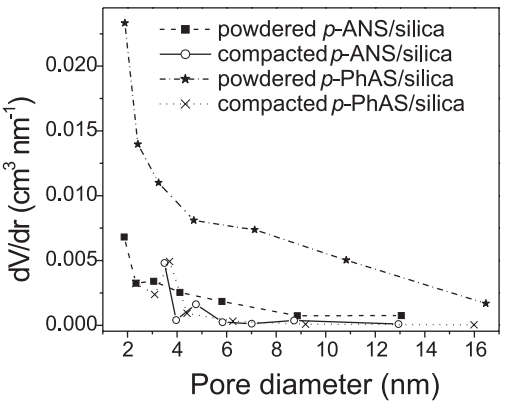

FIGURE 4 Pore-size distribution of the *p*-PhAS/silica and *p*-ANS/silica hybrid materials, powdered and compacted at 7.7 GPa

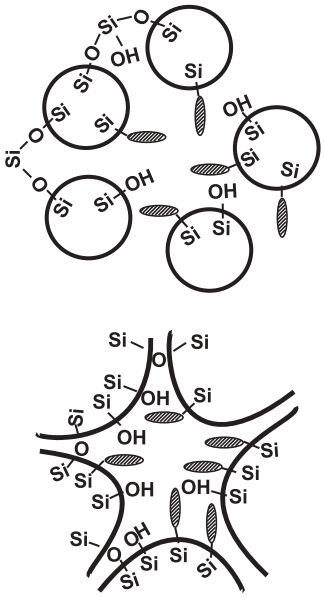

FIGURE 5 Model for the structure effects in a cold sintering process in the presence of the organics

cessing produced an increase in the surface area (see Table 1), which is confirmed by a lower remaining organic grade as already explained.

In general, when we apply high pressure to powdered samples, using a quasi-hydrostatic transmitting medium, the energy is dissipated in a sample-volume reduction, with a decrease of porosity, or in phase transitions [24–26]. For the

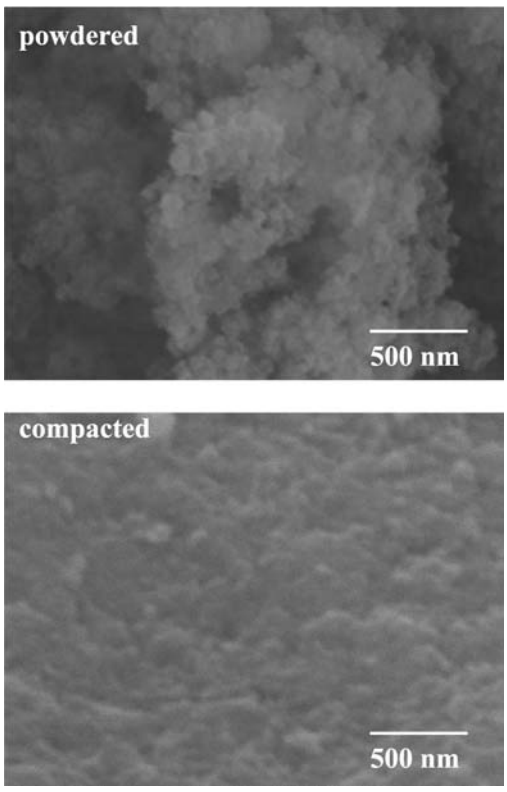

FIGURE 6 SEM images of *p*-PhAS/silica hybrid material, powdered and compacted at 7.7 GPa. The magnification was 60 000 times

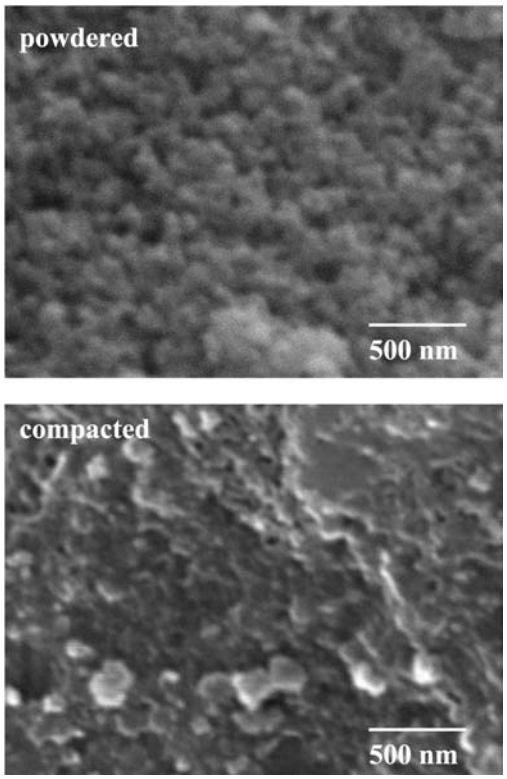

FIGURE 7 SEM images of *p*-ANS/silica hybrid material, powdered and compacted at 7.7 GPa. The magnification was 60 000 times

p-PhAS/silica, a porous sample, the energy dissipation occurred by the reduction of porosity; however, this process was not so impressive as already observed for pure silica [17], due to the presence of organics. For the powdered *p*-ANS/silica hybrid, this kind of dissipation process could be hindered because this material has a relatively lower porosity even in the powdered form (Table 1 and Fig. 4) and, additionally, presents surface organic groups. Therefore, the energy dissipation in *p*-ANS/silica material could happen by a shearing process between particles, causing microstructural defects formed at the onset of plastic deformation in the particles.

The SEM images obtained for *p*-PhAS/silica and *p*-ANS/silica hybrid materials that are shown in Figs. 6 and 7, respectively, confirm the above propositions. The decrease of the porosity for *p*-PhAS/silica material is evident after applying the high pressure. However, for the *p*-ANS/silica, the reduction of porosity is not clearly observed; the samples were very similar in this respect. The compacted samples showed a platelet microstructure that could confirm the hypothesis of the dissipation of energy by shearing or plastic deformation of particles.

4 Conclusions

The porous powdered *p*-PhAS/silica hybrid material, when submitted to high pressure, undergoes a surface-area and porosity reduction with consequent entrapment of organics in closed pores. This effect was not so impressive when compared to pure silica, and it could be explained considering that the surface organic groups partially hinder the cold sintering process. On the other hand, for the less porous

powdered *p*-ANS/silica hybrid material, the high pressure produces an amazing increase in surface area with an opening of the pores, observed by the liberation of the organics after the heat treatment, in a vacuum cell. This behavior was interpreted considering that the energy applied during the high-pressure processing is dissipated by shearing between the particles, causing the opening of the pores.

ACKNOWLEDGEMENTS We thank FAPERGS (Fundação de Amparoà Pesquisa no Estado do Rio Grande do Sul, Brasil) and CNPq (Conselho Nacional de Desenvolvimento Científico e Tecnológico, Brasil) for financial support and grants. We also thank the CME-UFRGS for the use of the SEM.

REFERENCES

1 O. Lev, Z. Wu, S. Bharathi, V. Glezer, A. Modestov, J. Gun, L. Rabinovich, S. Sampath: Chem. Mater. **9**, 2354 (1997)
2 Z. Lu, E. Lindner, H.A. Mayer: Chem. Rev. **102**, 3543 (2002)
3 W. Que, Y. Zhou, Y.L. Lam, Y.C. Chan, C.H. Kam: Appl. Phys. A **73**, 171 (2001)
4 M.M. Collinson: Trends Anal. Chem. **21**, 30 (2002)
5 P. Yang, C.F. Song, M.K. Lu, G.J. Zhou, D. Xu, D.R. Yuan: Appl. Phys. A **74**, 689 (2002)
6 T. Salesch, S. Bachmann, S. Brugger, R. Rabelo-Schaefer, K. Albert, S. Steinbrecher, E. Plies, A. Mehdi, C. Reye, R.J.P. Corriu, E. Lindner: Adv. Funct. Mater. **12**, 134 (2002)
7 S.V.M. de Moraes, J.B. Passos, P. Schossler, E.B. Caramão, C.C. Moro, T.M.H. Costa, E.V. Benvenutti: Talanta **59**, 1039 (2003)
8 F.A. Pavan, T.M.H. Costa, E.V. Benvenutti: Colloids Surf. A **226**, 95 (2003)
9 D.A. Loy, K.J. Shea: Chem. Rev. **95**, 1431 (1995)
10 L.T. Arenas, T.A.S. Aguirre, A. Langaro, Y. Gushikem, E.V. Benvenutti, T.M.H. Costa: Polymer **44**, 5521 (2003)
11 F.A. Pavan, S.A. Gobbi, T.M.H. Costa, E.V. Benvenutti: J. Therm. Anal. Calorim. **68**, 199 (2002)
12 M.R. Gallas, A.R. Rosa, T.M.H. Costa, J.A.H. da Jornada: J. Mater. Res. **12**, 764 (1997)
13 T.M.H. Costa, V. Stefani, N. Balzaretti, L.T.S.T. Francisco, M.R. Gallas, J.A.H. da Jornada: J. Non-Cryst. Solids **221**, 157 (1997)
14 T.M.H. Costa, M.R. Gallas, E.V. Benvenutti, J.A.H. da Jornada: J. Phys. Chem. B **103**, 4278 (1999)
15 E. Ol'khovik, O. Figovsky, V. Feigin: Mater. Res. Innov. **2**, 115 (1998)
16 M.A. Springuel-Huet, J.L. Bonardet, A. Gédéon, Y. Yue, V.N. Romannikov, J. Fraissard: Micropor. Mesopor. Mater. **44–45**, 775 (2001)
17 T.M.H. Costa, M.R. Gallas, E.V. Benvenutti, J.A.H. da Jornada: J. Non-Cryst. Solids **220**, 195 (1997)
18 L.G. Khvostantsev: High Temp. High Pressures **16**, 171 (1984)
19 W.F. Sherman, A.A. Stadmuller: *Experimental Techniques and High-pressure Research* (Wiley, New York 1987)
20 J.L. Foschiera, T.M. Pizzolato, E.V. Benvenutti: J. Braz. Chem. Soc. **12**, 159 (2001)
21 S. Brunauer, P.H. Emmett, E. Teller: J. Am. Chem. Soc. **60**, 309 (1938)
22 E.P. Barret, L.G. Joyner, P.P. Halenda: J. Am. Chem. Soc. **73**, 373 (1951)
23 F.A. Pavan, S. Leal, Y. Gushikem, T.M.H. Costa, E.V. Benvenutti: J. Sol–Gel Sci. Technol. **23**, 129 (2002)
24 A. Jayaraman: Sci. Am. **250**, 54 (1984)
25 L. Spain, P. Bolsaitis: *Phase Transformation at High Pressure* (Marcel Dekker, New York 1977)
26 S.N. Achary, G.D. Mukherjee, A.K. Tyagi, S.N. Vaidya: J. Mater. Sci. **37**, 2501 (2002)

ANALYTICAL SCIENCES MAY 2005, VOL. 21

Notes

7-Amino-4-azaheptyl Grafted onto a Silica Gel as a Sorbent for the On-line Preconcentration and Determination of Iron(III) in Water Samples

Sandra V. M. de Moraes,* Mateus M. Tisott,* Caroline D. Milcharek,* Jorge L. Brasil,* Tania M. H. Costa,* Márcia R. Gallas , Edilson V. Benvenutti,* and Eder C. Lima*†**

**Colégio Militar de Porto Alegre, Av. José Bonifácio, 363, 90040-130, Porto Alegre, RS, Brazil*
***Universidade Federal do Rio Grande do Sul-Instituto de Física, Porto Alegre, RS, Brazil*

A new sorbent was synthesized by anchoring 7-amino-4-azaheptyltrimetoxisilane, freshly prepared, to silica gel, producing 7-amino-4-azaheptyl anchored silica gel (AAHSG). This material was characterized by infrared spectroscopy (IR), elemental analysis (CHN), and nitrogen adsorption-desorption isotherms. Isotherms of the adsorption of Fe^{3+}, Fe^{2+} and Cu^{2+} on AAHSG were recorded, which indicated that Fe^{3+} presents a higher affinity by the sorbent. Therefore, AAHSG was successfully employed as a sorbent in a simple flow system for the preconcentration of Fe^{3+} in natural water samples, such as, river water, lagoonwater, springwater, stream water, well water and two water reference materials (NIST-SRM 1640, NIST-SRM 1643d). The obtained preconcentration factor was 82.2, and the detection limit achieved was 5.9 ng ml^{-1}. The recovery of spiked water samples ranged from 95.0 – 103.1%.

(Received October 25, 2004; Accepted December 13, 2004)

The determination of metal ions at low concentration levels usually requires the use of expensive analytical techniques, such as graphite-furnace atomic absorption spectrometry (GFAAS)[1,2] and/or inductively coupled plasma mass spectrometry (ICP-MS).[3,4] Although these techniques present very low detection limits for the determination of several elements in the more difficult kinds of samples, these techniques require a high investment for their implementation and maintenance,[1-4] precluding their extensive application in developing and underdeveloped countries. In order to overcome these difficulties, preconcentration of the elements increases the detection power of less-sensitive analytical techniques, such as flame atomic absorption spectrometry (FAAS) and visible spectrophotometry.

The preconcentration procedure most often employed is solid-phase extraction, because it does not require the use of hazardous solvents, which generate waste to be subsequently treated. Most kinds of the sorbents employed for the preconcentration of the elements in environmental samples are polymeric resins,[5] controlled pore silica glass,[6] modified silica obtained by a grafting process,[7,8] or by the sol-gel method.[9,10] The use of modified silicas with different organic groups is one of the most successful sorbents employed in analytical laboratories, because the silica supports do not swell or shrink such as the polymeric resin;[5] it allows the modified silica sorbent to be used during several cycles of preconcentration, because the retention process (adsorption, chelation, ion exchange) is reversible;[11] the modified silica may be employed in aqueous and organic solvent media;[11] they present good thermal stability[9,10] and appropriated accessibility of the ions to the attached chelanting groups, which allows high preconcentration factors.[11]

In the present work, a new modified silica was synthesized by reacting 7-amino-4-azaheptyltrimetoxisilane with silica gel, forming 7-amino-4-azaheptyl silica (AAHSG). This sorbent was characterized by infrared spectroscopy, CHN elemental analysis and N_2 adsorption-desorption isoterms; it was successfully employed for the preconcentration of iron(III) in natural water samples. A flow system for the on-line preconcentration of the analyte was employed with spectrophotometric detection at 480 nm.

Experimental

Synthesis and characterization of the 7-amino-4-azaheptyl silica (AAHSG)

The amount of 15 mmol of 1,3-diaminepropane was firstly activated using 15 mmol of sodium hydride in 10 ml of a mixture of aprotic solvent (toluene:tetrahidrofurane) (1:1) for 30 min; then, 15 mmol of 3-chloropropyltrimethoxisilane (CPTMS, ACROS) was added. The mixture was stirred under argon at the solvent-reflux temperature for a period of 5 h. The solution was then centrifuged, to eliminate the by-product sodium chloride. The product of the reaction, 7-amino-4-azaheptyltrimetoxisilane, was then used as an organic precursor reagent for the silica grafting reaction.

Silica gel (Merck) having particle size at 0.02 – 0.05 mm and a surface area of 250 m^2 g^{-1} was activated at 150˚C under a vacuum (10^{-1} Pa) for 5 h. The 7-amino-4-azaheptyltrimetoxisilane was dissolved in 300 ml of toluene and activated silica (10 g) was then added. The mixture was stirred for 48 h under argon at the solvent-reflux temperature. The modified silica was filtered under argon in a Schlenk apparatus, and washed with toluene, hexane, ethyl alcohol, doubly distilled water and ethyl ether (Merck). The resulting sorbent, 7-amino-4-azaheptyl silica (AAHSG), was dried for 2 h under a vacuum at 120˚C.

An infrared analysis was carried out using self-supporting disks of the AAHSG sorbent and pure silica, with an area of 5

† To whom correspondence should be addressed.
E-mail: ederlima@iq.ufrgs.br

cm², weighing *ca.* 100 mg. The disks were heated for 1 h up to 250°C, under a vacuum (10^{-2} Torr), using an IR cell, described elsewhere.[9,10] The self-supporting disk was analyzed in the infrared region using a Shimadzu FTIR (Model 8300). Spectra were obtained with a resolution of 4 cm^{-1}, with 100 cumulative scans.

The organic functionalization grade was obtained using a CHN Perkin Elmer M CHNS/O Analyzer (Model 2400). The analysis was performed in triplicate, after heating at 100°C, under a vacuum, for 1 h.

The nitrogen adsorption-desorption isotherm of degassed solid, at 150°C, was determined at the liquid-nitrogen boiling point in a homemade volumetric apparatus, with a vacuum line system employing a turbo molecular Edward vacuum pump (Crawley Sussex, England). Pressure measurements were made using a capillary Hg barometer, and also an active Pirani gauge. The specific surface areas of the pure silica and AAHSG sorbent were determined by the BET (Brunauer, Emmett and Teller) multipoint method,[12] and the pore size distribution was obtained using the BJH (Barret, Joyner, and Halenda) method.[13]

Instruments for analytical applications

A 600 S Femto spectrophotometer provided with a 150 µl flow-cell and a serial port RS232C connected to an AMD K6II 350 MHz personal computer for data acquisition were employed throughout for analytical measurements. Two four-channel Milam bp-200 peristaltic pumps provided with Tygon® and silicone tubes of different diameters were used to propel the solutions in the flow system. For pH measurements, a Digimed pH-meter provided with combined glass electrode was used.

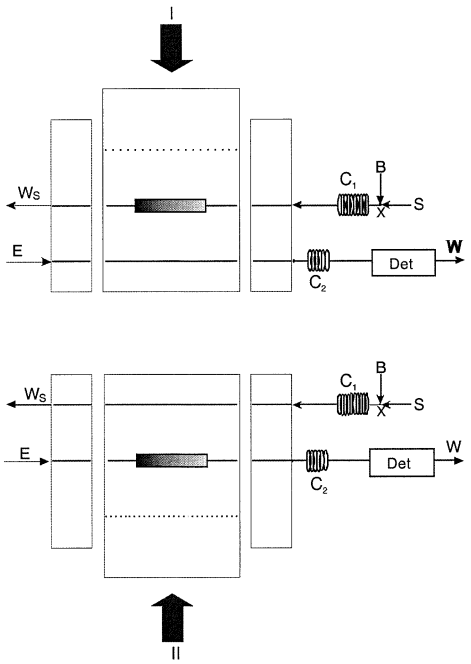

Fig. 1 Flow system for the preconcentration of Fe^{3+}. B, Buffer solution (pH 6.2), 2.5 ml min^{-1}; S, sample solution (pH 1), 4.5 ml min^{-1}; C_{R1} and C_{R2}, coil reactors; Ws, waste; E, eluent at 1.2 ml min^{-1}; Det, spectrophotometric flow-cell, 150 µl, λ = 480 nm.

Reagents, solutions, samples and reference materials

Doubly distilled water was employed throughout.

Solutions containing 0.1 – 1.0 mol l^{-1} of hydrochloric acid (Merck) plus 0.5 – 5.0% m/v KSCN were employed as an eluent. A 1.00 g l^{-1} iron stock solution was prepared from $FeSO_4{\cdot}NH_4SO_4{\cdot}6H_2O$. The Fe^{2+} solution was aerially oxidized to Fe^{3+} in an acidic medium. Calibration solutions within 30.0 – 600.0 ng ml^{-1} (preconcentration) and 2000 – 12000 ng ml^{-1} (without preconcentration) of Fe^{3+} range were prepared by suitable serial dilution of the stock solution with doubly distilled water and adjusting the final acidity to pH 1.0 with HCl.

For buffer preparations, glacial acetic acid, sodium acetate, ammonium acetate, and sodium hydroxide were employed.

For interference studies, the following salts of the elements were employed: NaCl, KCl, $MgSO_4{\cdot}7H_2O$, $CaSO_4{\cdot}2H_2O$, $AlCl_3{\cdot}6H_2O$, $CoSO_4{\cdot}7H_2O$, $Ba(NO_3)_2$, $CrCl_3{\cdot}6H_2O$, Cu metallic dissolved in 10% v/v HNO_3, $MnSO_4{\cdot}H_2O$, $ZnSO_4{\cdot}7H_2O$, $NiSO_4{\cdot}6H_2O$.

Ordinary water samples (river, lagoon, stream, spring, well) were filtered with Whatman paper, and the pH adjusted to 1.0 with HCl; they were then analyzed employing preconcentration procedure.

In order to attain the accuracy of the proposed method, the following water reference materials were employed: Trace Elements in Water NIST-SRM 1643d, and Trace Elements in Natural Water NIST-SRM 1640 from National Institute of Standards and Technology (NIST).

Isotherms of the adsorption of Fe^{3+},Fe^{2+}, and Cu^{2+} on AAHSG

A 10.00 ml sample solution containing individually Fe^{3+} or Fe^{2+} (8.95×10^{-6} – 1.79×10^{-2} mol l^{-1}), a Cu^{2+} (7.87×10^{-6} – 1.55×10^{-2} mol l^{-1}) solution plus 10.0 ml of a $NaCH_3CO_2$–HCH_3CO_2 buffer solution (pH 6.0) were transferred to a 50 ml conical polyethylene flask containing 20.0 mg of the sorbent. These flasks were placed in a horizontal shaker and agitated for 180 min in order to adsorb the analytes. Subsequently, the solid phase was separated from the aqueous phase by filtration, being the aqueous phase retained for analysis.

The elements, which were not retained in the sorbent, were spectrophotometrically determined. The element Cu^{2+} was determined using 0.15% m/v sodium diethyldithiocarbamate (DDTC); Fe^{3+} was determined using 2.0% m/v KSCN; and Fe^{2+} using 0.25% m/v 1,10-phenantroline. The measurements were carried out using a FEMTO 600 S spectrophotometer, according to the following procedure: an aliquot of 500 µl of the aqueous phase and/or an analyte standard solution plus 1000 µl of acetate buffer (pH 5.0) plus 500 µl of a chromogenic reagent were added to a Hellma glass curvette (10 mm of optical path). The analyte solutions with concentrations higher than those cited above were properly diluted with distilled water. The metal-ion adsorption capacity of the solid phase (N_f), obtained in the saturation plateau was calculated by applying the equation $N_f = (C_s - C_e) \times V/m$, where C_s is the initial metal concentration, C_e is the metal concentration at the equilibrium found in the solution in equilibrium with the solid phase, V is the volume of the solution put with the sorbent, and m is the mass of the solid phase.

Flow system

For the preconcentration of iron in water samples, a manifold made of a Perspex proportional injector-commutator was used, as depicted in Fig. 1. In position I, the sample solution (S, Fe^{3+}) and the buffer solution (B) are merged in the confluence point X; these solutions are subsequently mixed in a coil (C_{R1}) and directed to a glass microcolumn (3 cm, i.d. 3 mm, 0.12 g of sorbent), for sorbing the analyte present in the sample solution, and the aqueous phase is directed to the waste (W_s). In the second line, the eluent solution (E-KSCN + HCl) feeds the

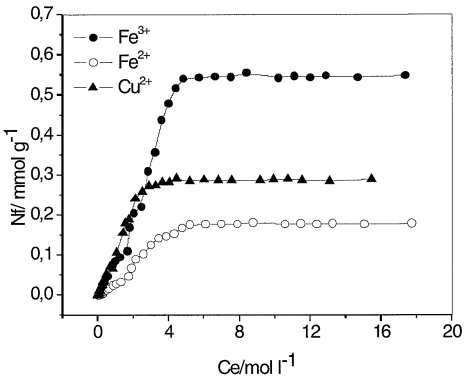

Fig. 2 Adsorption isotherms of Fe^{2+}, Fe^{3+}, and Cu^{2+} on DAPPS. Time of agitation, 180 min.

second coil (C_{R2}), and this solution passes in the flow-cell of the spectrophotometer, producing the line base; subsequently, this solution is directed to the waste (W). After a 120 s preconcentration period, unless otherwise stated, the central part of the injector commutator is slided to position II, and the microcolumn is inserted in the eluent line, stripping out the retained analyte. The KSCN present in the eluent solution forms an intense red complex with iron $[Fe(SCN)_x]^{x-3}$, (x ranging 1 – 6),[14] which absorbs at 480 nm. This solution is mixed in the C_{R2}, and subsequently directed to the spectrophotometer (480 nm), and finally to the waste. After a suitable elution time (60 s, unless otherwise stated), the central part of the injector-commutator is positioned at position I, and the column is reconditioned with water and a buffer solution. After a period (30 s, unless otherwise stated), the water channel is substituted by the sample solution and a further preconcentration cycle is carried-out. The total time for a preconcentration cycle and regeneration of the sorbent is 210 s, unless otherwise stated.

Results and Discussion

Synthesis and characterization of the 7-amino-4-azaheptyl anchored silica gel (AAHSG)

The organofunctionalization grade of the AAHSG sorbent obtained by CHN elemental analysis was 0.70 mmol of groups 7-amino-4-azaheptyl per gram of the sorbent. The presence of the organic groups was also confirmed by infrared spectroscopy.

The specific surface area of the AAHSG sorbent was 230 m^2 g^{-1}, slightly lower than that of pure silica, 250 m^2 g^{-1}, as was expected considering a homogeneous monolayer covering of the surface. The obtained pore-size distribution curves presented a distribution between 5 and 11 nm in diameter.

Isotherms of the adsorption of Fe^{2+}, Fe^{3+} and Cu^{2+} on AAHSG

The ions Fe^{2+}, Fe^{3+}, and Cu^{2+} were placed into contact with the AAHSG adsorbent for 180 min in order to evaluate the adsorption capacity of this sorbent for these analytes using a batch procedure (Fig. 2). The maximum adsorption capacity of Fe^{2+}, Fe^{3+} and Cu^{2+} were 0.18, 0.55 and 0.29 mmol g^{-1} (9.1, 31, and 18 mg g^{-1}), respectively. These results indicate that Fe^{3+} presents a higher affinity by the AAHSG sorbent in relation to Cu^{2+} and Fe^{2+} at pH 6. Other ions were also tested, and presented a lower affinity by the sorbent at pH 6. These results will be shown in the detection concerning to the interference studies.

In this work, no further investigations were carried out with Fe^{2+}, since it is aerially oxidized to Fe^{3+} in water samples, because this kind of sample is usually preserved in 0.1 – 0.2% v/v HNO_3. Usually, the iron contents are expressed as the total iron concentration form. For the reasons presented above, Fe^{3+} was chosen for its determination in natural water samples employing an on-line preconcentration system, optimized as described below.

Optimization of the flow system for the preconcentration and figures of merit

The amount of Fe^{3+} that percolates the column is an important variable to be optimized. The more analyte that percolates the column, the higher is the obtained analytical signal, up to the adsorption capacity of the column, is not surpassed. It was observed that when 4.5 ml min^{-1} of 400 ng ml^{-1} Fe^{3+} was passed through the column, the highest analytical signal was achieved. For lower sample flow rates, the repeatability of the measurements was worse, but with an increase of the sample flow rate, the %RSD of the measurements (n = 3) was better than 1.5%. The sample flow rate was fixed at 4.5 ml min^{-1} for improving this work.

It was observed that the maximum signal was obtained when the pH of the buffer solution for the preconcentration was fixed at 6.0 – 6.5. At lower pH values, there is a competition of the amino groups by protons, since these sites are not available for complex formation. At pH values higher than 7, Fe^{3+} forms iron hydroxides species, decreasing its sorption on the AAHSG. In order to obtain the maximum signal, the acidity of the buffer solution was adjusted to pH 6.2 using acetic acid/sodium acetate.

Another variable optimized was the flow rate of the buffer solution; it was observed that the best results were obtained when this variable was set at 2.0 – 2.5 ml min^{-1}. For lower flow rates, the buffer solution (pH 6.2) was not efficient for mixing with the sample solution (400 ng ml^{-1} Fe^{3+}, pH 1), flowing at 4.5 ml min^{-1}, in order to keep the amino groups of the sorbent non-protonated. It was also observed that, for flow rates lower than 2.0 ml min^{-1} of the buffer solution, the time to generate the sorbent for a subsequent preconcentration cycle should be increased, while reducing the sample throughput. For flow rates higher than 2.8 ml min^{-1}, the dispersion was increased, resulting in a decrease of the analytical signal. As a compromise between the sensitivity and the sample throughput, the flow rate of the buffer solution for the preconcentration of Fe^{3+} was fixed at 2.5 ml min^{-1}.

Other important variable for the preconcentration of elements in the flow system is the composition of the eluent. In our previous experiments, only HCl was used as an eluent, and KSCN was added in a confluence point, after the column. In this configuration, the concentration of HCl required for the elution was at least 1.0 mol l^{-1}. This high acid concentration utilized in the eluent required a regeneration step, using a buffer solution at pH 6.2, for a period of at least 60 s, because the amino groups of the AAHSG were protonated. This inconvenience leads a diminution of the sample throughput. In order to overcome these difficulties, a configuration of the flow system, as described in Fig. 1, was employed, where the eluent was formed by a mixture of HCl with KSCN. This latter component served for stripping out Fe^{3+} from the AAHSG, as well as a chromogenic agent for detecting the analyte. The effect of the concentration of KSCN presented on the eluent for the preconcentration of Fe^{3+} was also studied. It was observed

Table 1 Determination of Fe^{3+} in water samples (n = 5) employing an on-line preconcentration system

Sample	$[Fe^{3+}] \pm$ %RSD/ng ml^{-1}		
	Added	Found	Recovery, %
NIST-SRM 1640[a]	0.00	35.6 ± 1.1	—
	30.0	66.7 ± 1.9	103.1
NIST-SRM 1643d[b]	0.00	90.4 ± 1.3	—
	30.0	118.9 ± 2.0	98.3
Countryside river water	0.00	243 ± 1.2	—
	30.0	276 ± 2.1	101.2
Lagoon water	0.00	238 ± 3.0	—
	30.0	275 ± 2.9	102.9
Springwater I	0.00	50 ± 2.0	—
	30.0	79.3 ± 2.4	98.6
Springwater II	0.00	101 ± 2.1	—
	30.0	126 ± 1.7	95.0
Springwater III	0.00	48.8 ± 1.7	—
	30.0	77.8 ± 1.9	98.0
Stream water	0.00	181 ± 1.3	—
	30.0	210 ± 1.7	99.4
Streamlet water	0.00	197 ± 3.3	—
	30.0	220 ± 2.5	96.4
Well water I	0.00	429 ± 1.4	—
	30.0	468 ± 1.1	102.1
Well water II	0.00	228 ± 2.3	—
	30.0	259 ± 1.8	100.4
Well water III	0.00	191 ± 2.4	—
	30.0	219 ± 2.0	99.0

The samples were spiked with 30 ng ml^{-1} Fe^{3+}.
a. Certified value 34.3 ± 5% ng ml^{-1}.
b. Certified value 91.2 ± 4% ng ml^{-1}.

that 4.0% m/v KSCN is the best concentration for obtaining higher signals. The effect of the HCl concentration presented on the eluent for the preconcentration of Fe^{3+} was also studied, since 0.2 mol l^{-1} HCl is sufficient for obtaining the maximum signal. Based on these results, the best composition of the eluent for the preconcentration was 4.0% KSCN plus 0.2 mol l^{-1} HCl.

The eluent flow rate was also optimized. It was observed that the best eluent flow rate was 1.0 – 1.2 ml min^{-1}. For eluent flow rates lower than 1.0 ml min^{-1} the analytical signal was significantly diminished, and the reproductivity of the measurements was compromised. For eluent flow rates higher than 1.5 ml min^{-1} the analytical signal was also diminished, probably due to dilution of the analyte stripped out from the AAHSG sorbent; it was also observed that the standard deviation of the measurements increased. For these reasons, the eluent flow rate was fixed at 1.2 ml min^{-1}.

The last variable to be studied was the preconcentrantion time. The Fe^{3+} preconcentration linearly increased with the time of preconcentration up to 210 s; after that the preconcentration levelled off. In order to not decrease the sample throughput, the preconcentration time was fixed at 120 s. In this situation, the sample throughput was 17 measurements per hour.

Using all of the optimized conditions for the preconcentration of Fe^{3+} on the AAHSG sorbent, an analytical curve for the preconcentration was achieved ($A = 3.78 \times 10^{-3} + 2.27 \times 10^{-3}[Fe^{3+}]$, $r = 0.99984$, and Fe^{3+} expressed in ng ml^{-1}). The linearity was obtained for a Fe^{3+} solution ranging from 30 to 600 ng ml^{-1}. The obtained preconcentration factor was 82.2 and the detection limit, defined as [3σ/slope analytical curve], where σ is the standard deviation of a blank determination n = 20, was 5.9 ng ml^{-1}. The quantification limit [10σ/slope analytical curve] was 19.6 ng ml^{-1} (n = 10).

Table 2 Comparison among procedures for Fe^{3+} preconcentration

Sorbent	Characteristics	Ref.
Silica immobilized brow alga	On-line preconcentration, ICP-AES detection; preconcentration factor, 7; DL 11 ng ml^{-1}; total preconcentration time, 2 min	16
Chelex 100-iminodiacetic resin	On-line preconcentration, ICP-AES detection; preconcentration factor, 58.6; total preconcentration time, 2.73 min; DL, 8.4 ng ml^{-1}	17
8-Hydroxy-quinoline immobilized on controlled pore glass	On-line preconcentration, IC-HPLC; postcolumn detection; visible spectrophotometry; DL, 50 mg l^{-1}	18
DAPPS	On-line preconcentration, visible spectrophotometry detection; adsorption capacity, 0.55 mol g^{-1}; preconcentration factor, 82.2; total time of preconcentration, 3.5 min; DL, 5.9 ng ml^{-1}	This work

DL: detection limit.

Interference studies

The effect of several elements on the sorption of 400 ng ml^{-1} Fe^{3+} on the AAHSG sorbent (0.12 g) was investigated. The tolerance level was established at 100 ± 5% as a reference. Na^+ and K^+ ions could be tolerated up to 5000 mg l^{-1}, Ca^{2+} and Mg^{2+} up to 1000 mg l^{-1}, Al^{3+} up to 10 mg l^{-1}, Ba^{2+} up to 20 mg l^{-1}, Co^{2+} up to 10 mg l^{-1}, Cu^{2+} up to 10 mg l^{-1}, Cr^{3+} up to 5 mg l^{-1}, Mn^{2+} up to 10 mg l^{-1}, Ni^{2+} up to 10 mg l^{-1}, Zn^{2+} up to 20 mg l^{-1}. Based on these results, it can be concluded that the method could be successfully applied to the determination of Fe^{3+} in natural water samples, and brackish water, since the concentration of the concomitant species in these kind of samples are usually lower than the proposed preconcentration method can tolerate.[15]

Determination of Fe^{3+} in water samples using the proposed preconcentration system

The proposed preconcentration system using AAHSG as a sorbent was employed for the determination of Fe^{3+} (n = 5) in nine ordinary natural water samples and two reference materials, which were employed for attaining the accuracy of the method (Table 1). Besides that, a recovery study was also carried out, by spiking the natural water samples with 30 ng ml^{-1} Fe^{3+}. The recoveries ranged from 95.0 to 103.1%.

Based on the results of Table 1, it can be inferred that Fe^{3+} can be successfully determined in natural water samples, with good accuracy, employing a simple preconcentration system using AAHSG as a sorbent and spectrophotometric detection.

Comparison among several preconcentration methods for iron(III)

In Table 2 are presented some preconcentration procedures for Fe^{3+} determination, employing different sorbents with on-line column preconcentration systems.

As can be seen, the detection limit of this work is slightly lower than the already published on-line preconcentration procedures for iron(III) determination. This analytical characteristic can be attributed to the higher adsorption capacity (0.55 mmol g^{-1}) of the AAHSG sorbent, which permits higher preconcentration factors with good detection limits, able to determine this analyte in real samples.

A simple flow preconcentration system for the determination of Fe^{3+} using KSCN as a chromogenic agent and AAHSG as a sorbent was successfully employed for the determination of the analyte in natural and brackish water samples. The AAHSG sorbent used presents a suitable particle size, surface area and porosity, with homogeneous organic chelating groups covering. A preconcentration factor of 82.2 became the proposed method with a detection limit suitable for iron(III) determination in natural water samples.

Acknowledgements

We acknowledge Pró-Reitoria de Pesquisa da Universidade Federal do Rio Grande do Sul, FAPERGS and CNPq for financial support and fellowships.

References

1. E. C. Lima, J. L. Brasil, and A. H. D. P. Santos, *Microchim. Acta*, **2004**, *146*, 22.
2. J. L Brasil, E. C. Lima, R. C. Veses, and M. M. Tisott, *At. Spectrosc.*, **2004**, *25*, 94.
3. N. G. Becka, R. P. Franks, and K. W. Bruland, *Anal. Chim. Acta*, **2002**, *455*, 11.
4. K. Oshita, J. Xu, Y. H. Gao, K. H. Lee, M. Oshima, and S. Motomizu, *Bull. Chem. Soc. Jpn.*, **2003**, *76*, 1555.
5. C. E. Harland, "*Ion Exchange: Theory and Practice*", 2nd ed., **1994**, Royal Society of Chemistry, Cambrige, UK.
6. P. Liu, Q. Pu, and Z. Su, *Anal. Sci.*, **2003**, *19*, 409.
7. S. Zhang, Q. Pu, P. Liu, Q. Sun, and Z. Su, *Anal. Chim. Acta*, **2002**, *452*, 223.
8. M. Zougagh, A. G. Torres, and J. M. Pavón, *Talanta*, **2002**, *56*, 753.
9. J. C. P. Vaghetti, M. Zat, K. R. S. Bentes, L. S. Ferreira, E. V. Benvenutti, and E. C. Lima, *J. Anal. At. Spectrom.*, **2003**, *18*, 376.
10. L. T. Arenas, J. C. P. Vaghetti, C. C. Moro, E. C. Lima, E. V. Benvenutti, and T. M. H. Costa, *Mater. Lett.*, **2004**, *58*, 895.
11. C. Airoldi and R. F. Farias, *Quim. Nova*, **2000**, *23*, 496.
12. S. Brunauer, P. H. Emmett and E. Teller, *J. Am. Chem. Soc.*, **1938**, *60*, 309.
13. E. P. Barret, L. G. Joyner, and P. P. Halenda, *J. Am. Chem. Soc.*, **1951**, *73*, 373.
14. A. I. Vogel, "*Química Analítica Qualitativa*", Editora Mestre Jou, **1981**, São Paulo-SP, 274 – 275.
15. Database of Natural Matrix Reference Materials, compilation prepared by International Atomic Energy Agency (IAEA), last update January **2003**, http://www.iaea.org/programmes/nahunet/e4/nmrm/browse.htm, website visited on September 10th, 2004.
16. E. N. V. M. Carillho, J. A. Nóbrega, and T. R. Gilbert, *Talanta*, **2003**, *60*, 1131.
17. C. Pons, M. Miro, E. Becerra, J. M. Estela, and V. Cerda, *Talanta*, **2004**, *62*, 887.
18. M. R. B. Adas, I. A. Takruni, Z. Abdullah, and N. M. Tahir, *Talanta*, **2002**, *58*, 883.

Available online at www.sciencedirect.com
SCIENCE DIRECT
Spectrochimica Acta Part A 62 (2005) 398–406
SPECTROCHIMICA ACTA PART A
www.elsevier.com/locate/saa

Use of 1,3-diaminepropane-3-propyl grafted onto a silica gel as a sorbent for flow-injection spectrophotometric determination of copper (II) in digests of biological materials and natural waters

Sandra V.M. de Moraes [a], Jorge L. Brasil [a], Caroline D. Milcharek [a], Lucas C. Martins [a], Marina T. Laranjo [a], Márcia R. Gallas [b], Edílson V. Benvenutti [a], Eder C. Lima [a,*]

[a] *Instituto de Química, UFRGS, CP 15003, CEP 91501-970 Porto Alegre, RS, Brazil*
[b] *Universidade Federal do Rio Grande do Sul-Instituto de Física, Porto Alegre, RS, Brazil*

Received 13 October 2004; received in revised form 17 January 2005; accepted 17 January 2005

Abstract

The 1,3-diaminepropane-3-propyl-anchored silica gel (DAPPS) was successfully employed as a sorbent in a spectrophotometric flow system for the preconcentration of Cu^{2+} in digests of biological materials (maize powder, soybean, citrus leaves, corn stalks) as well as water samples (river, stream, streamlet, springwater and well). The system presented a minicolumn packed with DAPPS, where the sample solution was passed through it for a period of time, and subsequently, an eluent solution, stripped-out the retained analyte which was further determined with DDTC at 460 nm.

The better preconcentration conditions utilized were: 120 s loading, 60 s elution, 30 s regeneration of the column, loading flow rate 6.5 ml min^{-1}, buffer solution for the preconcentration and regeneration of the column-borate buffer pH 8.5, elution flow rate 2.3 ml min^{-1}, time of elution 60 s, eluent composition, 0.4 mol l^{-1} HNO_3. Under these conditions, the preconcentration factor obtained was 36, and the detection limit achieved was 8.4 ng ml^{-1} in water samples and 0.84 μg g^{-1} in biological material. The maximum adsorption capacity of DAPPS to Cu^{2+} was 0.49 mmol g^{-1} (31.1 mg g^{-1}) obtained in a batch system.

The recovery of copper in the water samples ranged from 96.9 to 102.4% and in the biological materials ranged from 97.0 to 102.6%.

Keywords: Preconcentration of copper; Flow-injection spectrophotometry; Biological materials and waters; Organo-functionalized silica gel

1. Introduction

Spectrophotometry is not usually employed for the determination of analytes in real samples because it suffers severe interferences of concomitants present in the sample matrix. Therefore, its use for determination of analytes in real samples requires a separation procedure. Among the several separation procedures, solid-phase extraction is the most attractive because it does not require the use of hazardous solvents, which generates large volumes of waste that need to be treated subsequently [1], besides being a time-consuming procedure that leads to a decrease of the sampling throughput. Modified silica with different organic groups is one of the most successful sorbents employed in the analytical laboratories, because the silica supports does not swells or shrinks such as the polymeric resin [2], and unmodified natural occurrence materials [3]; allows the modified silica sorbent to be used during several cycles of preconcentration, because the retention process (adsorption, chelation, ion exchange) are reversible [4,5]; the modified silica may be employed in aqueous and organic solvents media [4,5]; they present good thermal stability [4,5] and appropriated accessibility of the ions to the attached chelating groups; in addition, the modified silica gel exhibits sorption capacities higher than polymeric resins, because the number of organic molecules immobilized on the support surface is higher, allowing high preconcentration factors [1,4,5].

The organofunctionalized silica may be obtained by just impregnating the support with an organic substance [6,7],

* Corresponding author. Tel.: +55 51 3316 7175; fax: +55 51 3316 7304.
E-mail address: ederlima@iq.ufrgs.br (E.C. Lima).

1386-1425/$ – see front matter © 2005 Elsevier B.V. All rights reserved.
doi:10.1016/j.saa.2005.01.007

by sol–gel method [8–11], or by grafting an organic pendant group to silica [12–19]. The first procedure does not produce a suitable material for the preconcentration of metals because surface coverage of organic substances in the silica support is low, leading as consequence to low preconcentration factors, in addition, the achieved analytical signal decreases with the number of preconcentration cycles. The silica obtained from the sol–gel method for preconcentration of metals has few analytical applications to real samples [9,11], because this kind of silica synthesis leads to a microporous materials which are not compatible for reversible preconcentration systems [10]. The grafting of organic groups to silica material is the most efficient method for modeling sorbents with desired chelating properties [4,5,20].

Flow-injection preconcentration systems using mini-columns packed with a suitable sorbent for the preconcentration of several analytes in the most different kinds of sample has been successfully employed [18,19,21–26]. This procedure presents several advantages over conventional column preconcentration procedures such as diminution of total time of preconcentration of several hours to carry out just one cycle [21–26] to just few minutes which increases the sampling throughput remarkably; higher repeatability of the measurements acquired with flow systems [27]; diminution of risk of contamination because the manual operation is diminished [21,22,27]. However, flow-injection preconcentration systems present several advantages; it has been coupled to mainly to flame atomic absorption spectrometry (FAAS) [18,19,24,28–32] and inductively coupled plasma atomic emission spectrometry (ICP-AES) [23–26,33]. On the other hand, the applications of flow-injection preconcentration system coupled to spectrophotometry for the determination of metallic ions are scarce [34], there being a need to be explored more extensively. In order to achieve this application, more selective sorbents should be employed, since spectrophotometry alone, does not provide enough selectivity for the determination of analytes in real sample matrices.

In this paper, 1,3-diaminepropane-3-propylsilica (DAPPS) as a selective copper (II) sorbent was successfully employed for its preconcentration in digests of botanic material as well as natural water samples. It was observed that at pH 8, measured at the effluent of the column, the ions Fe^{3+}, Mn^{2+}, Zn^{2+}, Al^{3+}, Cr^{3+}, Co^{2+}, Ni^{2+} were not sorbed on DAPPS.

2. Experimental

2.1. Instruments

A 600 S Femto spectrophotometer (São Paulo, SP, Brazil) provided with 150 μl flow cell (Femto) and a serial port RS232C connected to AMD K6II 350 MHz personal computer for data acquisition were employed throughout for the analytical measurements. Two four-channel Milam bp-200 peristaltic pumps (Colombo, PR, Brazil) provided with Tygon® and silicone tubes of different diameters were used for the propulsion of the solutions in the flow system. For the pH measurements, a pH/mV hand-held meter handylab 1 Schott (Mainz, Germany) provided with combined glass electrode model BlueLine 23 pH was used.

2.2. Reagents and solutions

Doubly distilled water was employed throughout. Solutions containing 0.1–1.0 mol l^{-1} of nitric acid (Merck, Rio de Janeiro, RJ, Brazil) was employed as eluent. A 1.00 g l^{-1} copper (II) stock solution was prepared dissolving 0.5 g of metallic copper, weight with the precision of the tenth of milligram (Merck, Rio de Janeiro, RJ, Brazil) in 10 ml of (1 + 1, v/v) nitric acid–water and this solution was quantitatively transferred to a 500-ml calibrated flask and the volume was completed to the mark with distilled water. The calibration solutions within 25–400 ng ml^{-1} (preconcentration) and 1000–5000 ng ml^{-1} (without preconcentration) of Cu^{2+} range were prepared by suitable serial dilution of the stock solution with doubly distilled water and adjusting the final acidity to pH 1.0 with HNO_3.

A 0.15% (m/v) of sodium diethyldithiocarbamate (DDTC; Merck, Darmstadt, Germany) solution was daily prepared by dissolving 0.375 g of DDTC in 5 ml of ethanol; afterwards this solution was mixed with 150 ml of hot water (≈70–80 °C), and then filtered to 250 ml volumetric flask and the volume completed to the mark with distilled water.

For the buffer preparations, glacial acetic acid (Merck, Rio de Janeiro, Brazil), sodium acetate (Merck, Rio de Janeiro, Brazil), ammonium acetate (Merck, Rio de Janeiro, Brazil), boric acid (Merck, Rio de Janeiro, Brazil), sodium tetraborate decahydrate (Vetec, Rio de Janeiro, RJ, Brazil), potassium hydroxide (Reagen, Rio de Janeiro, RJ, Brazil), hydrochloric acid (Merck, Rio de Janeiro, Brazil) were employed.

For the interference studies, the following salts of elements were employed: NaCl (Merck, Rio de Janeiro, RJ, Brazil), $NaH_2PO_4{\cdot}7H_2O$ (Reagen, Rio de Janeiro, RJ, Brazil), $Na_2SO_4{\cdot}10H_2O$ (Merck, Rio de Janeiro, RJ, Brazil), KCl (Merck, Rio de Janeiro, RJ, Brazil), $MgSO_4{\cdot}7H_2O$ (Merck, Rio de Janeiro, RJ, Brazil), $CaSO_4{\cdot}2H_2O$ (Merck, Rio de Janeiro, RJ, Brazil), $AlCl_3{\cdot}6H_2O$ (Merck, Rio de Janeiro, RJ, Brazil), $CoSO_4{\cdot}7H_2O$ (Vetec, Rio de Janeiro, RJ, Brazil), $Ba(NO_3)_2$ (Reagen, Rio de Janeiro, RJ, Brazil), $CrCl_3{\cdot}6H_2O$ (Vetec, Rio de Janeiro, RJ, Brazil), $FeSO_4{\cdot}NH_4SO_4{\cdot}6H_2O$ (Merck, Rio de Janeiro, RJ, Brazil), $MnSO_4{\cdot}H_2O$ (Reagen, Rio de Janeiro, RJ, Brazil), $ZnSO_4{\cdot}7H_2O$ (Nuclear, Diadema, SP, Brazil), $NiSO_4{\cdot}6H_2O$ (Reagen, Rio de Janeiro, RJ, Brazil).

2.3. Synthesis and characterization of the 1,3-diaminepropane-3-propylsilica (DAPPS)

An amount of 15 mmol of 1,3-diaminepropane was first activated using 15 mmol of sodium hydride in 10 ml

of a mixture of aprotic solvent (toluene:tetrahydrofuran) (1:1) (Merck, Hohenbrunn, Germany) for 30 min, and then 15 mmol of 3-chloropropyltrimethoxisilane (CPTMS, Acros Organics, New Jersey, USA) was added. The mixture was stirred under argon at solvent-reflux temperature for a period of 5 h. The solution was than centrifuged, to eliminate the byproduct sodium chloride. The product of reaction, 1,3-diaminepropane-3-propyltrimethoxysilane (AMSIL) was then used as organic precursor reagent for the silica grafting reaction.

Silica gel (Merck, Darmstadt, Germany) 0.02–0.05 mm of particle size and a surface area of 250 $m^2\,g^{-1}$ was activated at 150 °C under vacuum (10^{-1} Pa) for 5 h. The AMSIL was dissolved in 300 ml of toluene and the activated silica (10 g) was then added. The mixture was stirred for 48 h under argon at solvent-reflux temperature. The modified silica was filtered under argon in a Schlenk apparatus, washed with toluene, hexane, ethyl alcohol, doubly distilled water and ethyl ether (supplied by Merck, Hohenbrunn, Germany). The resulting sorbent 1,3-diaminepropane-3-propylsilica (DAPPS) was dried for 2 h under vacuum at 120 °C. The DAPPS presented a specific surface area 230 $m^2\,g^{-1}$ and a coverage of silica surface of 0.70 mmol of 1,3-diaminepropane groups per gram of sorbent.

2.4. Samples

Ordinary samples of maize powder, soybean, citrus leaves, corn stalks and water samples (river, stream, streamlet, springwater and well) were employed. The following reference materials were employed for attaining the accuracy of the method, Chlorella (NIES-CRM-03) from National Institute for Environmental Studies (NIES, Ibaraki, Japan), Apple Leaves (NIST-SRM 1515) and Trace Elements in Natural Water (NIST-1640) from National Institute of Standards and Technology (NIST, Gaithersburg, USA).

The ordinary water samples were filtered with Whatman paper pH adjusted to 1.0 with HNO_3 and analyzed employing the procedure of preconcentration.

The solid samples were digested in triplicate with nitric acid plus hydrogen peroxide using a block digestor (Tecnal, Piracicaba, SP, Brazil) according to the following procedure [37]: 0.5 g of sample was accurately weighed with a precision of the tenth of milligram, and transferred to a 25-cm long borosilicate digestion tube (25 mm internal diameter), followed by the addition of 5.0 ml concentrated HNO_3; the mixture was digested at temperatures not exceeding 160 °C for 8 h. Afterwards, the digestion tubes were stand to reach the room temperature. Thereafter, 2.0 ml of 30% (m/m) H_2O_2 (Merck, Rio de Janeiro, Brazil) were dropwise added, and the block digestor was heated to 100 °C for about 30 min, obtaining a colorless solution. The excess of HNO_3 was driven off by gently heating, and during this procedure water was added to the tubes to avoid dryness. The volume was made up to 50 ml with water (1.0%, v/v, HNO_3 final acidity) and the resulting solution was analyzed in the flow system.

2.5. Isotherms of adsorption of Cu^{2+} on DAPPS

A 10-ml of sample solution containing 7.87×10^{-6} to 1.55×10^{-2} mol l^{-1} of Cu^{2+} solution plus 10.0 ml of borate buffer solution (pH 8.0) was transferred to a 50-ml conical polyethylene flask containing 20 mg of sorbent. These flasks were placed in a horizontal shaker and agitated for 180 min in order to adsorb the analyte. Subsequently, the solid phase was separated from aqueous phase by filtration, being the aqueous phase retained for analysis.

The Cu^{2+} contents, which were not retained in the sorbent, were spectrophotometrically determined, using 0.15% (m/v) sodium diethyldithiocarbamate (DDTC) as chromogenic agent. The measurements were carried out using a FEMTO 600 S spectrophotometer, according to the following procedure: an aliquot of 1.00 ml of aqueous phase and/or analyte standard solution plus 1.00 ml of chromogenic reagent plus 1.00 ml of water were added to a Hellma glass cuvette (10 mm of optical path). The analyte solutions with concentration higher than those cited above were properly diluted with distilled water. The metal ion adsorption capacity of the solid phase (N_f), obtained in the saturation plateau, was calculated by applying the equation $N_f = (C_s - C_e) \times V/m$, where C_s is the initial metal concentration, C_e the metal concentration at the equilibrium found in the solution in equilibrium with the solid phase, V the volume of the solution put with the sorbent, and m the mass of the solid phase.

2.6. Flow system

For the determination of Cu^{2+} in the samples, a home-made injection valve made of Perspex was used [38]. The glass minicolumn (4 cm, ID 2.5 mm, 0.11 g of sorbent) was placed in the central position of the injection valve and was utilized for the analyte preconcentration. Also, two peristaltic pumps, 0.8 mm ID polyethylene transmission lines, Perspex connectors, flow cell and spectrophotometer were mounted as depicted in Fig. 1. Initially, for developing the method, the system employed a loop instead of a minicolumn. In the preconcentration position (position I), the sample solution (25–400 ng ml^{-1} Cu^{2+}, 6.5 ml min^{-1}, pH 1) and the buffer solution B_1 (0.8 mol l^{-1} borate buffer, pH 8.5; 4.3 ml min^{-1}) are merged in the confluence point X, subsequently these solutions are mixed in the coil C_1 (100 μl) and directed to the minicolumn, for sorbing the analyte present in the sample solution and the aqueous phase is directed to the waste W_s (pH 8 measured at the effluent of column). In the second channel, the carrier solution E (0.4 mol l^{-1} HNO_3; 2.3 ml min^{-1}) is being pumped to the system where at confluence point Y it merges with B_2 buffer solution (0.8 mol l^{-1} borate buffer, pH 8.5; 2.3 ml min^{-1}) and mixed in the coil mixer C_2 (200 μl), then the buffered sample zone reaches the

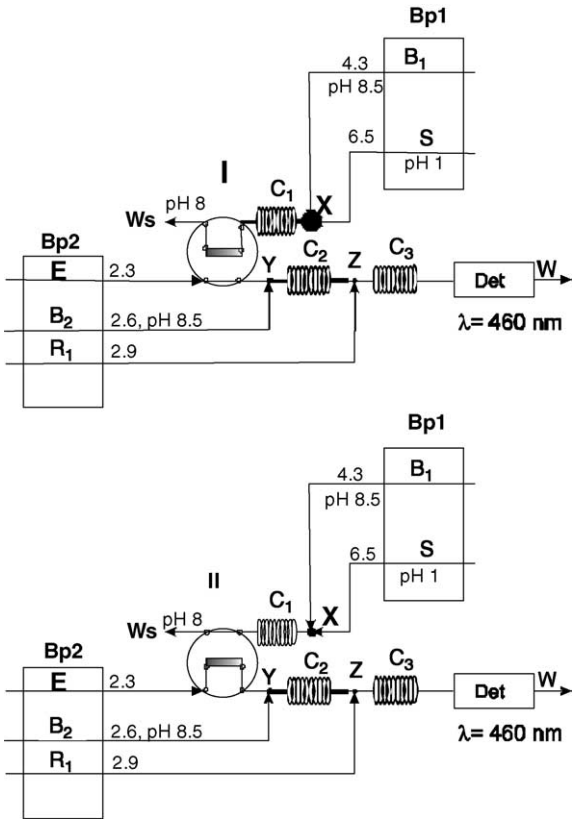

Fig. 1. Manifold employed for the determination of Cu^{2+} in the samples. I, preconcentration position; II, eluting position. B_1, 0.8 mol l^{-1} borate buffer solution; S, sample solution (pH 1); W and W_s, wastes; E, eluent 0.4 mol l^{-1} HNO_3; R_1, 0.15% DDTC; B_2, 0.8 mol l^{-1} borate buffer solution; C_1, C_2 and C_3, coil reactors, 100, 100, and 200 μl, respectively; Bp1 and Bp2, peristaltic pumps; Det, spectrophotometric flow cell, 150 μl, λ = 460 nm. X, Y, Z, confluence points. The flow rates are expressed in ml min^{-1}.

confluence point Z, where it merges with reagent R_1 (0.15%, m/v, DDTC; 2.9 ml min^{-1}) and subsequently it reaches the mixture coil C_3 (200 μl) and this sampling zone passes in the flow cell (150 μl) of the spectrophotometer (460 nm) producing the baseline and subsequently this solution is directed to the waste (W). After 120 s of preconcentration period, unless otherwise stated, the injection valve is positioned in the elution position (position II), and the minicolumn is inserted in the eluent line, eluting the retained analyte at flow rate of 2.3 ml min^{-1}. At the confluence point Y, the sample zone merges with B_2 buffer solution and mixed in the coil mixer C_2, then the buffered sample zone reaches the confluence point Z where it merges with the chromogenic reagent and then mixed in the coil mixer C_3 (200 μl) forming the $Cu(DDTC)_2$ complex [39]. This zone is subsequently directed to the flow cell of the spectrophotometer (460 nm), producing a transient signal, and finally this zone is directed to the waste (W). During the elution and reaction color developing step, the sample solution is replaced by water and this plus the B_1 buffer solution are directed to the waste (W_s). After the suitable elution time (60 s, unless otherwise stated), the injection valve is positioned in the position I, and the column is reconditioned with water and buffer solution. After a period (30 s, unless otherwise stated), the water channel is substituted by sample solution and a further preconcentration cycle is carried out. The total time for a preconcentration cycle and regeneration of the sorbent is 210 s, unless otherwise stated.

3. Results and discussion

3.1. Optimization of flow system conditions without preconcentration

The first variable investigated for the optimization of the reaction between Cu^{2+} and DDTC was the pH. Several 0.5–2.0 mol l^{-1} buffer solutions, in order to support higher acidic concentration of real samples, with pH ranging from 4.5 to 10.5 were tested. It was observed that the pH interval for Cu^{2+} determination with DDTC is large ranging from 5.5 to 9.0. Then at first approach, 0.8 mol l^{-1} borate buffer with pH adjusted to 8.5 was chosen for the color forming reaction. The flow rate of the buffer solution was also investigated from 2.0 to 5.0 ml min^{-1}. It was observed that the best sensitivity occurred at flow rates of 2.6 ml min^{-1}.

The concentration of DDTC was fixed at 0.15% (m/v) because of the limited solubility of this reagent however the chromogenic agent flow rate was investigated. It was observed that DDTC flow rates ranging from 2.6 to 4.0 ml/min did not presented significant changes in the analytical signals. A flow rate of 2.9 ml min^{-1} DDTC was employed throughout this work.

The dimensions of coil reaction C_2 and C_3 were also investigated, and the dimensions that promoted the highest and sharpest analytical signal was 100 and 200 μl, respectively. The C_2 reaction coil serves to buffer the sample zone previously to the addition of the chromogenic agent. After adding the DDTC to the buffered sample zone, this reaction zone is mixed in the reaction coil C_3. It should be stressed that higher volumes of reaction coils (C_2 and C_3) leaded to broad peak profiles that lasted more than 25 s to return the baseline after the appearing of the maximum of the peak.

The sample loop was varied from 75 to 500 μl. As a compromise between the sensitivity and sharpness of the peak profile, a sample loop of 375 μl (75 cm) was chosen. For sample loop of 500 μl (100 cm) the analytical signal achieved was broaden. Also it was observed that the time for the analytical signal to return to the baseline after the maximum of peak appearance was more than 25 s.

The last variable investigated for the optimization of the flow system without preconcentration, for the color forming reaction was the concentration of the HNO_3, used as carrier solution, ranging from 0.1 to 1.0 mol l^{-1}, and also its flow rate. The best conditions were obtained when 0.4 mol l^{-1} HNO_3 at flow rate of 2.6 ml min^{-1} were employed. Under these conditions the analytical calibration curve, without pre-

concentration, was performed obtaining the following equation $A = -4.24 \times 10^{-3} + 6.06 \times 10^{-5}$ [Cu^{2+}], $r = 0.99801$ for copper (II) concentration expressed in ng ml^{-1}.

3.2. Optimization of the flow system for the preconcentration and figures of merit

The amount of Cu^{2+} that percolates the column is an important variable to be optimized. The more analyte percolates the column, higher is the analytical signal obtained until the saturation of the sorbent is attained [21,22]. In Fig. 2A is shown the effect of sample flow rate on the analytical signal. It was observed that 6.5 ml min^{-1} of 250 ng ml^{-1} Cu^{2+} passing through the column, the highest analytical signal was achieved, being this sample flow rate chosen for improving this work.

The DAPPS sorbent presents two amino groups which chelate the metal ion, as depicted in Scheme 1. The formation of five and six member rings chelates are thermodynamically favorable leading to a high complex formation constants (K_f), however, the conditional complex formation constant depends strongly on the pH the reaction [35,36]. In Fig. 2B is presented the effect of the pH, of the buffer solution in the exit of the minicolumn, on the sorption of Cu^{2+} on the DAPPS. As can be seen, the maximum signal was obtained, when the pH of the buffer solution in the exit of the minicolumn was fixed 7.0–8.5. Based on these results, the buffer solution employed for the preconcentration of Cu^{2+} in acidic water samples (pH 1) was 0.8 mol l^{-1} borate buffer pH adjusted 8.5, which allow a solution at the exit of the minicolumn with pH 8.

In Fig. 2C is presented the effect of the flow rate of the buffer solution (pH 8.5) on the sorption of Cu^{2+} on the DAPPS sorbent. It is observed that the higher sensitivity obtained was when the flow rate of the buffer solution was set at 3.4–4.5 ml min^{-1}. For lower flow rates, the buffer solution (pH 8.5) was not efficient for mixing with the sample solution (250 ng ml^{-1} Cu^{2+}, pH 1) flowing at 6.5 ml min^{-1}, in order to keep the amino groups of the sorbent non-protonated. It was also observed that, for flow rates lower than 2.7 ml min^{-1} of the buffer solution, the time for the regeneration of the sorbent for a subsequent preconcentration cycle should be increased, reducing the sample throughput. For flow rates higher than 4.8 ml min^{-1}, the dispersion was increased resulting in a decrease of the analytical signal [27]. As a compromise between sensitivity and sample throughput, the flow rate of the buffer solution for the preconcentration of Cu^{2+} was fixed at 4.3 ml min^{-1}.

Other important variable for the preconcentration of elements in flow system is the composition of the eluent [21,22]. In previous studies, using the flow system with sample loop, the best sample carrier used was 0.4 mol l^{-1} HNO_3, which was suitable for removing the analyte from DAPPS column completely. Then the eluent was fixed as 0.4 mol l^{-1} HNO_3.

The eluent flow rate was also optimized (Fig. 2D). As can be seen, the best eluent flow rate is 2–2.5 ml min^{-1}. For eluent flow rates lower than 1.8 ml min^{-1} the analytical signal was significantly diminished, probably the amount of acid was not enough to strip-out all the retained analyte from the DAPPS minicolumn. For eluent flow rates higher than 2.9 ml min^{-1} the analytical signal also diminished, probably due to dilution of the analyte stripped out from the DAPPS sorbent [21,22]. By these reasons, the eluent flow rate was fixed at 2.3 ml min^{-1}.

The last variable to be studied was the time of preconcentration (Fig. 2E). The Cu^{2+} preconcentration was linearly increased with the time of preconcentration up to 180 s, after that the preconcentration was levelled off. In order to not decrease the sample throughput, the preconcentration time was fixed at 120 s. In this situation, the sample throughput was 17 measurements per hour.

Using all the optimized conditions of the preconcentration of Cu^{2+} on the DAPPS sorbent, the analytical curve for the analyte determination in water samples was achieved (Fig. 2F). The linearity was obtained for Cu^{2+} solution ranging from 50 to 400 ng ml^{-1}. For the copper determination in digests of biological materials, the linearity of the analytical curve ranged from 25 to 200 ng ml^{-1}.

The preconcentration factor obtained was 36 and the detection limit defined as ((blank + 3σ)/slope analytical curve), where σ is the standard deviation of blank determination ($n = 20$) was 8.4 ng ml^{-1}. The quantification limit ((blank + 10σ)/slope analytical curve) was 13.4 ng ml^{-1} ($n = 20$). Multiplying the detection limit and quantification limit by the dilution factor (100 ml g^{-1}), the detection and quantification limits attained for the biological materials were 0.84 and 1.34 μg g^{-1}, respectively.

In order to evaluate the adsorption capacity of DAPPS sorbent for Cu^{2+}, solutions of this element were placed into contact under agitation with the DAPPS adsorbent for 180 min using a batch procedure. The maximum adsorption capacity of Cu^{2+} was 0.49 mmol g^{-1} (31.1 mg g^{-1}) (see Fig. 3).

3.3. Interferences and recoveries studies

As it is known that DDTC form complexes with Cu^{2+}, Mn^{2+}, Zn^{2+}, Fe^{3+}, Co^{2+}, Ni^{2+}, Pb^{2+}, Cd^{2+}, Hg^{2+} [39], it is necessary to know if these ions will be retained in the DAPPS minicolumn. As the ions Pb^{2+}, Cd^{2+} and Hg^{2+} are always present in very lower concentrations than Cu^{2+} in biological materials and waters [40] these ions were not studied. In Fig. 4 is presented the sorption of 250 ng ml^{-1} Cu^{2+}, 5 mg l^{-1} Mn^{2+}, 5 mg l^{-1} Zn^{2+}, 50 mg l^{-1} Fe^{3+}, 5 mg ml^{-1} Co^{2+}, 5 mg ml^{-1} Ni^{2+} on DAPPS in function of the pH of the exit of the minicolumn, using 0.15% (m/v) DDTC as chromogenic reagent, and monitoring the analytical signal at $\lambda = 460$ nm, and all other Cu^{2+} optimized conditions. As can be seen at pH 8, all the tested concomitant species were not sorbed on DAPPS minicolumn. Therefore it is expected that the proposed method for Cu^{2+} preconcentration will be free from interferences with samples having up to 5 mg l^{-1} Mn^{2+}, 5 mg l^{-1} Zn^{2+}, 50 mg l^{-1} Fe^{3+}, 5 mg ml^{-1} Co^{2+}, 5 mg ml^{-1} Ni^{2+}.

A more extensive interference effects of other elements on the sorption of 250 ng ml^{-1} Cu^{2+} on the DAPPS sorbent (0.11 g) was also investigated (Fig. 5), employing the copper optimized conditions. The recovery value is defined as 100 times the relationship between the signal of Cu^{2+} plus concomitants divided by the signal of Cu^{2+} alone. The tolerance level was established at 100 ± 5% as a reference. The Na^{+} and K^{+} ions could be tolerated up to 5000 mg l^{-1}, Mg^{2+} up to 1000 mg l^{-1}, Ca^{2+} up to 500 mg l^{-1}, Al^{3+} up to 50 mg l^{-1}, Ba^{2+} up to 50 mg l^{-1}, Cr^{3+} up to 20 mg l^{-1}, SO_4^{2-} up to 500 g l^{-1}, PO_4^{3-} up to 200 g l^{-1}, and Cl^{-} up to 5000 g l^{-1}. Based on these results, it can be concluded that the method could be successfully applied to the determination of Cu^{2+} in digests of biological materials as well as natural waters, since

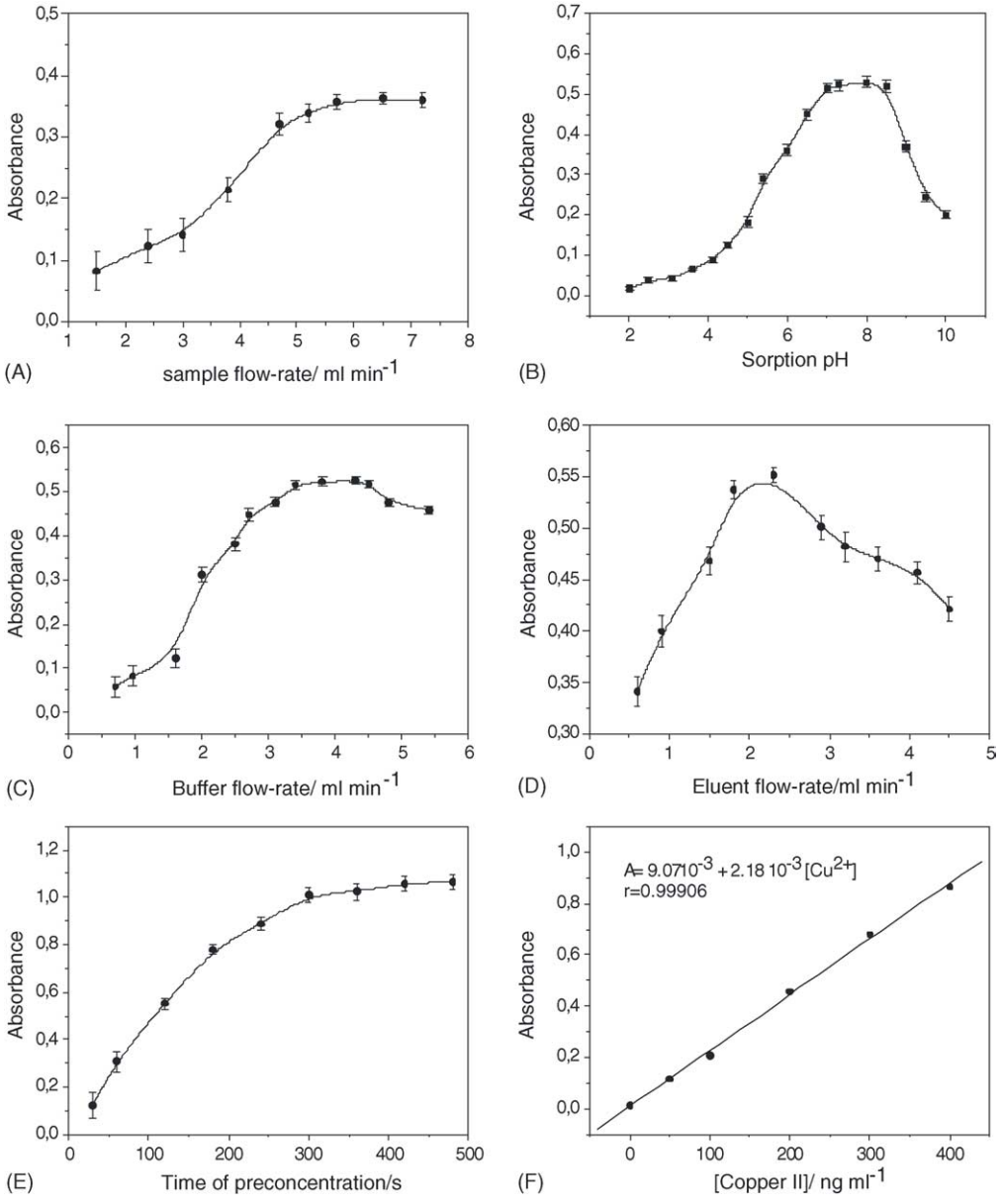

Fig. 2. Optimization of preconcentration flow system. Chromogenic agent 0.15% DDTC, 2.9 ml min^{-1}; buffer for color forming reaction, 0.8 mol l^{-1} borate buffer solution (pH 8.5), 2.6 ml min^{-1}: (A) effect of sample flow rate, 250 ng ml^{-1} Cu^{2+}; time of preconcentration 120 s; buffer solution pH 7.0; buffer flow rate, 3.4 ml min^{-1}; eluent, 0.5 mol l^{-1} HNO_3, 1.8 ml min^{-1}; time of elution, 60 s; time of regeneration, 60 s. (B) Effect of pH on the sorption, 250 ng ml^{-1} Cu^{2+}; sample flow rate, 6.5 ml min^{-1}; time of preconcentration, 120 s; buffer flow rate, 3.4 ml min^{-1}; eluent, 0.5 mol l^{-1} HNO_3, 1.8 ml min^{-1}; time of elution, 60 s; time of regeneration, 30 s. (C) Effect of the buffer flow rate for the copper preconcentration, 250 ng ml^{-1} Cu^{2+}; sample flow rate, 6.5 ml min^{-1}; time of preconcentration, 120 s; buffer solution pH 8.5; eluent, 0.5 mol l^{-1} HNO_3, 1.8 ml min^{-1}; time of elution, 60 s; time of regeneration 30 s. (D) Eluent flow rate, 250 ng ml^{-1} Cu^{2+}; sample flow rate, 6.5 ml min^{-1}; buffer solution pH 8.5; buffer flow rate, 4.3 ml min^{-1}; time of preconcentration, 120 s; eluent, 0.4 mol l^{-1} HNO_3; time of elution, 60 s; time of regeneration, 30 s; (E) Time of preconcentration, 250 ng ml^{-1} Cu^{2+}; sample flow rate, 6.5 ml min^{-1}; buffer solution pH 8.5; buffer flow rate, 4.3 ml min^{-1}; eluent, 0.4 mol l^{-1} HNO_3, 2.3 ml min^{-1}; time of elution, 60 s; time of regeneration, 30 s. (F) Analytical curve, sample flow rate, 6.5 ml min^{-1}; buffer solution pH 8.5; time of preconcentration, 120 s; buffer flow rate, 4.3 ml min^{-1}; eluent, 0.4 mol l^{-1} HNO_3, 2.3 ml min^{-1}; time of elution, 60 s; time of regeneration, 30 s.

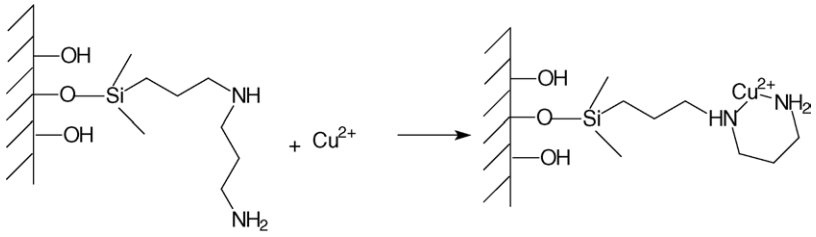

Scheme 1. Sorption of Cu^{2+} on the DAPPS.

the concentration of the concomitant species in these kind of sample are usually lower than the proposed preconcentration method can tolerate [40].

3.4. Determination of Cu^{2+} in the samples using the proposed preconcentration system

The proposed preconcentration system using DAPPS as a sorbent was employed for the determination of Cu^{2+} ($n = 3$) in seven ordinary natural water samples and one water reference material (Table 1), which was employed in order to achieve the accuracy of the preconcentration procedure. In addition, a recovery study was also carried out, by spiking the natural water samples with 100 ng ml^{-1} Cu^{2+}. The recoveries ranged from 96.9 to 102.4%.

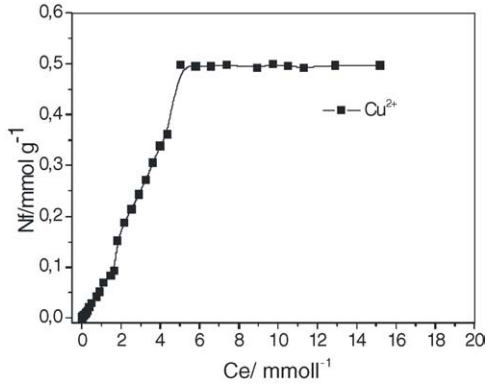

Fig. 3. Adsorption isotherm of Cu^{2+} on DAPPS. Time of agitation 180 min.

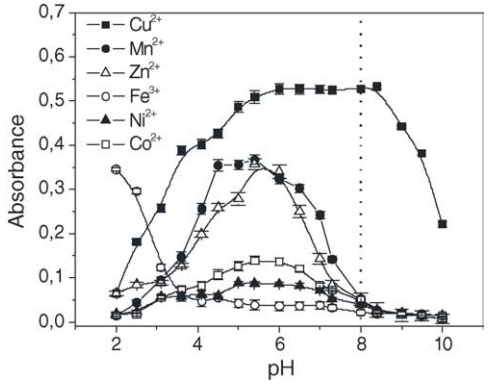

Fig. 4. Sorption of several metals on DAPPS in function of the pH.

Also, the preconcentration system using DAPPS as sorbent was also employed for the determination of Cu^{2+} in digests of biological materials (Table 2). The contents of copper were determined in four ordinary biological materials and for obtaining the accuracy of the method two biological

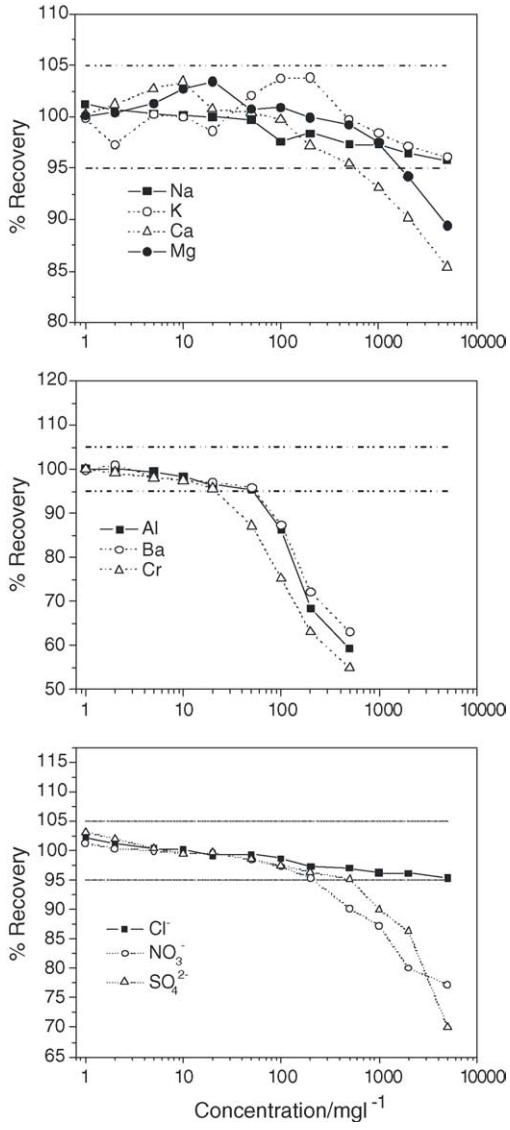

Fig. 5. Interference of several elements on the sorption of 250 ng ml^{-1} Cu^{2+} on the DAPPS sorbent. For details of the optimized conditions of flow system, see Fig. 2.

Table 1
Determination of Cu^{2+} in water samples ($n = 3$) employing an on-line preconcentration system

Samples	$[Cu^{2+}] \pm$ S.D. (ng ml^{-1})	Found with spike 100 ng ml^{-1}	%Recovery
NIST 1640[a]	85.6 ± 1.7	185.7 ± 2.7	100.1
Countryside river water	79.2 ± 2.9	179.1 ± 2.4	99.9
Urban river water	218.2 ± 3.4	311.4 ± 2.2	96.9
Streamlet water	160.0 ± 11.8	258.1 ± 2.4	98.9
Stream water	199.4 ± 1.6	304.2 ± 2.2	102.4
Springwater	216.0 ± 3.7	319.9 ± 1.4	101.8
Well water I	236.8 ± 3.7	342.0 ± 1.6	102.2
Well water II	206.1 ± 4.4	304.4 ± 1.7	99.2

Results are expressed as average value ± S.D. ($n = 3$). The samples were spiked with 100 ng ml^{-1} Cu^{2+}.
[a] Certified value 85.2 ± 0.9 ng ml^{-1}.

Table 2
Determination of Cu^{2+} in biological materials ($n = 3$) employing an on-line preconcentration system

Samples	$[Cu^{2+}] \pm$ S.D. (μg g^{-1})	$[Cu^{2+}] \pm$ S.D. (ng ml^{-1})	Found with spike 50 ng ml^{-1}	%Recovery
Maize powder	4.71 ± 0.16	47.13 ± 0.7	97.41 ± 0.20	100.6
Soybean	6.65 ± 0.17	66.48 ± 0.8	114.46 ± 0.66	97.0
Citrus leaves	5.10 ± 0.12	51.02 ± 0.4	102.33 ± 0.75	102.6
Corn Stalks	7.79 ± 0.14	78.01 ± 0.4	126.44 ± 0.05	98.0
NIST-SRM 1515[a]	5.69 ± 0.11	56.96 ± 0.4	106.78 ± 0.56	99.7
NIES-CRM-03[b]	3.47 ± 0.12	34.74 ± 1.6	85.28 ± 0.30	101.6

Results are expressed as average value ± S.D. ($n = 3$). The samples were spiked with 50 ng ml^{-1} Cu^{2+}. Dilution factor 100 ml g^{-1}.
[a] Certified value 5.64 ± 0.23 μg g^{-1}.
[b] Certified value 3.5 ± 0.3 μg g^{-1}.

certified materials were employed. In addition, to improve the accuracy of the proposed method with the ordinary samples, the digests of the biological materials were spiked with 50.0 ng ml^{-1} Cu^{2+}, and the recoveries ranged from 97.0 to 101.6%.

Based on the results of Tables 1 and 2 it can be inferred that Cu^{2+} can be successfully determined in natural waters as well as in biological materials, with good accuracy, employing a simple preconcentration system using DAPPS as a sorbent and spectrophotometric detection.

4. Conclusion

A simple flow preconcentration system for the determination of Cu^{2+} using DDTC as chromogenic agent with spectrophotometric detection and DAPPS as a sorbent was successfully employed for the determination of the analyte in biological materials as well as natural water samples. Although the attained preconcentration factor of 36 for Cu^{2+} determination in real samples is not one of the highest values achieved when compared with an off-line column preconcentration, which use 3 l of sample solution attaining a preconcentration factor of 300 [17], this value is a little bit better when compared with a flow system with employing reversed-phase C_{18} as a sorbent, and ethanol as eluent and detection with FAAS, whose preconcentration factor was 19 [31]. In addition, the preconcentration factor attained in this work was also better than that obtained with algae immobilized in silica gel using ICP-AES as a detector in a flow system, whose value was 13 [25].

The detection limit obtained in this work was 0.84 μg g^{-1} for biological materials, which is comparable with the detection limit of 0.64 μg g^{-1} obtained with ETAAS for copper determination in biological materials [41]. It is important to point out that the cost of the implementation of the proposed procedure, employing a homemade flow-injection system was less than US $4000. It also should be stressed that a graphite furnace spectrometer cost not less than US $50,000. Therefore, when the flow preconcentration systems coupled to selective sorbents as DAPPS, became widespread, the analysis of low concentration of elements could be attained at any simple analytical laboratory which are numerous in underdeveloped countries.

Acknowledgements

We acknowledge Flávio André Pavan from Instituto de Química da Universidade de Campinas (IQ-UNICAMP) for donating some peristaltic tubes and also Boaventura Freire dos Reis from Centro de Energia Nuclear na Agricultura da Universidade de São Paulo (CENA-USP) for donating some polyethylene propulsion tubes. Also, we are grateful to Fundação de Amparo à Pesquisa do Estado do Rio Grande do Sul (FAPERGS) and Conselho Nacional de Desenvolvimento Científico e Tecnológico (CNPq) for financial support and fellowships.

References

[1] A. Goswami, A.K. Singh, Talanta 58 (2002) 669.
[2] C.E. Harland, Ion Exchange Theory and Practice, 2nd ed., Royal Society of Chemistry, Cambridge, UK, 1994.
[3] Y. Baba, H. Noma, R. Nakayama, Y. Matsushita, Anal. Sci. 18 (2002) 359.
[4] C. Airoldi, R.F. Farias, Quim. Nova 23 (2000) 496.
[5] P.K. Jal, S. Patel, B.K. Mishra, Talanta 62 (2004) 1005.
[6] B. Perez-Cid, S. Rio-Segade, C. Bendicho, Microchem. J. 55 (1997) 319.
[7] H. Bagheri, A. Gholami, A. Najafi, Anal. Chim. Acta 424 (2000) 233.
[8] J. Seneviratne, J.A. Cox, Talanta 52 (2000) 801.
[9] J.C.P. Vaghetti, M. Zat, K.R.S. Bentes, L.S. Ferreira, E.V. Benvenutti, E.C. Lima, J. Anal. At. Spectrom. 18 (2003) 376.
[10] L.T. Arenas, J.C.P. Vaghetti, C.C. Moro, E.C. Lima, E.V. Benvenutti, T.M.H. Costa, Mater. Lett. 58 (2004) 895.
[11] J.C. Yu, S.M. Chan, Z. Chen, Anal. Bioanal. Chem. 376 (2003) 728.
[12] P.S. Roldan, I.L. Alcântara, G.R. Castro, J.C. Rocha, C.C.F. Padilha, P.M. Padilha, Anal. Bioanal. Chem. 375 (2003) 574.
[13] N. Tokman, S. Alman, M. Ozcan, U. Koklu, Anal. Bioanal. Chem. 374 (2002) 977.
[14] M.M. Osman, S.A. Kholeif, N.A. Abou-Al-Maaty, M.E. Mahmoud, Michrochim. Acta 143 (2003) 25.
[15] K.S. Abou-El-Sherbini, I.M.M. Kenawy, M.A. Hamed, R.M. Issa, R. Elmorsi, Talanta 58 (2002) 289.
[16] A. Goswami, A.K. Singh, Anal. Chim. Acta 454 (2002) 229.
[17] A. Goswami, A.K. Singh, B. Venkataramani, Talanta 60 (2003) 1141.
[18] S. Zhang, Q. Pu, P. Liu, Q. Sun, Z. Su, Anal. Chim. Acta 452 (2002) 223.
[19] P. Liu, Z. Su, X. Wu, Q. Pu, J. Anal. At. Spectrom. 17 (2002) 125.
[20] J.A.A. Sales, F.P. Faria, A.G.S. Prado, C. Airoldi, Polyhedron 23 (2004) 719.
[21] H. Bergamin-Filho, B.F. Reis, A.O. Jacintho, E.A.G. Zagatto, Anal. Chim. Acta 117 (1980) 81.
[22] M.M. Santos-Filha, B.F. Reis, H. Bergamin-Filho, N. Baccan, Anal. Chim. Acta 261 (1992) 339.
[23] M. Zougagh, P.C. Rudner, A.G. Torres, J.M.C. Pavón, Anal. Bioanal. Chem. 378 (2004) 423.
[24] T.P. Rao, J.M. Gladis, Anal. Sci. 18 (2002) 517.
[25] E.N.V.M. Carrilho, J.A. Nóbrega, T.R. Gilbert, Talanta 60 (2003) 1131.
[26] M. Zougagh, A.G. Torres, J.M. Pavón, Talanta 56 (2002) 753.
[27] J. Ruzicka, E.H. Hansen, Flow Injection Analysis, 2nd ed., Willey, New York, 1988.
[28] Q. Pu, P. Liu, Q. Sun, Z. Su, Michrochim. Acta 143 (2003) 45.
[29] P. Liu, Q. Sheng, Q.Y. Sun, Z.X. Su, Fresenius' J. Anal. Chem. 366 (2000) 816.
[30] M.C. Yebra, M.F. Enríquez, A. Garcia, A. Moreno-Cid, Fresenius' J. Anal. Chem. 370 (2001) 64.
[31] A. Ali, Y. Ye, X. Guangming, X. Yin, Fresenius' J. Anal. Chem. 365 (1999) 642.
[32] M.C. Yebra-Biurrun, A. Bermejo-Barrera, M.P. Bermejo-Barrera, M.C. Barciela-Alonso, Anal. Chim. Acta 303 (1995) 341.
[33] J. Wang, E.H. Hansen, J. Anal. At. Spectrom. 16 (2001) 1349.
[34] H. Bagheri, A. Gholami, A. Najafi, Anal. Chim. Acta 424 (2000) 233.
[35] I.M. Kolthoff, E.B. Sandell, E.J. Meehan, S. Bruckentein, Quantitative Chemical Analysis, 4th ed., Macmillan, London, 1969, p. 108.
[36] M.G. Fonseca, C. Airoldi, J. Therm. Anal. Calorim. 64 (2001) 273.
[37] E.C. Lima, F.J. Krug, A.T. Ferreira, F. Barbosa, J. Anal. At. Spectrom. 14 (1999) 269.
[38] E.A.G. Zagatto, A.O. Jacintho, B.F. Reis, F.J. Krug, H. Bergamin-Filho, L.C.R. Pessenda, J. Mortatti, M.F. Giné, Manual de Análises de Plantas e Águas empregando sistemas de injeção em fluxo, Universidade de São Paulo, Centro de Energia Nuclear na Agricultura, Piracicaba, SP, 1981, 45 pp.
[39] H. Cesur, J. Trace Microprobe Technol. 21 (2003) 627.
[40] Database of Natural Matrix Reference Materials, compilation prepared by International Atomic Energy Agency (IAEA), last update January 2003. http://www.iaea.org/programmes/nahunet/e4/nmrm/browse.htm.
[41] E.C. Lima, F. Barbosa, F.J. Krug, A. Tavares, Talanta 57 (2002) 177.

7. CONCLUSÕES

No presente trabalho usando-se o método sol-gel foi sintetizado um novo híbrido, pelo método sol-gel, a difenilaminapropril sílica (DFA Si), cujo grau de incorporação de matéria orgânica foi de 1,4 mmol/g. A adição de titânia (DFA Si/Ti) modificou significativamente a morfologia do híbrido, diminuindo a porosidade e a área superficial. O estudo da estabilidade térmica mostrou que a interface organo-inorgânica desse híbrido é de natureza covalente. O híbrido DFA Si mostrou-se termicamente mais estável na ausência de titânia e com menor fração de matéria orgânica oclusa em poros fechados.

O híbrido DFA Si apresenta potencialidade para a adsorção de nitrogenados aromáticos de interesse ambiental. A adição de titânia aumentou a capacidade de adsorção dos nitrogenados que foi interpretado como sendo devido: a) aos grupos Ti-OH que apresentam maior momento dipolar que os grupos Si-OH, adsorvendo melhor os analitos nitrogenados que possuem apreciável polaridade; b) a adsorção dos analitos ser maior na amostra contendo titânia porque essa amostra possui maior densidade de grupos orgânicos.

O estudo do efeito da compactação em altas pressões na microestrutura do híbrido inédito mostrou que esse processamento provoca uma diminuição na porosidade e na área superficial das amostras, efeito que está relacionado à compactação de partículas agregadas e ao fechamento de poros. A morfologia da amostra DFA Si compactada a 3,5 e a 6,0 GPa é bastante semelhante. Entretanto, na amostra contendo titânia a prensagem a 6 GPa provocou fissuras que não estavam presentes no híbrido compactado a 3,5 GPa. A diminuição da área superficial na amostra contendo titânia foi drástica, o que pode ser explicado pela baixa porosidade e pequena área superficial dessa amostra mesmo antes da compactação. Esse processamento praticamente eliminou a porosidade do material. O fechamento dos poros provocou o encapsulamento da matéria orgânica sendo mais evidente no material contendo titânia.

Neste trabalho foram sintetizados também pelo método sol-gel os híbridos *p*-fenilenodiaminapropril sílica (FNDA Si) e *p*-anisidinapropril sílica (ANS Si), híbridos de interesse do Grupo de Química do Estado Sólido da UFRGS, que já demonstraram eficiência na adsorção de metais e contaminantes orgânicos, além de apreciável estabilidade térmica. Esses materiais foram compactados a 7,7 GPa visando aprofundar as investigações sobre a influência da compactação em altas pressões na microestutura dos híbridos obtidos pelo método sol-gel.

No híbrido FNDA Si apenas uma pequena quantidade de grupos orgânicos foi encapsulada durante a síntese, já no híbrido ANS Si cerca de 57 % da matéria orgânica foi encapsulada em poros fechados, durante a hidrólise e policondensação. A área superficial e a porosidade do híbrido FNDA Si pó é maior que no híbrido ANS Si pó. A compactação em altas pressões provocou o fechamento de poros e a redução de cerca de 60% da área superficial do híbrido FNDA Si. É importante destacar que essa redução é pequena quando comparada à sílica pura. O fenômeno foi interpretado como uma conseqüência da presença dos grupos orgânicos. Foi proposto que esses grupos exerçam função amortecedora dificultando a aproximação das partículas e impedindo a reação dos grupos silanos, fenômeno que inibiu o processo de sinterização a frio.

No híbrido ANS Si a compactação a 7,7 GPa produziu trincas e um aumento na área superficial. O processo de dissipação de energia derivada dessa compactação foi prejudicado pela presença dos grupos orgânicos e pela baixa porosidade do material. Sugere-se que a dissipação de energia nesse material tenha levado a um processo de cisalhamento entre as partículas, causando defeitos microestruturais decorrentes da deformação plástica das partículas. Cisalhamento que explica a liberação da matéria orgânica que inicialmente encontrava-se encapsulada.

Conclui-se que a compactação em altas pressões pode ser uma alternativa para modificar a microestrutura dos híbridos sintetizados pelo método sol-gel, como também para densificar esses materiais. As modificações dependem tanto da pressão aplicada quanto da composição química do material.

Nesse trabalho foi sintetizado ainda pelo método enxerto o híbrido 7 amino-4-azaheptil sílica (AAH Si). A partir de termoanálise no infravermelho observou-se que a interface organo-inorgânica do material é de natureza covalente. Algumas características desse híbrido como a presença dos grupos quelantes e a área superficial despertaram interesse para sua utilização como adsorvente de cátions metálicos. Esse material mostrou potencialidade na pré-concentração de íons Cu (II) e Fe (III) presentes em amostras naturais, ao ser utilizado como fase estacionária num sistema de fluxo contínuo. A utilização desse híbrido na pré-concentração de íons metálicos mostra-se uma alternativa viável para aumentar o poder de detecção de técnicas menos sensíveis, como a espectrofotometria no UV e visível e a espectrometria de absorção atômica.